1994

Photophysics of a novel optical probe, 7-azaindole and an antiviral agent, hypericin

Feng Gai
Iowa State University

1

95

03554

Order Number 9503554

Photophysics of a novel optical probe, 7-azaindole and an antiviral agent, hypericin

Gai, Feng, Ph.D.

Iowa State University, 1994

U·M·I
300 N. Zeeb Rd.
Ann Arbor, MI 48106

Photophysics of a novel optical probe, 7-azaindole and an antiviral agent, hypericin

by

Feng Gai

A Dissertation Submitted to the

Graduate Faculty in Partial Fulfillment of the

Requirements for the Degree of

DOCTOR OF PHILOSOPHY

Department: Chemistry
Major: Physical Chemistry

Approved:

Signature was redacted for privacy.

In Charge of Major Work

Signature was redacted for privacy.

For the Major Department

Signature was redacted for privacy.

For the graduate College

Iowa State University
Ames, Iowa

1994

TABLE OF CONTENTS

CHAPTER I INTRODUCTION

The work described in this thesis centers about two biologically relevant molecules: 7-azaindole and hypericin. In order to study macromolecules, such as proteins, optically, an optical probe is needed. The conditions for a good probe are that it is easily accessible, simple, sensitive to environmental changes and that it does not obfuscate the observed signal of the molecules to be studied [1]. Also, its photophysics should be understood fully. Usually, tryptophan, a naturally occurring amino acid, is employed as the optical probe in protein studies [1]. However, tryptophan, tryptophan-containing peptides, and most proteins containing tryptophan afford nonexponential fluorescence decays [36], which complicate the interpretation of the results obtained. A model combining the existence of conformational isomers and charge transfer to the side chain from the indole moiety has been proposed to explain this nonexponential fluorescence decay [1]. Another disadvantage of using tryptophan as an optical probe is the mixed information coming from each individual chromophore in the multi-tryptophan-containing proteins. Thus, employing tryptophan as an optical probe has several limitations. Recently, we have proposed an alternative to tryptophan, 7-azatryptophan, as an optical probe. This proposal [31] is based on several considerations. (1) 7-azatryptophan can be incorporated into synthetic peptides and bacterial protein. (2) It is distinguishable optically from tryptophan, both in its emission and absorption spectra. Selective excitation and detection of only 7-azatryptophan in a mixture containing both 7-azatryptophan and tryptophan is possible. (3) Most importantly, 7-azatryptophan affords single exponential fluorescence decay [11] in water over most of the pH range when the entire emission band is collected. This single exponential is interpreted as an unfavorable charge transfer process from the 7-azaindole chromophore to the side chain compared to the case of tryptophan.

Except for the nonradiative processes in which the side chains are involved, the photophysics of tryptophan and 7-azatryptophan are determined mainly by their chromophores, indole and 7-azaindole, respectively. A thorough investigation of the photophysics of 7-azaindole is thus required in order to employ 7-azatryptophan as an optical probe. The most interesting chemistry happening after the 7-azaindole molecule absorbs a UV photon is excited-state double-proton transfer (ESPT) and photoionization [11a, 101].

The transfer of a proton represents a central reaction class in chemistry and biochemistry. Ground-state proton transfer has been one of the most important topics in chemistry for many years [166, 167]. Only recently, however, has the study of excited-state proton transfer become popular both experimentally and theoretically. Huppert [144] and Arnaut and Formosiho [166, 167] reviewed excited-state proton transfer reactions, respectively. These reviews include experimental results concerning inter- and intramolecular proton transfers in both the ground and the excited states. Two examples of molecules that exhibit excited-state proton transfer behavior are methyl salicylate, described by Weller [2], and 3-hydroxyflavone, described by Sengupta and Kasha [3]. Before fast laser sources were available, the methods employed to study excited-state proton transfer were mainly steady-state approaches. For example, the Förster cycle [10] is used to determine the pK_a change between ground state and excited state from the steady-state absorption and fluorescence spectra. Also, dual emission is taken as an indication of tautomerization in the excited-state. However, in the last decades, with the advent of fast pulsed laser light sources, kinetic data with ultrafast time resolution has become available for excited-state proton transfer processes. Many very interesting and important phenomena in the femtosecond range have been observed. Theoretically, approaches have emerged to permit one to cope with the quantum character of the proton at a molecular dynamics simulation level. Those include diabatic curve-crossing approaches [5], adiabatic quantum simulation techniques [6] and possible

nonadiabatic extensions, path-integral formulations [7], and semiclassical tunneling algorithms [8]. Computational studies using these methods have helped us a great deal to understand many features of proton-transfer reactions in solution [5,7a] and in biological systems [7b]. For example, Hynes et al. [9] have developed a dynamic theory for the proton transfer rate constant both in the nonadiabatic, weak coupling regime and in the adiabatic limit. The finite rate constant is expressed as resulting from an incoherent superposition of proton tunneling events in a distribution of inhomogeneous solvent environments. The classical Arrhenius behavior is determined by solvent and vibrational factors. Three coordinates have been shown to play an important role: the proton coordinate; the intramolecular separation of the two heavy atoms between which the proton is transferred; and the collective solvent coordinate. In this work, electrons were treated adiabatically, but the proton transfer was considered either nonadiabatically or adiabatically depending on the separation of the two heavy atoms. The transition between the adiabatic and nonadiabatic regions is at about 2.7 Å. When proton transfer is in the adiabatic region, small isotope effect is expected. Otherwise tunneling is considered to be important and a large isotope effect should be observed [9].

Kasha and co-workers [4] discovered that 7-azaindole can form dimers that undergo excited-state tautomerization through double-proton transfer. It has also been demonstrated that excited-state tautomerization occurs for 7-azaindole in alcohols. It is proposed that the excited-state double-proton transfer process of 7-azaindole in alcohols is mediated by a cyclic solute-solvent complex. By employing the proton inventory technique, Chen et al. showed that this process is concerted in nature [68].

The accepted description of the photophysics of indole is in terms of two overlapping $\pi \rightarrow \pi^*$ transitions, referred to by the Platt labels ^1L_a and ^1L_b [39]. Yamamoto and Tanaka [39c] determined that these two transitions are approximately orthogonal to one another in the plane of the indole ring by measuring the angular dependence of the absorbance of UV

light by oriented crystals of indole. Valeur and Weber [39a] resolved the excitation spectra for the ^1L_a and ^1L_b components by studying the fluorescence anisotropy of indole at low temperature. Rich et al. [33] reported similar results for 7-azaindole. Their study of the steady-state fluorescence excitation anisotropy of 7-azaindole at low temperature shows that the absorption spectrum of 7-azaindole consists of two overlapping electronic transitions whose transition dipole moments are at large angles to each other.

Photoionization has elicited considerable experimental and theoretical interest. Femtosecond laser pulses have been used to photoionize water molecules to generate photo-electrons biphotonically [168]. The instantaneous ejection of an electron into a polar medium provides the simplest case to study solvent response to an electronic perturbation. Experiments show that it takes about 100 fs [168] for a photoelectron to be localized and solvated in water. The fully solvated electron has broad featureless absorption spectra in polar solvents. In water the spectrum is centered around 720 nm [58]. The characteristic absorption spectrum and its quenching behavior by electron scavengers are used to identify the production of solvated electrons. Bent and Hayon [37] have studied the photoionization processes of indole and tryptophan by flash photolysis. They observed that for tryptophan a logarithmic plot of the yield of the solvated electron against the photolyzing pump intensity gave a straight line of slope 1.25 at pH 7.5. This result made them suggest a monophotonic ionization process. Nevertheless, because of the 3.6 ns pulse duration of their laser pulse, which is longer than the tryptophan fluorescence life time, they were unable to assign the ionizing states accurately.

Hypericin, a naturally occurring polycyclic quinone, is closely related, both structurally and spectrally, to the photoreceptor of the protozoan ciliates, *Stentor coerulus* [107] and *Blepharisma japonicum* [108, 109]. Carpenter and Kraus [106] demonstrated that hypericin has dramatic photoinduced antiviral activity against a lentivirus closely related to HIV, equine

infectious anemia virus. Song and co-workers [112, 114] have observed that the excited states of hypericin produce protons upon photoexcitation. Also it has been shown that hypericin generates singlet oxygen after absorbing light [106]. The x-ray structure of hypericin indicates that the aromatic polycycle is twisted and that intramolecular hydrogen bonding occurs between a hydroxyl and a carbonyl oxygen separated by about 2.5 Å [133, 155].

This thesis is organized as follows: Chapter II describes the instruments and methods used to obtain the experimental data and the construction of a new femtosecond Ti:sapphire laser system. Chapter III contains the discussion of the photoionization of indole, 7-azaindole and their derivatives. In this chapter, the similarities and differences between indole and 7-azaindole are discussed. Chapter IV and V are devoted to hypericin. In these chapters, the fluorescence species and the excited-state tautomerization of hypericin are described. The role of solvents in the proton transfer process of hypericin is discussed. Chapter VI outlines the isotope effect for a concerted and a step-wise double-proton transfer reaction as well as its application to the 7-azaindole/alcohol system.

CHAPTER II INSTRUMENTS

A. 30 Hz Dye Laser Amplifier

1. Introduction

Synchronous pumping of a dye laser by a CW mode-locked Nd:YAG laser makes it possible to produce tunable picosecond optical pulses with several kilowatt peak power. However, many applications need even more power, thereby requiring the development of a short pulse dye amplifier. Peak powers exceeding 3 GW have been obtained with such picosecond systems [15]. Femtosecond laser pulses generated from colliding-pulse mode-locked lasers can be amplified to the 10 GW level using a dye amplifier [16], which is high enough to generate a white light continuum.

One of the difficulties associated with high gain dye amplifiers is their short storage time (typically < 1ns). This means the seed pulse competes for gain with amplified spontaneous emission (ASE) during the several nanosecond profile of the pump pulse. Hence the subpicosecond seed pulse emerges from the amplifier on a background of ASE [17]. In order to suppress ASE, saturable absorbers, pinholes, or other devices may be used to isolate the different stages in the amplifier, thereby complicating the design of the dye amplifier. Even with isolation schemes, ASE is often several percent of the total energy coming out of the amplifier [26].

First Sizer [18], then Wokaun [19] realized that a shorter pumping pulse with duration much shorter than the gain storage time of the amplifier would reduce the ASE substantially. Because the seed pulse can be amplified only if it overlaps with the pump pulse both temporally and spatially, precise timing between pump and seed pulse must be maintained.

2. Pump Source and Dye Amplifier

In order to overcome these difficulties, we built a dye amplifier based on the design of Perry et al. [26]. The laser system begins with a cw mode-locked Nd:YAG laser (Coherent Antares 76s) operating at 76 MHz. The 100-ps, 1064 nm pulses are converted to 532 nm by employing a second harmonic generator. The second harmonic is separated from the fundamental by a dichroic beam splitter. 50% of the 2-watt green power is used to pump a Coherent 701-2 dye laser which in turn produces about 100 mW 1-ps duration tunable optical pulses in the wavelength range of 580-620 nm when Rhodamine 6G is used as the laser medium. The dye laser pulses, typically of nanojoule energy, are focused by a 12.5 cm focal length lens into the three stage dye amplifier. A small portion of the residual 1064 nm radiation from the Nd:YAG laser is sent to a Continuum regenerative amplifier as a seed pulse. The regenerative amplifier then produces pulses with a 30 Hz repetition rate, ~ 70-ps duration and typically 1.2-1.4 watts average power at 532 nm. This is an ideal short pulse pump source for the dye amplifier.

The dye amplifier consists of three flowing dye cells (see Figure 2.1) with concentrations of about 2×10^{-5} M for the first dye cell and 0.9×10^{-5} M for the second and the third. Using Kiton Red 620, the amplifier is tunable from 570 to 600 nm. The output beam is collimated by a pair of lenses at the end of the amplifier. A variable delay line composed of a prism mounted on a translation stage is used to maintain the precise timing between the seed pulse and the pump pulse. In the first and second delay lines, two focal lenses with focal lengths of 25 cm and 50 cm, respectively, are employed to focus the pump beam down to the size of the seed beam at respective stages in order to overlap the two beams spatially. With pump energy of 40 mJ per pulse, the amplifier can produce 1-2 mJ in a ~ 1-ps pulse at 30 Hz, depending on the adjustment and the cavity length of the dye laser.

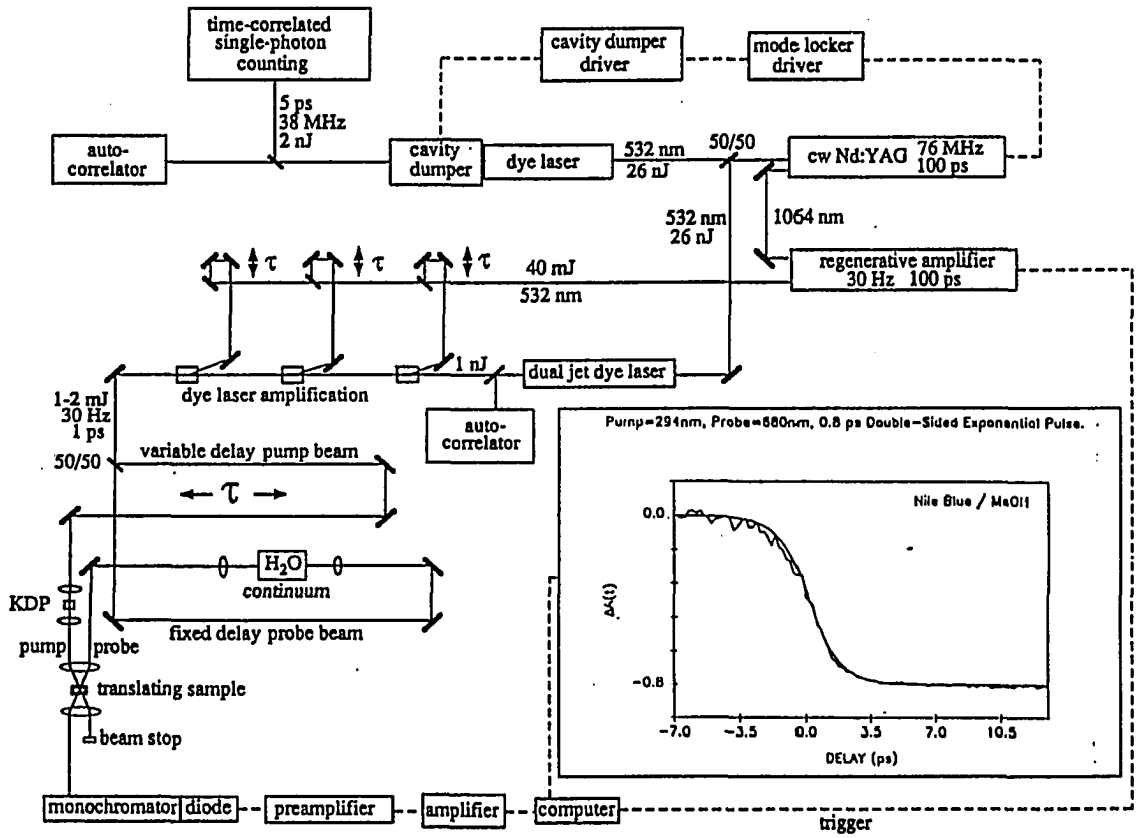

Figure 2.1. Experimental apparatus for pump-probe transient absorption measurements. Also displayed (inset) is the rise time of the induced bleaching of nile blue in methanol, λ_{ex} = 294 nm, λ_{probe} = 680 nm. The amplified laser pulse width is deconvoluted from the molecular response and is best described by a double-sided exponential of 0.8 ps full width at half-maximum.

The amount of amplified spontaneous emission presented in the output from the amplifier could be measured by separating the main pulse from the ASE using a grating. According to Perry et al. [26], a ratio of 10^3:1 between the main pulse and the ASE can be reached very easily even without a saturable absorber being used. However, this ratio is typically 10:1 for a nanosecond pumped dye amplifier.

3. Transient Absorption Spectrometer

Half of the amplified dye laser pulse train passes a fixed delay line and is focused into a cell containing water by a 75.6 mm focal length lens to generate a white light continuum, which is used as a probe pulse. Another half of the pulse train passes through a variable delay line as a pump pulse, which is either frequency doubled by a KDP crystal or the fundamental. The variable delay line consists of two mirrors mounted on a Klinger motorized translation stage. The movement of the translation stage is driven by a CD4.1 stepping motor driver which is controlled by a personal computer through a IEEE488 board. Both the pump and probe pulse are then focused into a 1 mm path length sample holder, which is translating at 30 cycles per minute. This makes the probe pulse strike a new spot each time. After the sample cuvette, the pump pulse is blocked and the probe pulse is collimated into a Jarrell-Ash 82-410 monochromater by another lens. The monochromater separates the different wavelengths contained in the probe pulse. A photodiode is placed at the exit of the monochromater to convert the light intensity into electrical signal. In order to correct for the laser intensity fluctuation, part of the probe energy is split before the sample holder and is directed into the same monochromater; the output is read by another photodiode. This signal is treated as a reference. Both probe and reference signals from the photodiodes are amplified by EG&G 142A preamplifiers and 571 main amplifiers before further processing.

The transient absorbance change induced by the pump pulse is derived from the probe signal difference before and after zero time. Here zero time refers to the temporal overlap of pump and probe pulses. The rise time of the transient signal is then determined only by the convolution of the pump and probe pulses. Data acquisition is achieved by a DT-2828 board. The simultaneous collection of both probe and reference signal is triggered by the synchronous TTL output from the regenerative amplifier. The delay between the signal reading and the trigger is controlled by a EG&G 416A delay generator. The program controlling the movement of the translation stage and the data acquisition is written in an advanced computer language, ASYST. In the directory of |asyst⟩, one can access the main menu by typing PP. After entering the main menu, one can chose different submenus, depending on the application. For the purpose of movement of the translation stage, one can chose the "motor control" submenu. The translation stage can be moved either forwards or backwards at different speeds depending on the input parameters. Two movement functions can be selected to determine the time interval corresponding to the distance the translation stage moved. In the Full.Step function, 75 steps correspond to 1 ps. And in Tenth.Step function, 750 steps correspond to 1 ps. For data acquisition, several controlling parameters should be given in advance. They are the output file name (e.g. xxxx.xxx), comments for the file (e.g. 7-azaindole/MeOH; ex = 298 nm; probe = 650 nm), time between two points (in ps, there are totally 100 data points, so the time window is 100 multiplied by this number), the number of shots for each point (typically 10), the lower limit of the reference signal (in volts), the upper limit of the reference signal (in volts), and the waiting time after the movement of translation stage (typically 1-2 seconds). The purpose of introducing lower and upper levels for the reference signal is to set a control window, only the probe signals corresponding to the reference signals in this window are collected. All the others are discarded. The data shown on the screen corresponds to transmittance, it will be saved automatically every 20 scans. In

order to obtain the absorbance change, one needs to take the logarithm of the inverse of these data.

To fit the experimental data, the pulse duration is measured first. Usually the instrument response is determined by fitting the bleaching signal of nile blue in ethanol, which is done by convoluting a guessed instrument function which is in turn the convolution of the pump and probe pulse (typically we use a double-sided exponential as the pulse envelope, see Figure 2.1) with an instantaneous response for nile blue. Once the instrument function is determined, one can use it to fit the real experimental signal (usually to an exponential) so that the kinetics of the event might be recovered.

B. Ti:sapphire Oscillator and Amplifier

1. Introduction

The broad gain bandwidth of Ti:sapphire makes it an excellent solid-state material both for a femtosecond oscillator and amplifier. Its gain bandwidth extends approximately from 670 to 1100 nm, providing both a large tuning range and the ability to produce ultrashort pulses. Using passively mode-locked mechanisms, the shortest pulse which can be generated scales inversely with the gain bandwidth multiplied by the square root of the saturable absorption [23]. Theoretically it is suggested that pulses as short as ~ 3 fs may be generated from Ti:sapphire lasers. Various mode-locking schemes have been employed in Ti:sapphire lasers whereby sub-100-fs pulses can be generated, one of them is so called self-mode-locking [21, 14]. Although the self-mode-locking mechanism is not fully understood, there is no doubt that the anomalous group velocity dispersion produced by a pair of intracavity prisms together with the nonlinearity χ_3 of the lasing medium plays a very important role in the ultrashort pulse generation process [20].

The amount of gain that one can extract from a laser material inside a amplifier with a short pulse is generally limited by the nonlinear effects, which may distort the spatial and temporal profile of the input pulse in the gain medium. In order to maintain low peak power in the amplification medium, the seed pulse has to be stretched first. After amplification the stretched pulse can be compressed back very close to its Fourier-transform limit. This type of amplification technique is called chirped-pulse amplification [22, 24].

2. Self-Mode-Locked Ti:sapphire Laser

The oscillator built in our lab is based on the design by Murnane and coworkers [13]. Pulses as short as 11-fs have been generated by such systems. The lasing medium of our oscillator is a 4.75 mm long Ti:sapphire rod, 0.015% doped, which is pumped by 5-6 W of the all lines output of an Ar^+ laser (Laser Ionics). A 12.5 cm focal length lens is used to focus this pump beam into the Ti:sapphire crystal. The oscillator cavity is folded by a high-reflector. A pair of fused silica prisms manufactured at a Brewster 63^o angle are used to minimize the third-order dispersion in the laser cavity. Two 10-cm radius of curvature mirrors are employed to focus the radiation inside the crystal. An output coupler dumps 10% of the cavity energy out, which is about 600-800 mW. The configuration of the oscillator is schematically shown in Figure 2.2. The total cavity length and the length on either arm of the laser are not critical, they can be varied considerably. However, the separation between the prisms is somewhat critical in order to get the shortest pulse duration. Also, the rod position and the separation between the two curved mirrors are very critical. The aligning procedures are simply described below [12]

(1) Align the pump beam so that it passes through the center of the focal lens, the first curved mirror, the crystal, and the second curved mirror. Make sure that the lens does not deviate the pump beam when translated and that the crystal surface reflects the pump beam

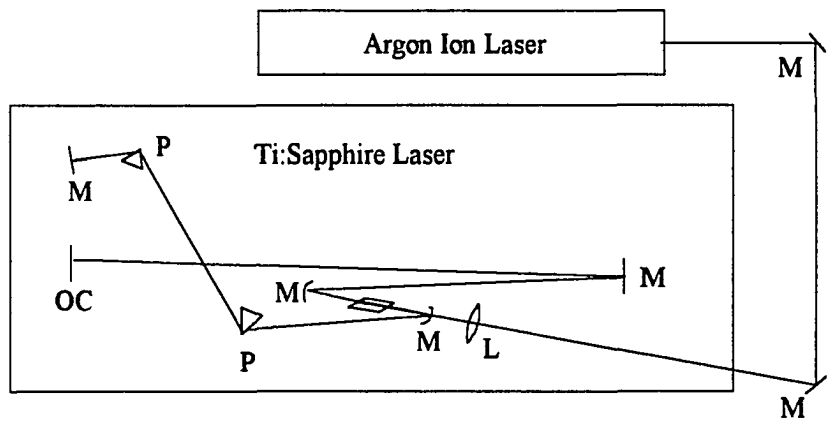

Figure 2.2. The schematic of the Ti:sapphire oscillator. M - Mirror, P - Prism, L - Lens, OC - Output coupler.

minimally (Brewster angle). A small rotation (~ 5^{o}) of the lens with respect to normal will slightly improve the overlap of the pump beam with the cavity mode.

(2) Place the folding mirror and the output coupler at one side of the rail and an aid mirror at another side of the rail (close to the output coupler). With 5 watts pumping energy, align for lasing (CW) by overlapping the fluorescence spots. Maximize the output power by alternately adjusting the horizontal and vertical controls both on the end mirror and output coupler, and translating the crystal, lens, and curved mirror. 600 mW should be obtained very easily.

(3) Place the first prism. Translate it to graze a bit of laser beam off the apex of the prism. Rotate it for minimum deviation of the laser beam. Place the second prism at the proper distance from the first one into this beam and rotate for minimum deviation.

(4) Insert an end mirror after the second prism and retroreflect the picked-off beam. Translate the prism fully into the beam. Remove the aid mirror and optimize the power by the end mirror and the output coupler. One should get > 600 mW with 5 watts pumping power.

(5) Adjust the crystal, curved mirrors, focal lens, and end mirrors for TEM_{00} mode and maximum power. Translate the prisms so that the beam is 1-2 mm from the edges. Disperse the output beam using a grating. Move the crystal and curved mirror far from the lens a small distance until the output beam looks oval. In the meantime, watch to see if the dispersed beam gets "jumpy" when the end mirror or output coupler is tapped. If this is so, mode-locking can be reached by either translating the 10 cm curved mirror far from the pump lens or tapping the output coupler.

(6) When the laser is running in mode-locked mode, adjust the prisms and the end mirror to get the full potential spectral width or the shortest pulse. Now the pulse width can be measured by an autocorrelator. For our system, sub-100-fs pulses are very easily obtained.

3. Ti:sapphire Amplifier and Femtosecond Transient Absorption Spectrometer

We amplify the Ti:sapphire oscillator by chirped amplification [14, 30]. The femtosecond pulse from the oscillator is first stretched to > 100 ps in a stretcher which consists of a 2000 g/mm gold-coated grating and gold-coated mirrors. The stretched pulse is then directed into the amplification cavity. The amplification medium is a 25-mm Ti:sapphire crystal which is pumped by a Laser Photonics KYD-300 YAG laser at a repetition rate of 10 kHz and 30 watt average power. The injection and ejection of the seed pulse and the amplified pulse is controlled by a Pockels cell (Medox). The exact timing between switching the Pockels cell on and off and firing the pump laser is maintained by a trigger signal originated from a photodiode output, which monitors the oscillation of the Ti:sapphire oscillator. After amplification, the pulse is compressed back to its Fourier transform limited shape by a two-grating compressor. The schematic of our amplifier and transient absorption spectrometer is shown in Figure 2.3.

After the compressor, we obtain 100-200 μJ in each pulse with around 100-fs duration. With this GW peak power, a white light continuum is generated very easily.

C. Pulse Broadening in Dispersive Media

When one works with subpicosecond laser pulses, pulse broadening must be considered if the short pulse propagates in dispersive media. The general treatment of such kind of broadening phenomena has been described by Tomov et al. [28].

For a short pulse with central frequency ω_0, its propagation vector $k(\omega)$ may be expanded in a Taylor's series with respect to frequencies nearby ω_0 [27]

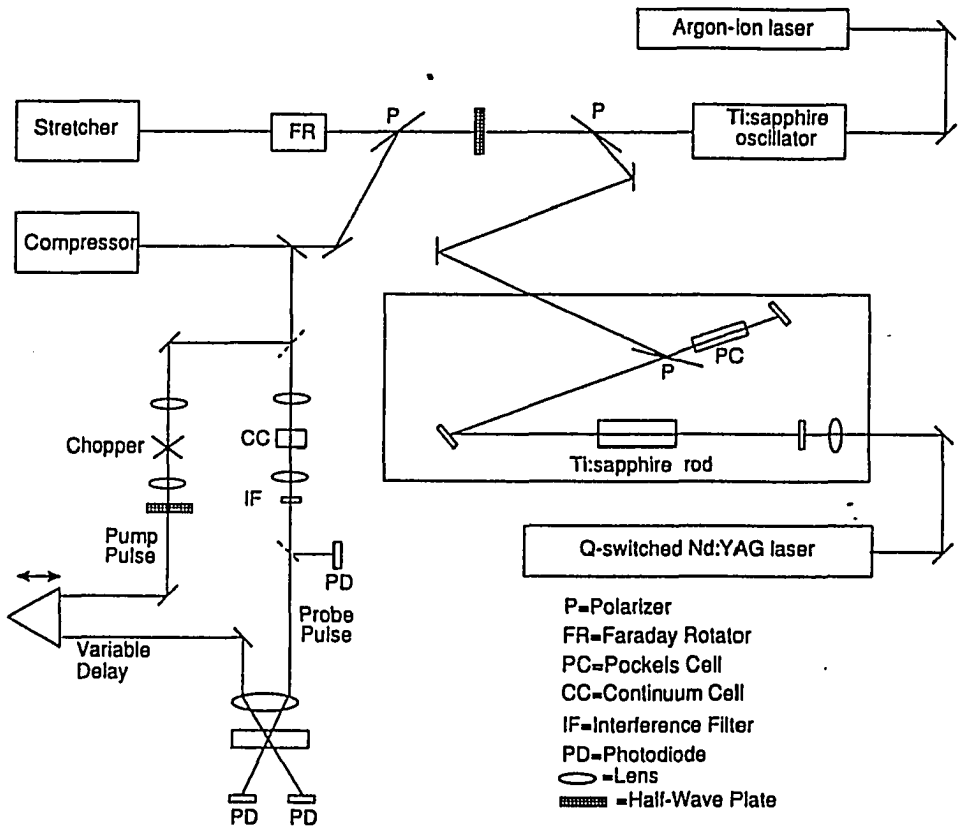

Figure 2.3. The schematic of the Ti:sapphire amplifier and the femtosecond transient spectrometer.

$$k(\omega) = k(\omega_0) + \left(\frac{\partial k}{\partial \omega}\right)_{\omega_0} d\omega + \frac{1}{2}\left(\frac{\partial^2 k}{\partial \omega^2}\right)_{\omega_0} d\omega + \cdots. \tag{2.1}$$

Here, the first term is the propagation vector of the light pulse at the central frequency. The second one is the inverse of the group velocity (v_g), and the third term is the group velocity dispersion (GVD). GVD determines the change of the pulse shape when it is propagating in a dispersive medium. All the higher terms may be neglected if one deals with a pulse duration greater than 10 fs [25].

1. Group Velocity Effects

The group velocity can be calculated from the dependence of the index of refraction on wavelength. The partial derivative of k with respect to ω in Eq (2.2),

$$k = \frac{n\omega}{c}, \tag{2.2}$$

gives rise to

$$\frac{\partial k}{\partial \omega} = \frac{n}{c} + \frac{\omega}{c}\frac{\partial n}{\partial \omega}, \tag{2.3}$$

where n is the index of refraction, c is the light velocity in vacuum, and ω is the wavelength. Because

$$d\omega = -\frac{2\pi c d\lambda}{\lambda^2}, \tag{2.4}$$

Eq (2.3) can be rewritten as

$$\frac{\partial k}{\partial \omega} = \frac{n}{c} - \frac{\lambda}{c}\frac{\partial n}{\partial \lambda}. \tag{2.5}$$

So the group velocity can be formulated as following [27, 28]

$$v_g(\lambda) = c\left[n(\lambda) - \lambda\left(\frac{\partial n}{\partial \lambda}\right)\right]^{-1}. \tag{2.6}$$

If the derivative of n with respect to wavelength, $\partial n/\partial \lambda$, is known for a dispersive medium, the group velocity can be calculated according to Eq (2.6).

When short pulses travel in linear optics, they are not affected by group velocity. But in nonlinear phenomena, such as second harmonic generation, the group velocity mismatch between the fundamental and the second harmonic may introduce a broadening of the second harmonic pulse [28]. This is because the fundamental pulse envelope travels faster than the frequency-doubled pulse inside the doubling crystal. A longer crystal length will produce a broader second harmonic pulse [29].

In order to keep the frequency-doubled pulse width no broader than that of the fundamental, the crystal length should be shorter than L_0 [28, 29], with

$$L_0 = \tau_p \Delta v_g \tag{2.7}$$

where τ_p is the fundamental pulse width and Δv_g is the group velocity mismatch between the frequency-doubled pulse and the fundamental, which is

$$\Delta v_g = \left| v_g(\omega)^{-1} - v_g(2\omega)^{-1} \right|^{-1}, \tag{2.8}$$

in units of velocity. For example, the phase matching angle is 60.46^{o} for a KDP crystal to double a 600 nm fundamental, but the group velocity matching angle cannot be reached at this point. The critical length for a 1-ps input pulse then can be calculated with Eqs (2.8) and (2.7). The result is about 5.3 mm. If a doubling crystal with length L is much longer than L_0, the second harmonic pulse will be broadened, and the resulting pulse duration may be expressed as [28, 29]

$$\tau_{SH} = \tau_p(1+L/L_0). \tag{2.9}$$

In general, the phase and group velocity matching can not be satisfied simultaneously in the visible and ultraviolet regions for most nonlinear crystals used today. This restricts the use of a long crystal length and consequently the conversion efficiency.

2. Group Velocity Dispersion

The group velocity dispersion (GVD) is the third term in Eq (2.1), which is

$$\mathrm{GVD} = \frac{\partial^2 k}{\partial \omega^2}. \tag{2.10}$$

GVD determines the change in shape of the wave packet during propagation in a dispersive medium. Similar to the group velocity, GVD can be related to the index of refraction of the dispersive medium. The derivative of Eq (2.5) with respect to ω yields

$$\frac{\partial^2 k}{\partial \omega^2} = \frac{1}{c}\left(2\frac{\partial n}{\partial \omega} + \frac{\omega \partial^2 n}{\partial \omega^2}\right). \tag{2.11}$$

Using Eq (2.4), the following result can be derived

$$\frac{\partial^2 n}{\partial \omega^2} = \frac{\partial}{\partial \omega}\left(\frac{\partial n}{\partial \omega}\right) = \frac{\lambda^2}{\pi c}\left(\frac{\partial n}{\partial \lambda}\right) + \frac{\lambda^3}{2\pi c}\left(\frac{\partial^2 n}{\partial \lambda^2}\right). \tag{2.12}$$

Combination Eqs (2.4), (2.11) and (2.12) gives rise to [27, 28, 30]

$$\frac{\partial^2 k}{\partial \omega^2} = \frac{\lambda^3}{2\pi c^2}\frac{\partial^2 n}{\partial \lambda^2}. \tag{2.13}$$

Group velocity dispersion can either compress a pulse with the right initial chirp, or broaden a pulse with the wrong initial chirp. In particular, the propagation of a short pulse with no initial chirp through a dispersive medium leads to pulse broadening and introduces chirp. As an example, we consider a gaussian pulse with a carrier frequency ω_0, which can be expressed as [30]

$$\varepsilon(t) = \exp(-at^2)\exp j(\omega_0 t + bt^2). \tag{2.14}$$

Here, the parameter b is a measure of the chirp. The instantaneous intensity associated with this gaussian signal can be written as

$$I(t) = |\varepsilon(t)|^2 = \exp(-2at^2). \tag{2.15}$$

Then the pulse width, defined in the usual FWHM fashion, is related to the parameter a as [30]

$$\tau_p = \sqrt{\frac{2\ln 2}{a}}. \tag{2.16}$$

An initially unchirped gaussian pulse with $b_0 = 0$ will vary its parameter a in a dispersive medium as following [30], after propagating a distance z,

$$a(z) = \frac{a_0}{1 + \left[2(GVD)^2 z\right]^2 a_0^2}. \tag{2.17}$$

So, if $GVD \neq 0$, a(z) will be less than a_0, which means the initial pulse width is broadened according to Eq (2.16). The final pulse width is related to the initial one as [30]

$$\tau_p^2(z) = \left[1 + (z/z_D)^2\right] \times \tau_{p0}^2, \tag{2.18}$$

with

$$z_D = \frac{\tau_{p0}^2}{(4\ln 2)GVD}. \tag{2.19}$$

Eqs (2.18) and (2.19) predict that after propagating a distance z_D the initial pulse width will increase by a factor of $\sqrt{2}$. For a pulse with 100-fs duration at 308 nm, this distance is about 44 m in air and about 3 cm in KDP or quartz [30].

When one works with a femtosecond laser system, care should be given to the selection of the optics. If possible, low dispersion materials such as fused silica or metal coated optics should be used. Where possible, one can correct for the group velocity dispersion by introducing an anomalous dispersion to eliminate the frequency chirp. This may

be done by a prism pair or a grating pair. Pulse broadening due to nonlinear processes cannot be corrected. The only way to minimize the group velocity mismatch is to select a shorter crystal length and low dispersive material if it is possible. Usually, BBO seems to be best both for high conversion efficiency and low group velocity mismatch [29].

D. Dispersion in Pairs of Prisms

In the generation of ultrashort optical pulses, one problem is how to minimize the phase distortion. Recent experimental work has shown that uncompensated cubic phase distortion limited the useful bandwidth of the compressed pulses [28d]. One may discuss this problem in terms of the Taylor series expansion of the phase:

$$\phi(\omega) = \phi(\omega_0) + \left(\frac{d\phi}{d\omega}\right)_{\omega_0} (\omega - \omega_0) + \frac{1}{2}\left(\frac{d^2\omega}{d\omega^2}\right)_{\omega_0} \times (\omega - \omega_0)^2 + \frac{1}{6}\left(\frac{d^3\omega}{d\omega^3}\right)_{\omega_0} (\omega - \omega_0)^3 + \cdots, \tag{2.20}$$

where ω_0 is the central frequency of the pulse spectrum. Treacy [28b] has shown that a pair of diffraction gratings can be used to compensate for the quadratic phase distortion of a frequency-broadened optical pulse. We describe, in the following, the use of prism pairs to compensate for the quadratic and cubic order phase distortions of an ultrashort pulse. We start from the optical path length, P [28c], with

$$P = \frac{\phi c}{\omega}, \tag{2.21}$$

here ϕ is the total phase, ω is the angular frequency, and c is the light velocity. The second order derivative of ϕ with respect to ω can be obtained through Eq (2.21), which is

$$\frac{d^2\phi}{d\omega^2} = \frac{2}{c}\frac{dP}{d\omega} + \frac{\omega}{c}\frac{d^2P}{d\omega^2}. \tag{2.22}$$

Considering only the second order in Eq (2.22), one obtains

$$\frac{d^2\phi}{d\omega^2} = \frac{\omega}{c}\frac{d^2P}{d\omega^2}. \tag{2.23}$$

From Eq (2.4), the following equation can be derived

$$d\omega^2 = \frac{4\pi^2 c^2}{\lambda^4} d\lambda^2. \tag{2.24}$$

Substitution of Eq (2.24) into Eq (2.23) gives rise to the quadratic phase distortion as

$$\frac{d^2\phi}{d\omega^2} = \frac{\lambda^3}{2\pi c^2}\frac{d^2P}{d\lambda^2}. \tag{2.25}$$

The derivative of Eq (2.22) with respect to ω yields

$$\frac{d^3\phi}{d\omega^3} = \frac{3}{c}\frac{d^2P}{d\omega^2} + \frac{\omega}{c}\frac{d^3P}{d\omega^3}. \tag{2.26}$$

From Eq (2.4), one has

$$d\omega^3 = -\frac{8\pi^2 c^3}{\lambda^6} d\lambda^3. \tag{2.27}$$

Then by substituting Eq (2.27) into Eq (2.26) one obtains the cubic term for phase distortion as

$$\frac{d^3\phi}{d\omega^3} = \frac{\lambda^4}{4\pi^2 c^3}\left(3\frac{d^2P}{d\lambda^2} - \lambda\frac{d^3P}{d\lambda^3}\right). \tag{2.28}$$

For double prism pairs, the total optical path that contributes to the dispersion is [28c]

$$P = 2l\cos\beta, \tag{2.29}$$

and

$$\frac{dP}{d\beta} = -2l\sin\beta, \tag{2.30}$$

$$\frac{d^2P}{d\beta^2} = -2l\cos\beta. \tag{2.31}$$

The definition of β is given in Figure 2.4. Employing the chain rule for derivatives, one has

$$\begin{aligned}\frac{d^2P}{d\lambda^2} &= \frac{d}{d\lambda}\left(\frac{dP}{d\lambda}\right) = \frac{d}{d\lambda}\left(\frac{dn}{d\lambda}\frac{d\beta}{dn}\frac{dP}{d\beta}\right) \\ &= \frac{d\beta}{dn}\frac{dP}{d\beta}\left(\frac{d^2n}{d\lambda^2}\right) + \frac{dn}{d\lambda}\frac{dP}{d\beta}\left(\frac{d^2\beta}{d\lambda d\beta}\right) + \frac{dn}{d\lambda}\frac{d\beta}{dn}\left(\frac{d^2P}{d\lambda d\beta}\right) \\ &= \left[\frac{d^2n}{d\lambda^2}\frac{d\beta}{dn} + \left(\frac{dn}{d\lambda}\right)^2\frac{d^2\beta}{dn^2}\right]\frac{dP}{d\beta} + \left(\frac{dn}{d\lambda}\right)^2\left(\frac{d\beta}{dn}\right)^2\frac{d^2P}{d\beta^2},\end{aligned} \tag{2.32}$$

here n is the index of refraction of the prism. For minimum deviation and Brewster angle incidence, Fork [28c] and co-workers have shown

$$\frac{d\beta}{dn} = -2, \text{ and } \frac{d^2\beta}{dn^2} = -4n + \frac{2}{n^3}. \tag{2.33}$$

Substitution of Eqs (2.30), (2.31) and (2.33) into Eq (2.32) yields [28d]

$$\frac{d^2P}{d\lambda^2} = 4l\sin\beta\left[\frac{d^2n}{d\lambda^2} + \left(2n - \frac{1}{n^3}\right)\left(\frac{dn}{d\lambda}\right)^2\right] - 8l\cos\beta\left(\frac{dn}{d\lambda}\right)^2. \tag{2.34}$$

The derivative of Eq (2.34) with respect to λ gives rise to

$$\begin{aligned}\frac{d^3P}{d\lambda^3} = {} & 4l\cos\beta\left[\frac{d^2n}{d\lambda} + \left(2n - \frac{1}{n^3}\right)\left(\frac{dn}{d\lambda}\right)^2\right]\frac{d\beta}{d\lambda} + 4l\sin\beta\frac{d^3n}{d\lambda^3} + \\ & 4l\sin\beta\left(2\frac{dn}{d\lambda} + \frac{3}{n^4} + \frac{dn}{d\lambda}\right)\left(\frac{dn}{d\lambda}\right)^2 + 8l\sin\beta\left(2n - \frac{1}{n^3}\right)\left(\frac{dn}{d\lambda}\right)\left(\frac{d^2n}{d\lambda^2}\right) + \\ & 8l\sin\beta\left(\frac{d\beta}{d\lambda}\right)\left(\frac{dn}{d\lambda}\right)^2 - 16l\cos\beta\left(\frac{dn}{d\lambda}\right)\left(\frac{d^2n}{d\lambda^2}\right).\end{aligned} \tag{2.35}$$

By substituting $\frac{d\beta}{d\lambda} = \frac{d\beta}{dn}\frac{dn}{d\lambda}$ and Eq (2.33) into Eq (2.35), one obtains

$$\begin{aligned}\frac{d^3P}{d\lambda^3} = {} & 4l\sin\beta\frac{d^3n}{d\lambda^3} - 24l\cos\beta\left(\frac{dn}{d\lambda}\right)\left(\frac{d^2n}{d\lambda^2}\right) + \\ & \left\{\left[-8l\cos\beta\left(2n - \frac{1}{n^3}\right) + 4l\sin\beta\left(2 + \frac{3}{n^4}\right) - 16l\sin\beta\right]\left(\frac{dn}{d\lambda}\right)^3 + \right. \\ & \left. 8l\sin\beta\left(2n - \frac{1}{n^3}\right)\left(\frac{dn}{d\lambda}\right)\left(\frac{d^2n}{d\lambda^2}\right)\right\}.\end{aligned} \tag{2.36}$$

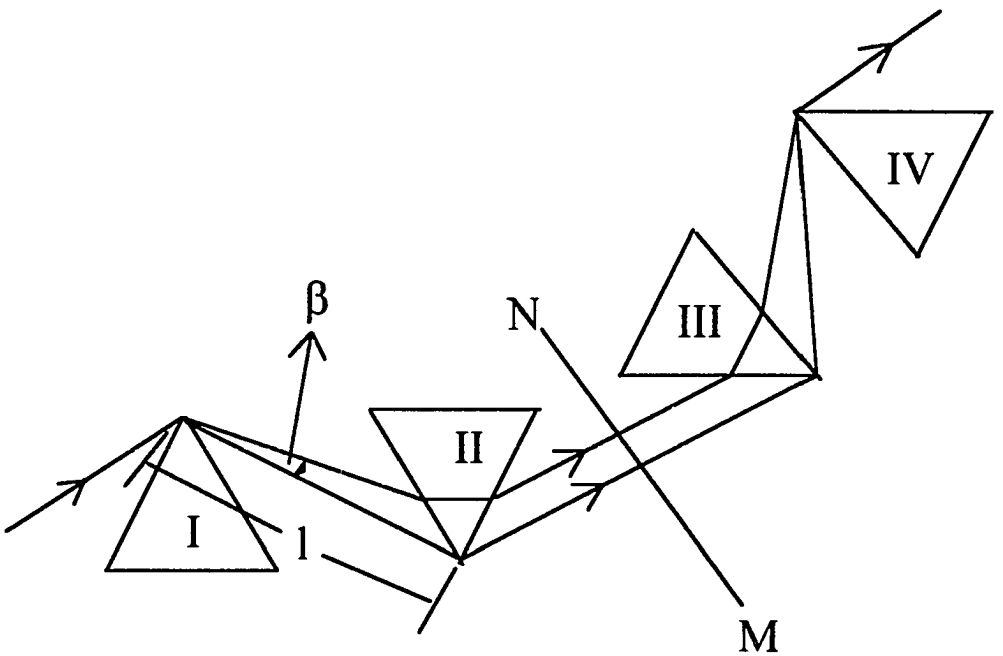

Figure 2.4. Two prism pairs having negative dispersion. The prisms are used at minimum deviation and oriented so that the rays enter and leave at Brewster's angle. The arrangement is symmetric about the plane NM.

It is important to recognize that it is the second derivative of the path length with respect to wavelength that determines the group velocity dispersion through following equation [28c]

$$\mathrm{GVD} = -\frac{\omega}{\lambda \mathrm{l}} \frac{\mathrm{d}^2\phi}{\mathrm{d}\omega^2}. \tag{2.37}$$

The variation in $\mathrm{d}^2\mathrm{P}/\mathrm{d}\lambda^2$ over the bandwidth of a pulse is relatively small for typical cases of interest; for example, 5% for a 60-fs pulse and quartz prisms [28c]. For significantly shorter pulses, these third derivative terms could become important.

CHAPTER III PHOTOIONIZATION OF INDOLE, 7-AZAINDOLE, AND THEIR DERIVATIVES

A. Introduction

7-Azaindole is the chromophoric moiety of the nonnatural amino acid, 7-azatryptophan, which we have proposed as an alternative to tryptophan as an optical probe of protein structure and dynamics [31-34] (Figure 3.1). One observation that renders 7-azatryptophan preferable to tryptophan as an optical probe is that its fluorescence lifetime over most of the pH range is single exponential when emission is collected over the entire band [32,35]. On the other hand, the fluorescence lifetime of tryptophan at neutral pH is nonexponential [36]. Characterization of the 7-azaindole chromophore as an optical probe requires an understanding of its nonradiative pathways of deactivation.

We have reported the monophotonic production of solvated electrons in 7-azaindole [35]. This observation is particularly intriguing because it indicates that its photophysics is more similar to those of indole, which also undergoes monophotonic ionization [37], than had previously been recognized. In fact, it is the ability of the indole moiety of tryptophan to undergo excited-state charge transfer to side-chain acceptors at various separation distances that has been suggested as the explanation for the nonexponential fluorescence decay in tryptophan [36]. A fundamental question, then, is if photoionization is also a significant nonradiative process in 7-azatryptophan, why is its fluorescence decay a single exponential of 780 ps [31,32]? In order to begin to address this question, in this article we discuss the monophotonic ionization of the 7-azaindole chromophore in detail, and we relate this ionization to the excited-state manifold of 7-azaindole.

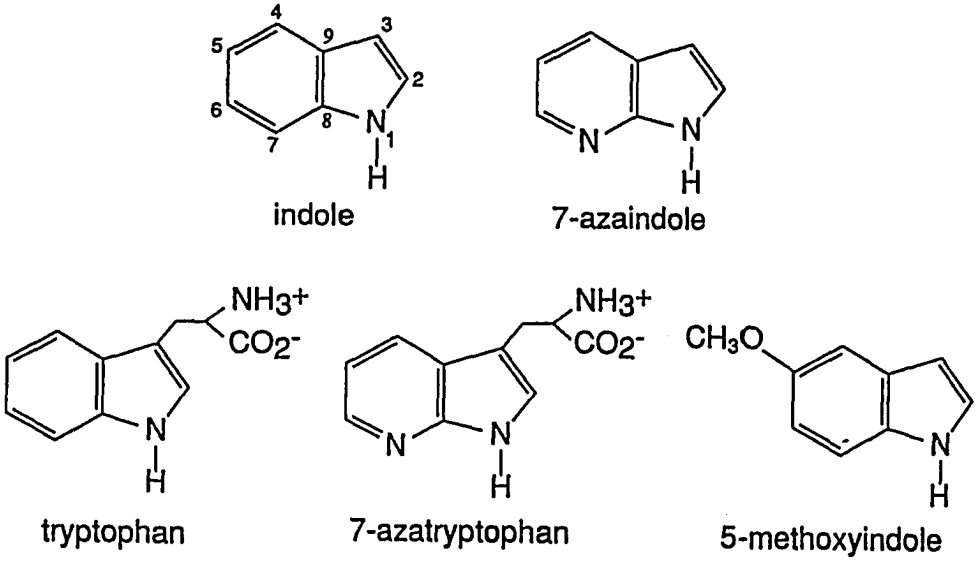

Figure 3.1. Structures of indole, 7-azaindole, zwitterionic tryptophan, zwitterionic 7-azatryptophan, 5-methoxyindole.

The arguments and conclusions that will be presented here depend on several diverse observations of the photophysics of indole and 7-azaindole. We summarize them here.

(1) Indole in water and methanol, 7-azaindole in water and methanol, 5-methoxyindole in water (methanol was not used as a solvent), and their analogs (investigated mostly in water) photoionize monophotonically and instantaneously to produce the solvated electron [35,37,38]. Unless otherwise indicated, the results reported here are obtained using water as the solvent. Because the fluorescent state of these analogs is always characterized by an average lifetime of at least hundreds of picoseconds, the solvated electron cannot originate from the lowest excited singlet.

(2) Fluorescence-excitation anisotropy spectra of 7-azaindole in propylene glycol glasses indicate, as for indole [33,39], the presence of closely-spaced ^1L_a and ^1L_b electronic states in 7-azaindole whose transition dipole moments are at large angles to each other [33].

(3) We demonstrate here that the fluorescence quantum yields, ϕ_F, of indole, 7-azaindole, and 5-methoxyindole, are all strongly dependent on excitation wavelength.

(4) The excitation-wavelength dependence of ϕ_F is used to assign the ^1L_b state to the photoionizable channel in these compounds.

(5) In zwitterionic tryptophan, the presence of the $-NH_3^+$ and $-CO_2^-$ sidechain groups brings considerable complexity to the indolyl photophysics. In particular, nonexponential fluorescence decay is observed [36]. These sidechains are not, however, a source of nonexponential fluorescence decay in zwitterionic 7-azatryptophan [31,32].

We argue that these data can be synthesized and comprehended by the following working hypotheses.

(a) The ^1L_b state is photoionizable and the ^1L_a state is not.

(b) The ^1L_a state is coupled to charge transfer states, which are the source of the nonexponential fluorescence decay in tryptophyl derivatives.

(c) Wave packet evolution away from the initial Franck-Condon region provides a means of rationalizing these data.

With this summary in mind, we shall now present and discuss our results in more detail.

B. Experimental

7-azaindole (7AI) (Sigma) was purified by flash chromatography [32,41] using ethyl acetate as a solvent. Indole, tryptophan (Trp), D,L-7-azatryptophan (7AT), 5-hydroxytryptophan (Sigma), 5-methoxyindole (5MeOI) (Aldrich), stilbene (Sigma), rhodamine B (Eastman Kodak Co.), p-terphenyl (Sigma), and quinine sulfate monohydrate (Aldrich) were used without further purification. N_1-methyl-7-azaindole (1M7AI) and 7-methyl-7H-pyrrolo[2,3-b]pyridine (7M7AI) were prepared as described elsewhere [32].

For steady-state anisotropy determinations, all compounds were dissolved in propylene glycol and experiments were performed as discussed previously [33]. Stilbene was used as a reference compound because it has been reported to have a limiting anisotropy of 0.4 [42].

Quantum yield determinations were performed as outlined by Teale and Weber [43] and by Chen [44]. Previous work [95] has demonstrated that Beer's Law is valid for indole at these concentrations. We assume the same holds true for the other species in this study. Quinine sulfate and p-terphenyl were used as standards. Verification of our experimental set-up and quantum yield calculations was performed using rhodamine B in ethylene glycol. We examined the wavelength regions, 530-570 nm, where excitation into the first excited-state singlet occurs for rhodamine B and the ultraviolet region, 240-320 nm, where the indoles absorb. Because the fluorescence quantum yield of quinine sulfate is excitation-wavelength dependent [96], all our analyses, therefore, are relative to the quantum yield of quinine sulfate

in 1.0 N H_2SO_4, which is 0.55 at λ_{ex} = 348 nm [44]. We observe the fluorescence quantum yield of rhodamine B to be 0.98 ± 0.05 at λ_{ex} = 555 nm. This quantum yield deviates less than 5% over the visible range of excitation wavelengths we employed (Figure 3.4d). The deviation in the quantum yield using ultraviolet excitation wavelengths (240-320 nm) was more significant (20%), but this may be due to the low absorbance of rhodamine B in this region as well as to impurities. Literature values for rhodamine B are 0.89 in ethylene glycol and 0.97 in ethanol [43]. If we do not include a correction for the refractive indices of the rhodamine B and quinine sulfate solutions (outlined below), we obtain a quantum yield of 0.88 at λ_{ex} = 555 nm for rhodamine B.

As an additional check of our procedures, we determined the fluorescence quantum yield of zwitterionic tryptophan by comparison to the quantum yield of another known standard, p-terphenyl (ϕ_F = 0.93 [97]). A range of values has been reported (0.06 - 0.20 [44-49]). Using an excitation wavelength of 280 nm, we obtain a fluorescence quantum yield of 0.18 ± 0.01 for zwitterionic tryptophan.

Indole, 7-azaindole, and 5-methoxyindole were dissolved in water. The quantum yield data listed in Table 3.1 of each compound were determined relative to quinine sulfate. Sample temperature was controlled with a M9000 Fisher refrigerated circulator connected to the cell holder and monitored directly at the sample by an HH-99A-T2 Omega thermocouple. Absorbance measurements were made using a Shimadzu UV-2101PC double-beam spectrophotometer. Steady-state fluorescence measurements were made using a Spex Fluoromax. All spectra were corrected for fluctuations in lamp intensity and detector response. A 0.6 - 4 nm band-pass was used for excitation and emission, depending on the quantum yield of each compound. For samples of high quantum yield, narrow slit widths are required to prevent signal saturation of the detector. We ensure that signal saturation does not occur for a given slit width by comparing the emission spectra of solutions having a range

of concentrations within Beer's Law. If the emission intensity decreases proportionally to the dilution factor and the spectral shape does not change, saturation does not occur.

The excitation-wavelength dependence of the fluorescence quantum yield of the indoles (Figures 3.4a-c) is a significant observation whose novelty required the investigation of many possible artifacts. Most significant is the possible reabsorption at the reddest excitation wavelengths when samples of high concentration are required. (Three solutions of various sample concentration ($0.05 \leq \text{O.D.}(\lambda_{ex}) \leq 0.15$) were prepared for each excitation wavelength examined in order to measure accurately the sample absorbance or to prepare a solution giving a large enough fluorescence signal.) This proved to be important in the rhodamine B analysis (since there is significant overlap between the absorption and emission spectra), but an almost negligible factor for the indoles. The true fluorescence quantum yield is given by (where $\tilde{\nu}$ is the energy in wavenumbers, $I^{obs}(\tilde{\nu})$ is the observed fluorescence spectrum, and A is the optical density):

$$\phi_F = \int_{-\infty}^{+\infty} I(\tilde{\nu})d\tilde{\nu} = \int_{-\infty}^{+\infty} I^{obs}(\tilde{\nu})10^{A(\tilde{\nu})}d\tilde{\nu}$$
$$\approx \int_{-\infty}^{+\infty} I^{obs}(\tilde{\nu})[1+2.303A(\tilde{\nu})]d\tilde{\nu}.$$

The correction was never more than 7%, and then only for rhodamine B at $\lambda_{ex} = 570$ nm.

Another correction was possible inner filter effects [98], which arise from not collecting all the fluorescence emitted from the sample. In our analyses, this inner filter effect does not occur since the fluorimeter sample cell holder blocks no portion of the cuvette face.

Corrections for the differences in the indices of refraction between two solvents were also considered. Such a correction affects the absolute quantum yield determined for each sample but does not change the excitation-wavelength dependent profile of an individual species. The quantum yields are corrected using the relationship [99]:

Table 3.1. Fluoresecnce Quantum Yields[a]

compound	λ_{abs}^{max}(nm)	ϕ_F^{max}[b]	ϕ_F (literature)[c]
indole	270	0.45 ± 0.05 (270 nm)	0.45 [43,50], 0.27 [51], 0.23 [48]
tryptophan	278	0.18 ± 0.01 (280 nm)[d]	0.13 [44], 0.12 [45], 0.2 [46], 0.14 [47,48], 0.06 [49]
7-azaindole	289	0.056 ± 0.007 (265 nm)	0.03 [50]
5-methoxyindole	270	0.43 ± 0.02 (260 nm)	0.22 [51]

[a] Data reported from our laboratory were obtained at 24.5 ± 0.5 °C. [b] The fluorescence quantum yield measurements were performed by varying the excitation wavelength in increments of 5 nm. The excitation wavelength that yields the maximum fluorescence quantum yield is therefore only approximate. [c] These quantum yield values were obtained over a range of 23 to 27 °C, or simply at "room temperature". We assume that most of these measurements were made at the absorbance maxima since excitation wavelengths are not given in the references. For purposes of comparison, we note that at the absorbance maxima of indole (270 nm) and of 7-azaindole (290 nm), we obtain fluorescence quantum yields of 0.45 ± 0.05 and 0.039 ± 0.002, respectively. [d] The wavelength dependence of the fluorescence quantum yield of zwitterionic tryptophan was not investigated for this work. The value we report here was determined at 280 nm.

$\phi_F = \phi^{uncorr}\left[n(s)^2/n(r)^2\right]$, where n(s) and n(r) are the refractive indices at the emission wavelengths of interest of the sample solvent and reference solvent, respectively. In our experiments, the correction was 11% for rhodamine B in ethylene glycol compared to quinine sulfate in water. Since the refractive index of water changes less than 2% from 300 to 589 nm (1.358-1.329) [100], and since the emission spectra of the indoles do not change with excitation wavelength, no correction for the index of refraction was required in comparing the fluorescence quantum yield at one excitation wavelength with respect to another.

We investigated the possibility that the variations in the plots of ϕ_F vs. λ_{ex} resulted from absorption by excited-state transients such as solvated electrons or triplets. For example, the extinction coefficient for a solvated electron (ε_{e^-}) is about 1000 M^{-1} cm^{-1} at 400 nm (and decreases towards higher energies) [58]. If we take the extreme case and assume that all of the ground-state population is projected into the excited state and if we take the quantum yield of photoionization as 0.2, then the maximum correction for absorption by electrons is less than 1%. Under normal conditions of excitation, the absorption by solvated electrons is insignificant. Similarly, the contribution due to absorption by triplets should be even smaller.

The fluorescence excitation spectra of indole, 7-azaindole, and 5-methoxyindole in water all differ from their respective absorption spectra. The differences are largest in 5-methoxyindole. In indole and 7-azaindole, the differences are small but reproducible. It is important to recognize that the magnitude of the difference between a fluorescence excitation spectrum and an absorption spectrum can be greatly underestimated because in order to compare the two they must be normalized. (A change between the two spectra will also be underestimated--or annulled--by normalization if it occurs in a region where the spectra change rapidly with wavelength, as occurs on the red edges of the indole spectra.) This

normalization usually takes the form of setting the value of the optical density and the fluorescence intensity to be arbitrarily equal at a given wavelength.

As a final indication of self consistency, we note that curves similar to the ones displayed in Figure (3.4a-c) can be constructed directly from the excitation spectra. If the emission spectral shape does not change with respect to excitation wavelength (we do not observe such a change), then the integrated area of the emission (the fluorescence quantum yield) is proportional to the emission intensity. When the fluorescence intensity at a given emission wavelength is monitored in order to obtain an excitation spectrum, the quantum yield over the range of excitation wavelengths is essentially what is observed if for each fluorescence intensity measured an accurate correction is made for the sample absorbance. Such a correction is similar to that used to obtain standard quantum yields, except that no factor to account for the fluorimeter lamp intensity is included since this has already been accounted for when obtaining the excitation spectrum itself. Of course, if the absorption and excitation spectra are exactly superimposable, this procedure yields a plot of the quantum yield that is independent of the excitation wavelength.

Fluorescence lifetime measurements were performed with the time-correlated single-photon counting apparatus described elsewhere [32]. In the course of this article, we make a distinction between anisotropies obtained from two types of experiments: r_0 is the anisotropy obtained from steady-state, low temperature measurements; r(0) is the limiting anisotropy obtained from time-dependent measurements in the liquid phase [33].

Pump-probe transient absorption measurements were performed with a system based on an Antares 76s cw-modelocked Nd:YAG synchronously pumping a Coherent 701-2 dye laser with 1 W of 532 nm radiation (Figure 2.1). The output of the dye laser was amplified to 1-2 mJ at 30 Hz with a Continuum regenerative amplifier that is seeded with residual 1064 nm radiation from the Antares. Half of the amplified dye-laser pulse train is focused into a cell

containing water to form a white light continuum that is used as a probe beam. The remainder of the pulse train is focused into a crystal of KDP to obtain the appropriate ultraviolet wavelength for excitation.

The pulsewidth of the amplified pulse train is determined by measuring the apparent rise time of the induced transmission or absorption of a standard (Figure 2.1). In the pump-probe experiments discussed here, the typical full scale is 800 ps. It is thus crucial that the translation stage (optical delay line) is adequately aligned so as to avoid drift in the overlap of the pump and probe beams during the course of the experiment. Our system was thus regularly aligned by reproducing the "flat" transient absorbance of the solvated electron produced from zwitterionic tryptophan or 7-azatryptophan (Figure 3.2). Geminate recombination of the electron does not occur on this time scale [38].

The quantum yield of photoionization was determined at various excitation wavelengths using the relation

$$\Delta A_{e^-} = \varepsilon_{e^-} l c_{e^-} = e_{e^-} l \phi_{e^-} I_{abs} \rho = \rho \varepsilon_{e^-} l \phi_{e^-} I_0 \left(1 - 10^{-A_{e^-}}\right) \tag{3.1}$$

where ε_{e^-} is the extinction coefficient of the solvated electron at the probe wavelength, l is the sample pathlength, c_{e^-} is the concentration of the solvated electron, ρ is a constant that is proportional to the overlap between pump and probe pulses, ϕ_{e^-} is the quantum yield of the solvated electron, and A_{e^-} is the optical density of the sample at the pump wavelength.

A similar expression can be obtained for the change in optical density for a reference molecule, such as nile blue (Figure 2.1):

$$|\Delta A_N| = \rho \varepsilon_N l I_0 \left(1 - 10^{-A_N}\right) \tag{3.2}$$

The absolute value sign is used because nile blue provides a transient bleaching instead of absorption. We are only concerned here in normalizing the optical density changes. It follows that

$$\phi_{e^-} = \frac{\Delta A_{e^-}\left(1-10^{-A_N}\right)\varepsilon_N}{\Delta A_N(1-10^{-A_{e^-}})\varepsilon_{e^-}} \tag{3.3}$$

C. Results

1. Monophotonic Ionization

The flash photolysis studies of indole and tryptophan by Bent and Hayon [37] are a natural point of comparison for our work on 7-azaindole. Bent and Hayon observed that for tryptophan a logarithmic plot of the absorbance of the solvated electron against the photolyzing pump intensity gave a straight line of slope 1.25 at pH 7.5. This result is consistent with monophotonic ionization [52]. Nevertheless, the electron appeared within their pulsewidth of 3.6 ns, leading them to suggest that an electronic state higher than S_1 or that a hot vibrational state of S_1 was the ionizing species. For tryptophan they observed that the zwitterion produced the solvated electron within the duration of their pump pulse; but that at pH 10.3, where the amino group is deprotonated and only the anion is present, about 10% of the solvated electron appears with a rise time equal to the ~ 8-ns decay time of the fluorescent species.

Figure 3.2 presents our results for tryptophan on a time scale of 800 ps using 1-ps pump and probe pulses. For zwitterionic tryptophan, the solvated electron appears within the duration of the pump pulse. On the other hand, at pH 12.3 where we measure the

fluorescence lifetime of anionic tryptophan to be 3.17 ns, a small amount of the solvated electron appears with a similar rise time, just as in the earlier experiment of Bent and Hayon.

That the transient absorption in Figure 3.2 is due to a solvated electron is demonstrated by the transient quenching in the presence of the electron scavenger, KNO_3 [53]. For 7-azaindole, the dependence of the logarithm of the absorption of the solvated electron at "zero time" upon the logarithm of the pump intensity is presented in Figure 3.3. The slope is 1.2 ± 0.3 indicating a monophotonic ionization.

Table 3.2 indicates that the quantum yield of the solvated electron is excitation-wavelength dependent for tryptophan. For 7-azaindole and 5-methoxyindole, because the electron yield is less than that in tryptophan and because of experimental error, the excitation-wavelength dependence is obscured. The data for tryptophan indicate that the electron yield is higher towards the red edge of the absorption spectrum and are thus consistent with the diminished fluorescence quantum yield at those wavelengths (Figure 3.4). The yields for the solvated electron production for a variety of compounds, relative to that for tryptophan, are listed in Table 3.3.

The motivation for measuring ionization yields for 7-azaindole in methanol was to determine whether the solvated electron originates from the normal or the tautomer form of 7-azaindole. If it originates from the tautomer form, the rise time for the solvated electron would be expected to be equal to the formation time for the tautomer, 140 ps. Such a rise time for the solvated electron is not observed.

2. Excited States

Low-temperature, steady-state fluorescence excitation anisotropy studies of 7-azaindole in propylene glycol indicate that, like indole [39], its absorption spectrum is composed of two overlapping electronic transitions whose transition dipole moments are at be

Figure 3.2. Transient absorption arising from the solvated electron at 23°C. (a) Zwitterionic tryptophan, pH 6.8; λ_{ex} = 304 nm, λ_{probe} = 650 nm. The decaying signal is obtained in the presence of 0.25 M KNO_3. The upper trace is flat on the time scale of the measurement. The maximum absorption change in the absence of scavenger is 0.16; in the presence of 0.25 M KNO_3, it is 0.05. The two traces are normalized to have the same maximum absorption change. Similar behavior is observed for 7AI, 1M7AI, and 7M7AI. (b) Tryptophan, pH 12.3; λ_{ex} = 294 nm, λ_{probe} = 580 nm. The data are fit to 10% of a rising component of duration 3.2 ns. Identical results are obtained with λ_{ex} = 304 nm. This rise time is identical to the value of the single-exponential decay time we obtain for tryptophan at pH 12.3 by means of time-correlated single-photon counting. (c) Zwitterionic 7-azatryptophan, pH 6.8, and anionic 7-azatryptophan, pH 12.3; λ_{ex} = 294 nm, λ_{probe} = 580 nm. Identical results are obtained using an excitation wavelength of 304 nm.

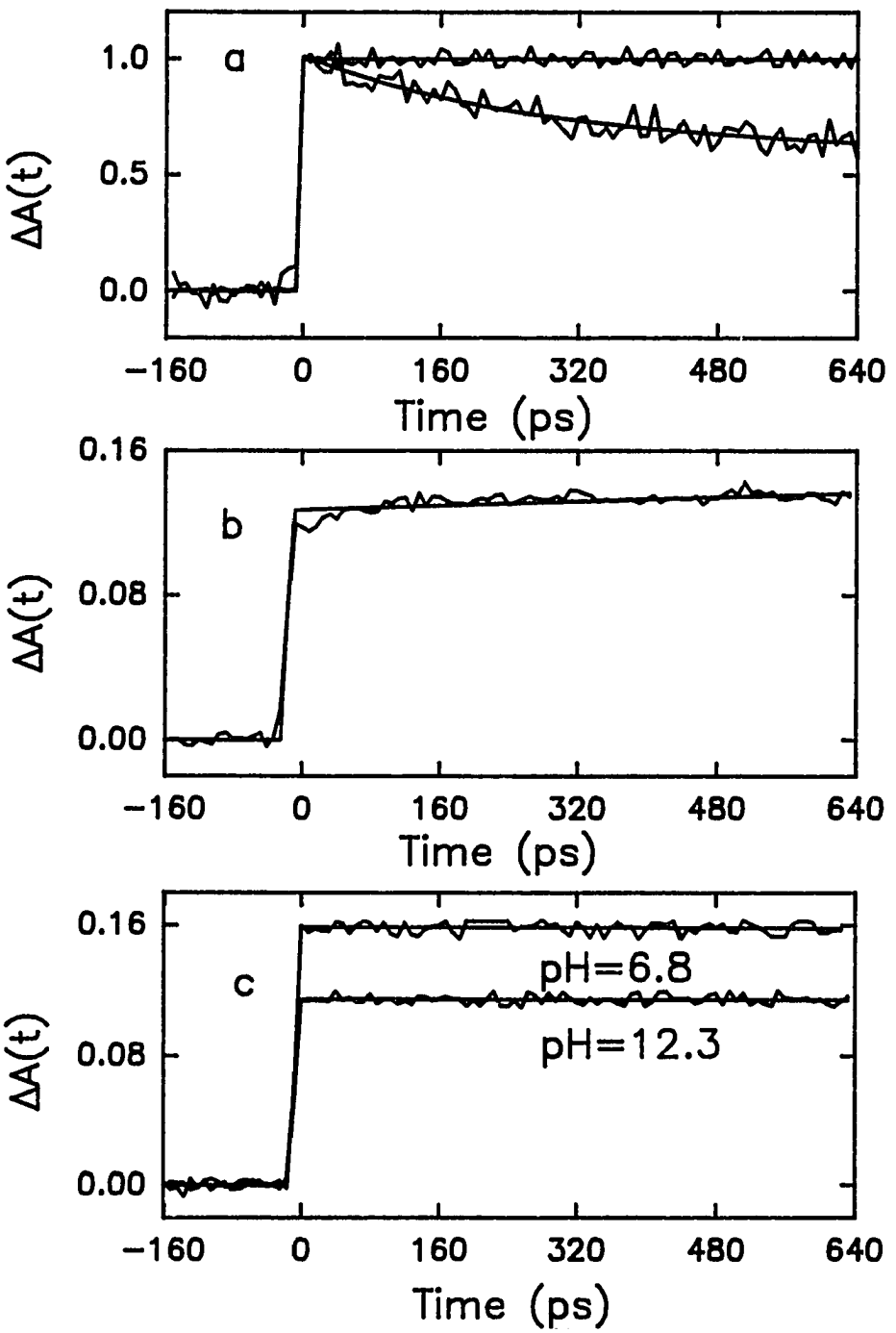
a
1.0
0.5
0.0
ΔA(t)
−160
0
160
320
480
640
Time (ps)
b
0.16
0.08
0.00
ΔA(t)
−160
0
160
320
480
640
Time (ps)
c
pH=6.8
pH=12.3
0.16
0.08
0.00
ΔA(t)
−160
0
160
320
480
640
Time (ps)

Table 3.2 Solvated Electron Yield[a] (ϕ_{e^-}) vs. Excitation Wavelength (λ_{ex})

	Excitation Wavelength			
Compound	294 nm	301 nm	303 nm	305 nm
Trp (pH 6.5)	0.14 ± 0.05	0.43 ± 0.05	0.35 ± 0.03	0.31 ± 0.08
7AI (pH 6.9)	0.08 ± 0.03	0.16 ± 0.04	0.14 ± 0.03	0.15 ± 0.04
5MeOI (pH 7.3)	0.23 ± 0.04			0.27 ± 0.02

[a] The probe wavelength for all measurements is 665 nm. At this wavelength the extinction coefficient for the reference compound, nile blue in ethanol, is approximately equal to that of the solvated electron: 1.8×10^4 M^{-1} cm^{-1}. All measurements were performed at 23° C. The absence of a value indicates that the measurement was not performed.

Table 3.3 Quantum Yield of Solvated Electron[a]

compound	ϕ_{e^-}
tryptophan, pH 6.8	1.00[b]
indole, pH 6.4	0.86
7AI (N_7, N_1H), pH 6.3	0.38
7AI (N_7H^+, N_1H), pH 2.1	0.16
7AT (N_7, N_1H), pH 6.7	0.28
7AT (N_7H^+, N_1H), pH 2.1	0.12
7M7AI (N_1), pH 12.3	0.30
7M7AI (N_1), pH 8.8	0.16
7M7AI (N_1H^+), pH 3.3	0.14
1M7AI (N_7), pH 6.8	0.32
7AI/methanol	0.17

[a] All yields are reported relative to that of zwitterionic tryptophan at 23 °C. λ_{ex} = 304 nm, λ_{probe} = 650 nm. In all cases, the solvated electron appears within our ~ 1-ps pulse width. The reported values reflect an uncertainty of ~ 15%. See experimental section for abbreviations. [b] Using an excitation wavelength of 265 nm, Bent and Hayon [37] obtain an absolute quantum yield of 0.08 for the production of photoelectrons from zwitterionic tryptophan (pH 6.0) at 25 °C.

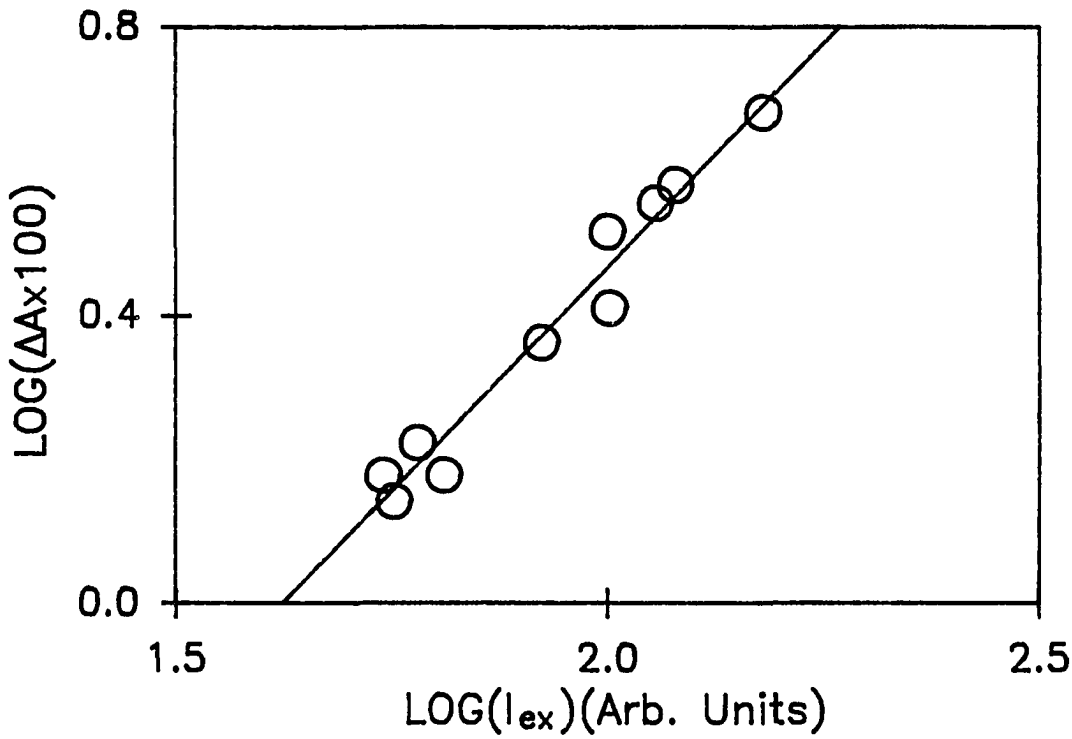

Figure 3.3. Plot of the logarithm of ΔA_{max} against the logarithm of the pump intensity for 7-azaindole. The plot yields a straight line with a slope of 1.2 ± 0.3, indicating a monophotonic ionization [42].

large angles to each other. The fluorescence excitation anisotropy spectrum and the decomposed fluorescence excitation spectra of 7-azaindole are displayed in Figure 3.5. The measurements of Bulska et al. [77] suggested the presence of ^1L_a and ^1L_b bands in 7-azaindole.

Valeur and Weber [39] resolved the fluorescence excitaion spectrum of indole into overlapping ^1L_a and ^1L_b bands at -58°C in propylene glycol and reported the ^1L_b transition to be quite structured with maxima at 282.5 and 289.5 nm. The ^1L_a transition is broader and absorbs farther to the red than does the ^1L_b transition. At wavelengths longer than 295 nm, only absorption resulting from the ^1L_a transition is observed. The excitation anisotropy of 7-azaindole is qualitatively similar to that of indole, but it possesses less pronounced structure. Anisotropy minima at 293.5 and 300.5 nm and a relative maximum at 297.0 nm give rise to the structure in the resolved excitation spectra.

Neither 7-azaindole, nor indole, nor 5-methoxyindole yield a limiting steady-state anisotropy, r_o of 0.4 at any excitation wavelength. The control experiment, stilbene, produced $r_o = 0.4$ at $\lambda_{ex} \geq 336$ nm. Our results for stilbene are qualitatively similar to those of Bobrovich et al. [54], who measured the excitation polarization spectrum of stilbene in butanol at 77 K.

The excitation-wavelength dependence of the photoionization process indicates that conventional methods of decomposing fluorescence excitation spectra of indole-like molecules into ^1L_a and ^1L_b absorption spectra based on measurements of polarized emission are inappropriate [39,40]: a fluorescence excitation spectrum can only be considered to represent the absorption spectrum if ϕ_F is independent of the excitation wavelength [33].

3. Excitation Wavelength Dependence of the Fluorescence Quantum Yield

If the instantaneous appearance of the electron has its origin in the upper of the two electronic states illustrated in Figure 3.5b, then the fluorescence quantum yield of 7-azaindole

Figure 3.4. Fluorescence quantum yield, ϕ_F, versus excitation wavelength, λ_{ex}, at neutral pH, for (a) indole, (b) 7-azaindole, (c) 5-methoxyindole, and (d) rhodamine B (in ethylene glycol).

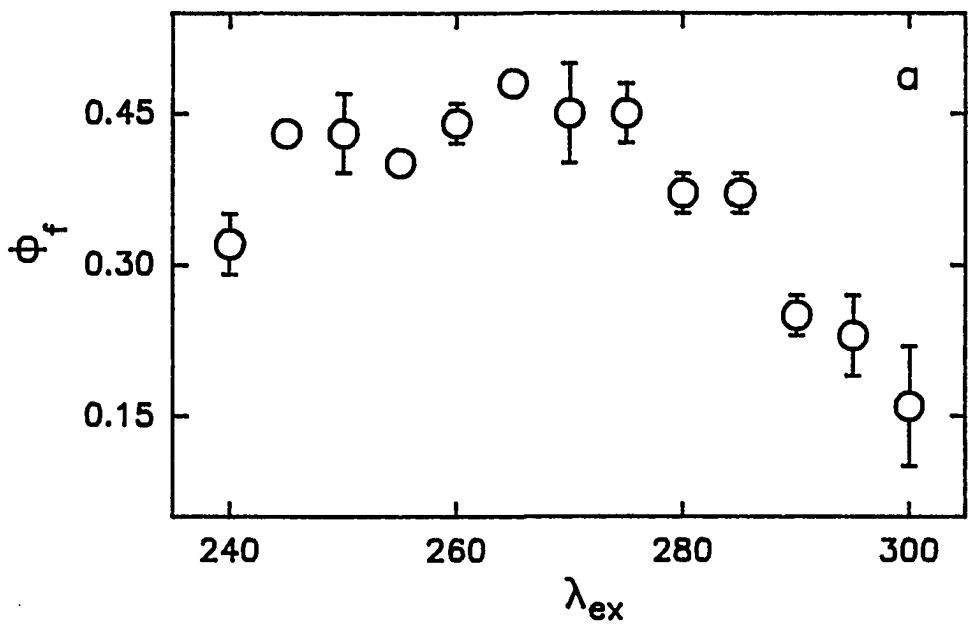
a
0.45
0.30
0.15
Φ_f
240
260
280
300
λ_{ex}

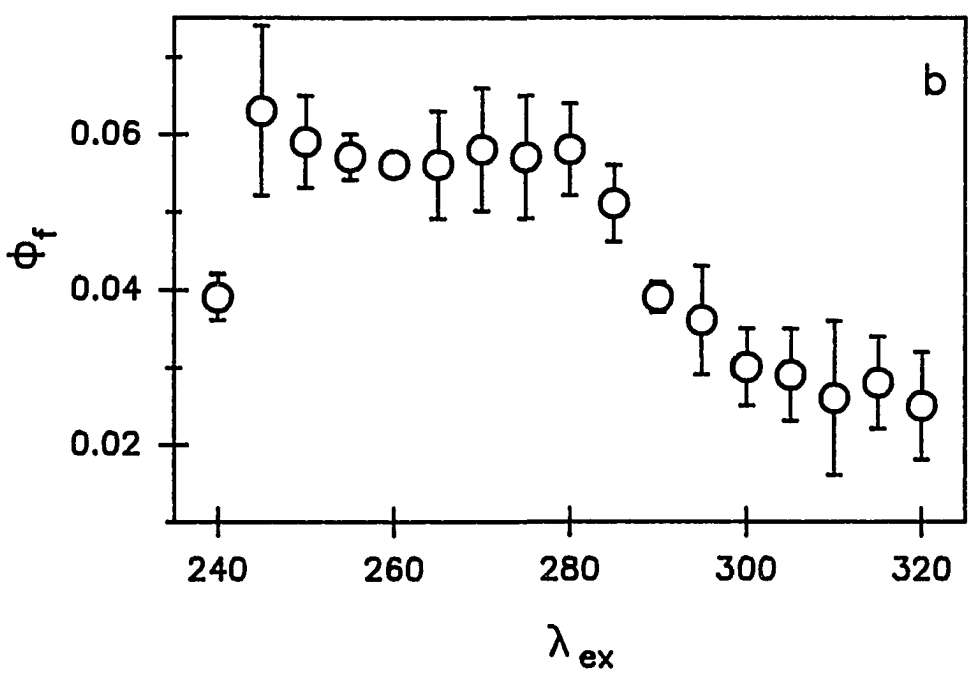
b
0.06
0.04
0.02
Φ_f
240
260
280
300
320
λ_{ex}

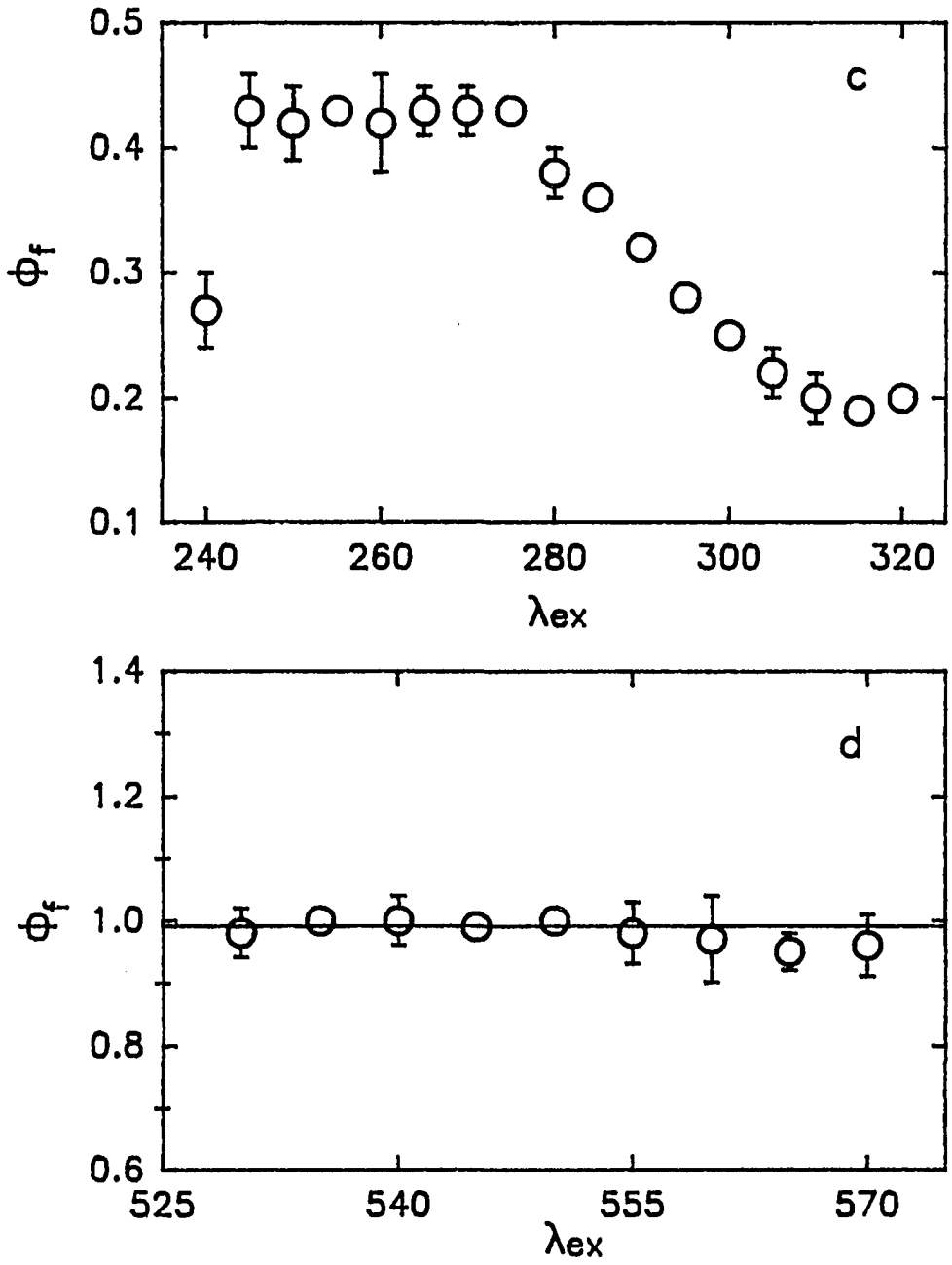

Figure 3.4. Continued

Figure 3.5. (a) The excitation anisotropy of 7-azaindole (7AI) (λ_{em} = 372 nm). (b) The corrected excitation spectrum of 7AI resolved into contributions from the ^1L_a and ^1L_b bands. $r_{oa} = 0.25$ and $r_{ob} = -0.13$. See reference 33 for a discussion of this analysis.

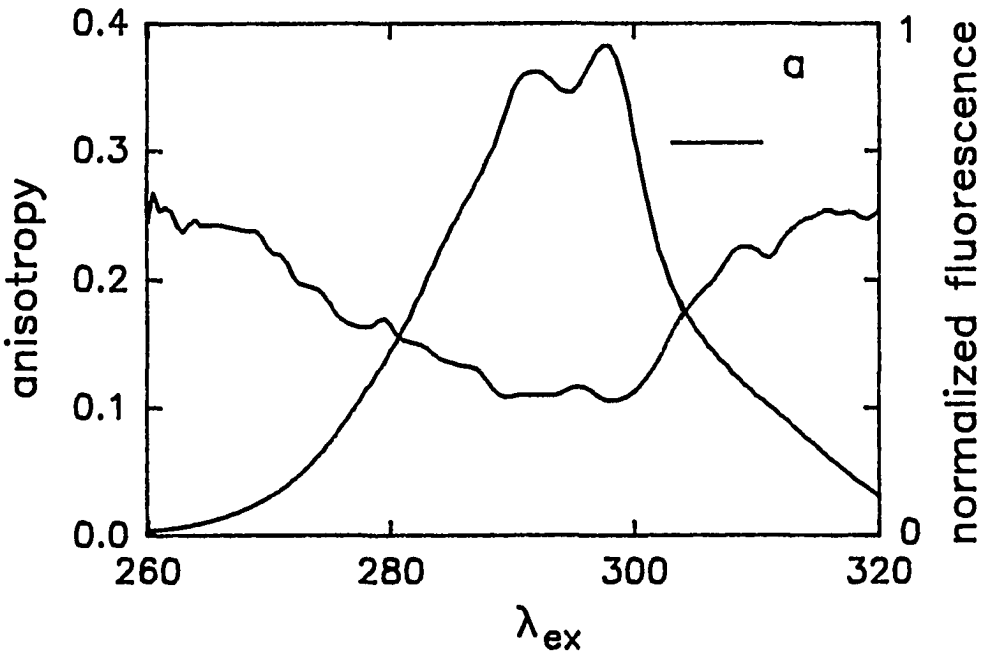
0.4
0.3
0.2
0.1
0.0
anisotropy
1
0
normalized fluorescence
a
260
280
300
320
λex

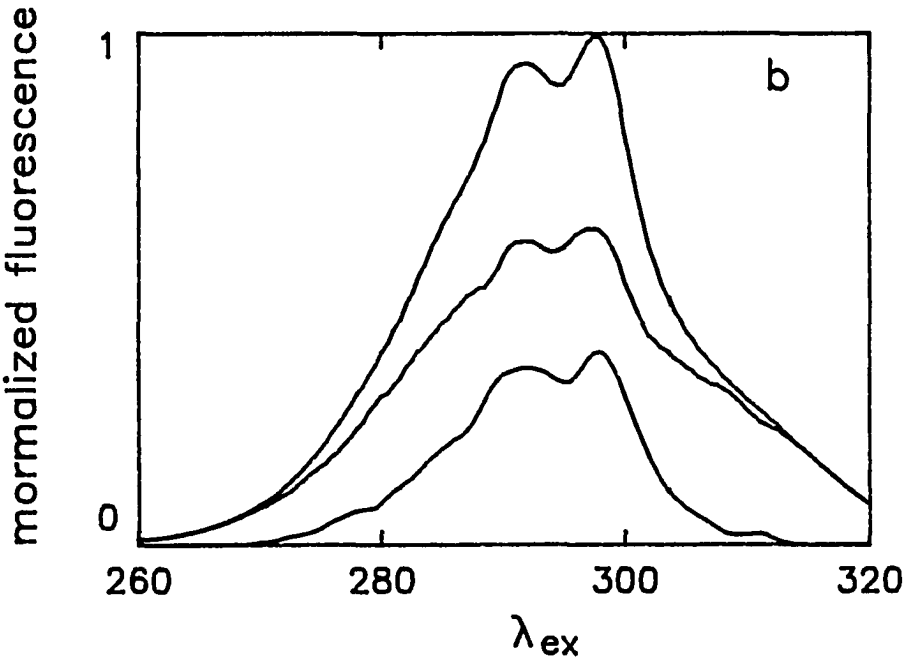
1
0
normalized fluorescence
b
260
280
300
320
λex

is expected to be excitation-wavelength dependent. The data presented in Figure 3.4 indicate that this is the case for 7-azaindole, indole, and 5-methoxyindole. The control experiment was performed for rhodamine B in ethylene glycol, for which no excitation-wavelength dependence on the fluorescence quantum yield was observed. The observation of an excitation-wavelength dependent fluorescence quantum yield is of significance because it is consistent with the excitation-wavelength dependence of the electron yield. These two observations argue cogently, along with the log-log plot (Figure 3.3), for the monophotonic ionization of 7-azaindole, indole, 5-methoxyindole, and their derivatives. The photoionization of indoles has been studied extensively [5,7,8,25,59,60,61]. The measurements of Steen [91] and Pigault et al. [90] suggest an excitation-wavelength dependence of the electron yield, but their data are not precise enough to demonstrate that this dependence exists at wavelengths greater than 250 nm.

D. Discussion

1. Temperature and Excitation-Wavelength Dependence of the ϕ_F

The low-temperature fluorescence anisotropy data indicate the presence of closely-spaced excited states in indole, 7-azaindole, and their derivatives. The instantaneous appearance of the solvated electron indicates that at least one of the excited states is dissociative. The fluorescence quantum yields of the compounds investigated here are very low at the red edge of the absorption spectrum, attain a maximum near--but usually not at--the absorption maximum, and subsequently decrease towards the blue edge of the absorption spectrum. This is in contrast to the fluorescence lifetime, which we observe to be constant over the range of wavelengths accessible to our laser system (285 to 310 nm). For example, our results for 7-azaindole indicate that the electron is generated monophotonically and

instantaneously. A time scale of ≤ 130 fs [38,86] is required for the electron to become "solvated." The excitation-wavelength dependent fluorescence quantum yield, $\phi_F(\lambda)$, is correspondingly diminished by the instantaneous production of electrons. This is especially clear in the case of indole and tryptophan (Figure 3.4 and Table 3.2). The wavelength dependence of ϕ_F and ϕ_{e^-} led us to investigate the role of both temperature and excitation wavelength on ϕ_F and ϕ_{e^-}. These measurements were performed to address the following questions. Assuming that the variation in ϕ_F arises only from changes in the yield of solvated electrons, by performing measurements of the fluorescence quantum yield as a function of both excitation wavelength and of temperature, can we obtain any information concerning the barrier--if there is one--to photoionization? Alternatively, can we obtain any information concerning the interaction of bound and dissociative excited-state surfaces?

Our experiments were based on the suggestions in the literature that photoionization is a thermally activated process [37,55,56]. It is possible (as opposed to the case illustrated in Figure 3.10a) that one dissociative surface intersects the bound state near its minimum (no barrier); and the other, at a higher energy (large barrier). Alternatively, because the Franck-Condon factors for predissociation are favorable only for the vibrational levels of the bound state that coincide with the crossing of the dissociative state, the rate of photoionization increases at both low and high excitation energies (Figure 3.10a). The former scheme predicts that excitation to vibrational levels lying between the two crossing points will yield solvated electrons with different activation energies depending on the energy separation between the initially excited vibrational level and the upper crossing point.

The data compiled in Table 3.4 indicate, however, that the Arrhenius parameters are essentially independent of excitation wavelength--although some fluctuations are observed for indole. The treatment of these temperature and excitation-wavelength dependent data is as follows. Because the solvated electron is produced on a time scale that is instantaneous

compared to steady-state or conventional time-correlated single-photon counting experiments, the apparent fluorescence quantum yield obtained in either of these two latter experiments must be corrected by the electron yield at "zero time"; thus,

$$\phi_F^{-1}(\lambda) = \int_0^\infty \left(1.0 - \phi_{e^-}(\lambda)\right) F(t)dt \qquad (3.4)$$

For a two-level system characterized by emitting ^1L_b and ^1L_a states [71,72], the fluorescence decay is given by $F(t) = \alpha_1 \exp(-t/\tau_1) + \alpha_2 \exp(-t/\tau_2)$. If $\tau_2 >> \tau_1$, then the fluorescence quantum yield is determined only by the long-lived component, and $\phi_F = \left[1.0 - \phi_{e^-}(\lambda)\right] k_R \tau_2$, where k_R is the radiative rate of the fluorescent species. Our measurements in water indicate that the radiative rate, k_R, is 1.05×10^8 s^{-1} for indole; 3.3×10^7 s^{-1}, for 7-azaindole; and 1.07×10^8 s^{-1}, for 5-methoxyindole. We define $y_0 = 1.0 - \phi_{e^-}(\lambda)$ and $\tau_2 = (k_R + k_0 + k(T))^{-1}$, where for simplicity we have assumed that there is only one temperature-dependent nonradiative process, k(T), and only one temperature-independent nonradiative process, k_0, such as intersystem crossing [35,56,88]. We have set k_0 equal to the rate for intersystem crossing, 3.3×10^7 s^{-1}. If $k(T) = A\exp(-E_a/RT)$,

$$\phi_F^{-1}(\lambda) = A_0 + A_1 \exp(-E_a/RT) \qquad (3.5)$$

where

$$A_0 = \frac{1}{y_0} + \frac{k_0}{y_0 k_R} \text{ and } A_1 = \frac{A}{y_0 k_R}$$

Plotting the experimental data as $\phi_F^{-1}(\lambda)$ vs. 1/T yields an exponential plus a background from which we may obtain A_0, A_1 and E_a (Figure 3.6a, Table 3.4). A similar

analysis has been performed by Kirby and Steiner [57]. Knowledge of k_R and k_0 permits the determination of y_0 and, consequently, ϕ_e.. Similarly, the activation parameters obtained from the fit permit the determination of the fluorescence lifetime, $\tau_F = \tau_2$, at any temperature

$$\tau_F = \left[k_R + k_0 + A\exp(-E_a/RT)\right]^{-1} \tag{3.6}$$

The self-consistency of this approach is demonstrated by the comparison of the measured fluorescence lifetimes (Figure 3.6b) and the fluorescence lifetimes obtained from the temperature-dependent quantum yield data (see below).

It is significant that one exponential is sufficient to describe the temperature dependence of the steady-state data in water (Table 3.4, Figure 3.6). We find that the Arrhenius parameters obtained from the temperature dependence of the fluorescence lifetimes in water are nearly identical to those obtained from the fluorescence quantum yields: indole (λ_{ex} = 288 nm), E_a = 9.3 kcal/mol, A = 1.2 × 10^{15} s^{-1}; 7-azaindole (λ_{ex} = 285 nm), E_a = 2.4 kcal/mol, A = 7.3 × 10^{10} s^{-1}; 5-methoxyindole (λ_{ex} = 288 nm), E_a = 7.8 kcal/mol, A = 6.1 × 10^{13} s^{-1}.

Because the fluorescence detected in our experiments is collected after the photoionization event, and because the steady-state and the time-resolved measurements yield identical activation energies, we conclude that the majority of photoelectrons are produced by means of a temperature-independent pathway and that the observed activation energies reveal the presence of another nonradiative process that is thermally activated. The photoelectrons are most likely produced by a temperature independent pathway, such as tunneling. It is possible, however, that thermal activation of the "fluorescent" state produces solvated electrons with the reported activation parameters. The yield of solvated electrons from the

Table 3.4 Dependence of Arrhenius Parameters on Excitation Wavelength

Indole

λ_{ex} (nm)	ϕ_F[a]	ϕ_{ϵ^-}[b]	E_a (kcal/mol)[b]	A (s^{-1})[b,c]
240	0.32 ± 0.03	0.18	12.8	3.2×10^{17}
255	0.40 ± 0.01	0.20	13.8	1.1×10^{18}
260	0.44 ± 0.02	0.14	14.8	5.2×10^{18}
270	0.45 ± 0.05	0.03	13.7	1.2×10^{18}
280	0.37 ± 0.02	0.20	12.6	2.0×10^{17}
285	0.37 ± 0.02	0.08	12.4	2.0×10^{17}
290	0.25 ± 0.02	0.23	9.5	2.4×10^{15}
295	0.23 ± 0.04	0.30	7.1	7.7×10^{13}
300	0.16 ± 0.06	0.81	10.0	2.5×10^{17}

7-azaindole

λ_{ex} (nm)	ϕ_F[a]	ϕ_{ϵ^-}[b]	E_a (kcal/mol)[b]	A (s^{-1})[b]
250	0.059 ± 0.006	0.13	2.2	3.3×10^{10}
260	0.056 ± 0.001	0.11	2.6	4.8×10^{10}
270	0.058 ± 0.008	0.21	2.8	5.5×10^{10}
280	0.058 ± 0.006	0.07	2.8	6.7×10^{10}
290	0.039 ± 0.002	0.05	2.7	7.6×10^{10}
300	0.030 ± 0.005	0.24	2.4	5.3×10^{10}
310	0.026 ± 0.010	0.07	2.1	4.6×10^{10}
320	0.025 ± 0.007	0.25	1.4	1.7×10^{10}

Table 3.4 Continued

5-methoxyindole

λ_{ex} (nm)	ϕ_F[a]	ϕ_{e^-}[b]	E_a (kcal/mol)[b]	A (s^{-1})[b,c]
240	0.27 ± 0.03	0.57	9.0	4.0×10^{14}
270	0.43 ± 0.02	0.17	9.9	1.2×10^{15}
300	0.25 ± 0.01	0.58	9.6	7.6×10^{14}
310	0.20 ± 0.02	0.74	9.8	5.1×10^{14}

[a] Fluorescence quantum yields are determined experimentally at 25 °C as described in the Experimental section. [b] The quantum yield of photoionization, ϕ_{e^-}, and the Arrhenius activation energies and prefactors, E_a and A, are obtained from the temperature dependence of the fluorescence quantum yield at the indicated excitation wavelength, as described in the text. For simplicity, it is assumed that nonradiative processes such as intersystem crossing and internal conversion are independent of temperature and excitation wavelength. [c] The data for indole reveal an enormous variation in the value of the Arrhenius prefactor, A--a factor of 10^5. We are uncertain whether these results are an anomaly of the fitting procedure or whether real physical significance should be attributed to them. Arrhenius prefactors greater than 10^{13} s^{-1} are inconsistent with the nonradiative process in question being controlled by nuclear motions. Kirby and Steiner [57] have performed similar experiments for indole and obtain a prefactor of 2.5×10^{16} s^{-1}. They do not, however, indicate their excitation wavelength. An unusually large prefactor may be a result of not fitting the data over a wide enough range of temperatures, or it may reveal an inappropriate form for the temperature dependence of the rate. Frauenfelder and coworkers have commented on large prefactors for the rates of ligand binding to myoglobin [92].

Figure 3.6. (a) Plots of $\phi_{F^{-1}}$ vs. T^{-1} for indole, 7-azaindole, and 5-methoxyindole at neutral pH. The plots are presented for only one excitation wavelength for each molecule: indole, λ_{ex} = 285 nm; 7-azaindole, λ_{ex} = 290 nm; 5-methoxyindole, λ_{ex} = 285 nm. In general, within experimental error (Table 3.4) identical Arrhenius parameters are obtained for a given molecule at all excitation wavelengths. The only difference in the data is that the plots are displaced along the ordinate owing to the excitation-wavelength dependence of the fluorescence quantum yield. (b) Plots for indole, 7-azaindole, and 5-methoxyindole at neutral pH obtained from the inverse of the fluorescence lifetimes (less the temperature-independent rates) using an excitation wavelength of 285 nm.

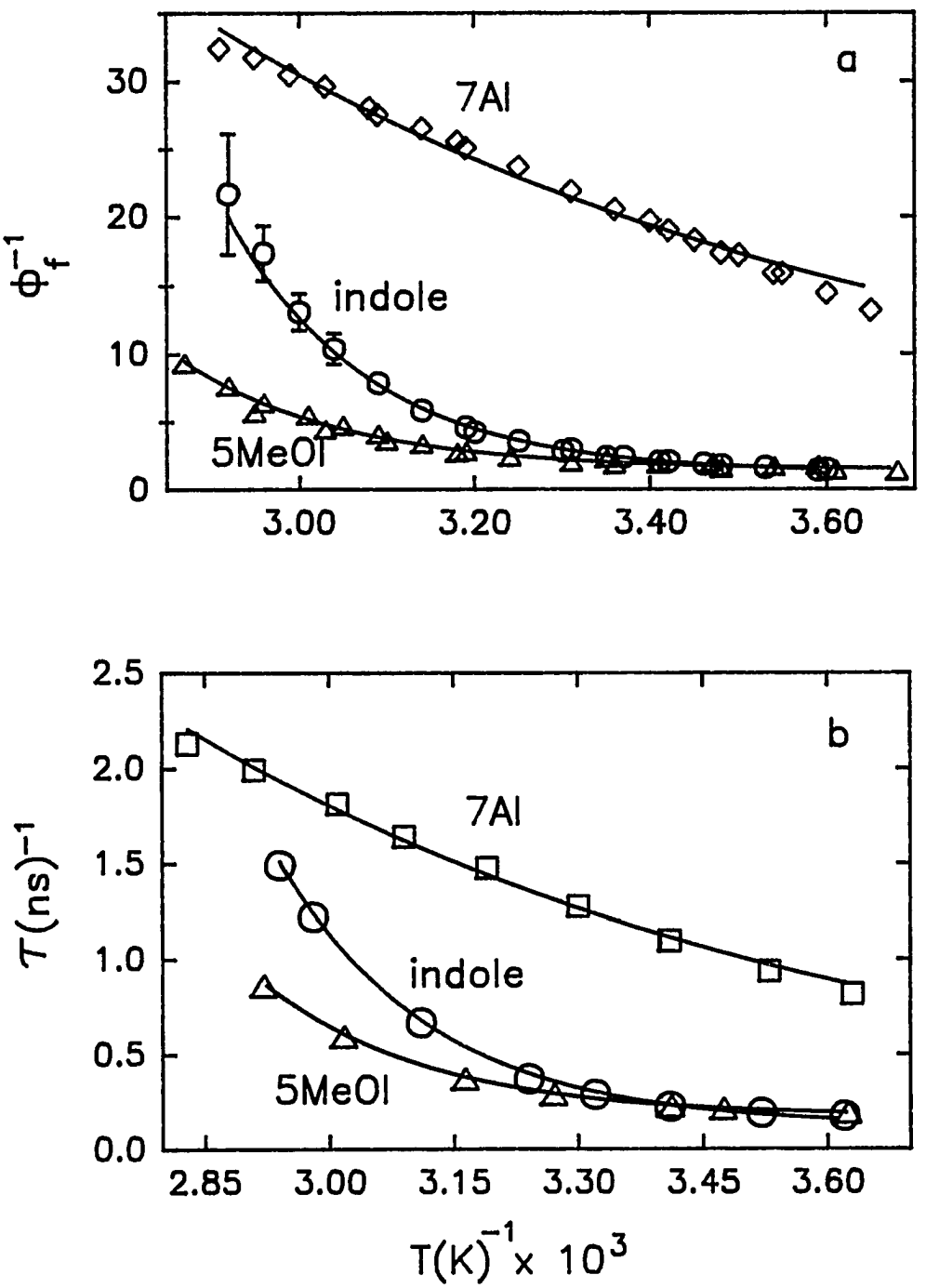
a
7Al
indole
5MeOI
Φ_f^{-1}
30
20
10
0
3.00
3.20
3.40
3.60
b
7Al
indole
5MeOI
$\tau(ns)^{-1}$
2.5
2.0
1.5
1.0
0.5
0.0
2.85
3.00
3.15
3.30
3.45
3.60
$T(K)^{-1} \times 10^3$

"fluorescent" state is not expected to be more than 10% of that produced instantaneously from the Franck-Condon region (Figure 3.2b).

Lee and Robinson [93] have performed an interesting, detailed, and original analysis of the nonradiative processes of indole in water/methanol mixtures using fluorescence lifetime and fluorescence quantum yield measurements. It is useful to compare and contrast our results and conclusions with theirs. Because of the agreement between lifetime measurements obtained with a neodymium/phosphate-glass laser and quantum yield measurements, they conclude that the nonradiative processes they observe result from monophotonic events. By analogy with previous work on photoionizing compounds such as anilino-naphthalene sulfonic acid (ANS) [94] and from evidence in the literature indicating that indole produces photoelectrons, Lee and Robinson assume that the nonradiative process measured in their experiments is photoionization. Since they do not directly monitor absorption from the solvated electron, their assignment of the nonradiative process is tentative. As we note in the previous paragraph and elsewhere in this article, we can never observe more than 10% of a contribution of solvated electron whose rise time coincides with the decay time of the fluorescent state. Below we suggest the importance of abstraction of the N_1 proton in deactivating the fluorescent state. Regardless of the identity of the nonradiative process for indole observed in the experiments of Lee and Robinson, it is clear that it is very sensitive to solvent. For example, from the temperature dependence of the nonradiative rate they obtain activation energies of 10.4 and ~ 0.0 kcal/mol in water and methanol, respectively [93]. Assuming that the nonradiative process is photoionization, Lee and Robinson suggest that in methanol trapping of the photoelectron by a solvent cage is unfavorable and that a rapid recombination occurs that reforms ground-state indole. The optimum cage is proposed to be formed from about four water molecules [93]. With regard to our photoionization measurements of 7-azaindole, the electron yield in water is greater by about a factor of two

than that in methanol. If this reduction in yield results from recombination with the parent cation, the back reaction must occur in < 1 ps (beyond our time resolution). We observe no geminate recombination 150 ps subsequent to photoionization [38]. Similarly, for indole in butanol, no recombination is observed on the 30-ps time scale investigated subsequent to photoionization [38].

Our conclusions are in contrast to those of Feitelson [55] and Bent and Hayon [37], which have significantly influenced the interpretation of indole photophysics over the past twenty years. Feitelson proposed that the production of photoelectrons from indole was temperature dependent based on indirect measurements of hydrogen evolution. Bent and Hayon performed direct flash photolysis measurements of the solvated electron. They observed that the optical density change, ΔA, at 650 nm due to the solvated electron produced from indole at pH 7.5 is temperature dependent. Figure 4 of their article presents these raw data. A plot of ΔA vs. 1/T yields an apparent activation energy of 0.37 kcal/mol. A plot of $\ln(\Delta A)$ vs. 1/T yields an apparent activation energy of 4.9 kcal/mol, when the absorbance data have been corrected for the shift of the spectrum of the solvated electron with temperature [58]. The interpretation of these results is not straightforward. The quantum yield of photoectrons is, by definition,

$$\phi_{e^-} = \frac{k_{e^-}}{k_{e^-} + \sum_i k_i} \tag{3.7}$$

where the k_i represent all the other processes, radiative and nonradiative, that deactivate the excited state. ϕ_{e^-} is proportional to k_{e^-} only if $k_{e^-} < \sum_i k_i$; and this is unlikely since in 7-azaindole the solvated electron appears in ≤ 130 fs [38] and, in every other example studied here, within a 1-ps pulse width. It is therefore inappropriate to attach any physical

significance to the activation energies obtained from the temperature dependence of the absorbance change resulting from the solvated electron.

The temperature dependence observed by Bent and Hayon for the electron yield may be attributed to changes in the ground-state absorption spectrum with temperature. As can be seen for indole in Figure 3.7, raising the temperature decreases the shoulder at 290 nm and increases the absorbance in the short-wavelength region of the spectrum. Such a temperature-dependent absorption increase occurs at 265 nm, the excitation wavelength used by Bent and Hayon. The increase in electron yield that they report may thus be attributed to shifts in the spectra resulting from the $^1A \rightarrow {}^1L_a$ and $^1A \rightarrow {}^1L_b$ transitions.

If the observed activation energy in indole derivatives does not reflect thermally activated photoionization, what nonradiative process is involved? Glasser and Lami [59] have proposed that in the vapor phase dissociation of the N_1-H bond is an important nonradiative process. Detailed information on the ^1L_a and ^1L_b states in jet-cooled indoles has become accessible [60-66]. Wallace and coworkers [65] undertook an investigation of 2,3-dimethylindole, which is known to have a low-lying ^1L_a state in all media [67]. Their work yielded evidence that the ^1L_b state was strongly coupled to the ^1L_a state, from which dissociation of the N_1-H bond could occur. These results deal with site-specific hydrogen-bonding interactions in the gas phase. We have performed [68] proton inventory experiments [69] of 7-azaindole in water and have suggested that abstraction of the N_1 hydrogen may be an important, temperature-dependent, nonradiative process in indoles, especially 7-azaindole. Barkley and coworkers [70] have recently discussed hydrogen abstraction as a possible nonradiative pathway in indoles.

We suggest that the excitation-wavelength dependence of the fluorescence quantum yield reflects the coupling (most likely vibronic, see below) of the zero order ^1L_a and ^1L_b states. These results argue against the utility of using zero-order pictures of ^1L_a and ^1L_b states

Figure 3.7. Temperature dependence of the absorption spectrum of the ground-state of indole derivatives: (a) indole; (b) 7-azaindole; (c) 5-methoxyindole. 10° (—), 40° (···), 79°C (---). The change in absorption spectra with temperature is suggested to explain the temperature dependence of the electron yield observed by Bent and Hayon [37].

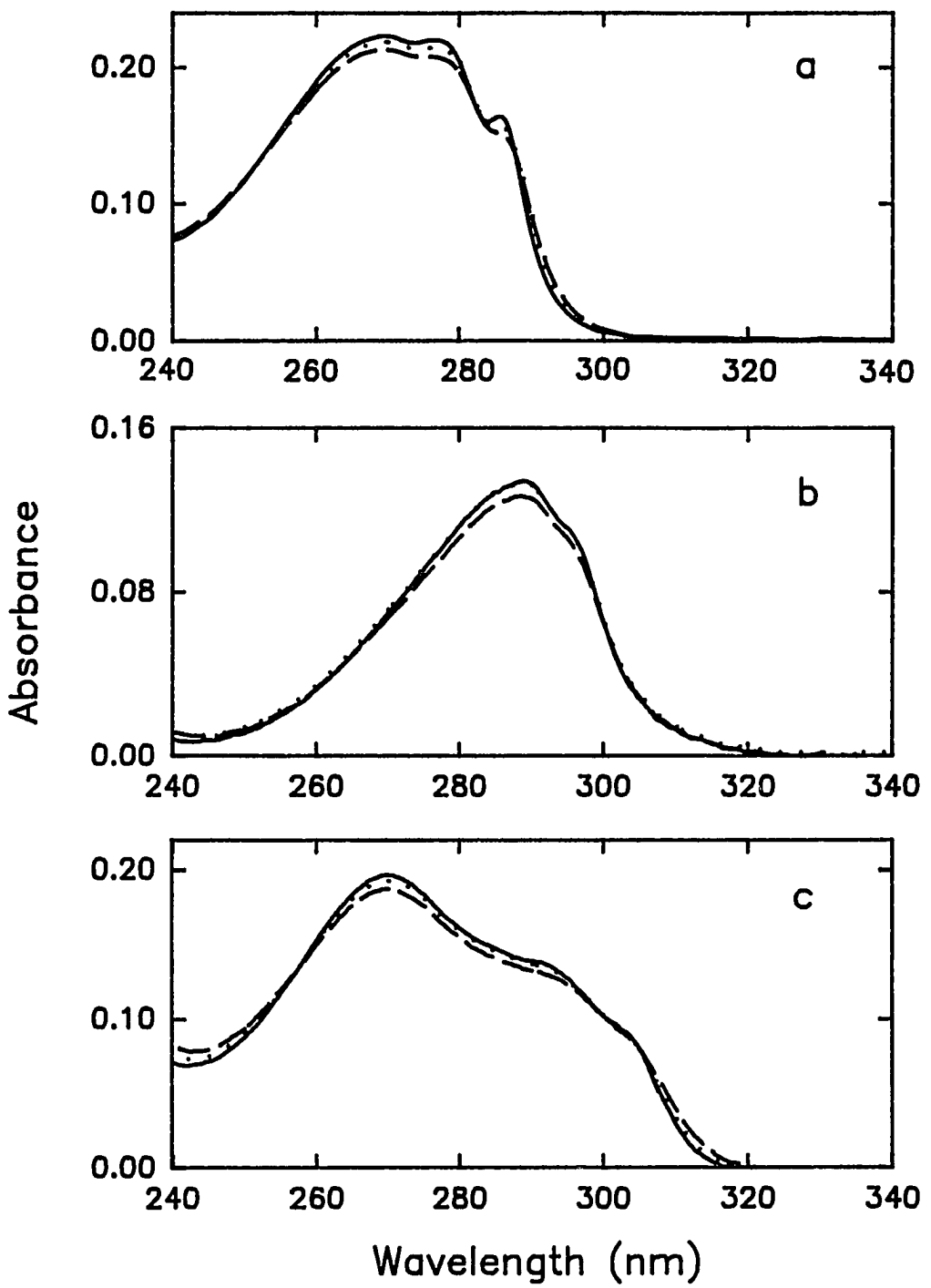
a
b
c
Absorbance
Wavelength (nm)
0.20
0.10
0.00
0.16
0.08
240
260
280
300
320
340

to describe the photophysics of indole and its derivatives. Similar conclusions have been obtained by Wallace and coworkers [65] and Fleming and coworkers [42].

2. The Effect of Closely-Spaced Excited States

First Cross et al. [71] and then Szabo [72] demonstrated how the presence of two excited electronic states whose energy gap is close to kT can influence the short time anisotropy decay and hence give rise to apparently anomalously low r(0) values if the anisotropy measurement is not performed with sufficient time resolution. Subsequently, Fleming and coworkers [42,73] experimentally observed these effects. Subpicosecond resolution reveals r(0) = 0.4 and rapid components of the anisotropy decay in the range of 1-4 ps.

In the specific case where there are two closely-spaced excited states, ^1L_a and ^1L_b, the measured anisotropy decay function is a function of both wavelength and time [42,71]:

$$r(\lambda,t) = \frac{k_R^a g^a(\lambda) r^a(t) K^a(t) + k_R^b g^b(\lambda) r^b(t) K^b(t)}{k_R^a g^a(\lambda) K^a(t) + k_R^b g^b(\lambda) K^b(t)} \tag{3.8}$$

where $k^{a,b}$ are the radiative rate constants, $K^{a,b}(t)$ are the population (fluorescence) decay laws, and $g^{a,b}(\lambda)$ are the emission line shapes, whose integrals are normalized to unity, of the ^1L_a and ^1L_b states. Thus, when two closely-spaced states can be reached from the ground state in an optical transition (or if the upper state can be thermally populated), the observed anisotropy decay is a superposition of the individual anisotropy decays. The form of the observed anisotropy decay will depend strongly on the extinction coefficient connecting the ground electronic state to ^1L_a or ^1L_b, which will determine $K^{a,b}(t=0)$. The decay will also depend on the relative contribution of emission from the two states that is detected at a given wavelength.

Using the level scheme depicted in Figure 3.8, the following rate constants [42,71] are defined.

$$k^a = k^b = k_R^a + k_{NR}^a \tag{3.9}$$

Here we assume that $k_R^a = k_R^b$. We also assume that the sum of the rate constants of the nonradiative processes depleting ^1L_a and ^1L_b, neglecting internal conversion, is the same for both levels: $k_{NR}^a = k_{NR}^b$. k_{ba} is the rate of ^1L_b to ^1L_a internal conversion. k_{ab} is rate at which ^1L_b is thermally populated by ^1L_a and is determined using the appropriate ^1L_b–^1L_a energy gap and an estimated value of k_{ba}.

In order to evaluate the limiting anisotropies obtained from steady-state and time-domain measurements [33], r_o and r(0) respectively, we employ the following relationships [74].

$$\begin{aligned} k^a(t) = &\left(\frac{1}{2}Q\right)\left\{K^a(0)[Q-\delta]+2k_{ba}K^b(0)\right\}\exp(l_1 t)+ \\ &\left(\frac{1}{2}Q\right)\left\{K^a(0)[Q+\delta]-2k_{ba}K^b(0)\right\}\exp(l_2 t) \end{aligned} \tag{3.10}$$

$$\begin{aligned} K^b(t) = &\left(\frac{1}{2}Q\right)\left\{K^b(0)[Q+\delta]+2k_{ab}K^a(0)\right\}\exp(l_1 t)+ \\ &\left(\frac{1}{2}Q\right)\left\{K^b(0)[Q-\delta]-2k_{ab}K^a(0)\right\}\exp(l_2 t) \end{aligned} \tag{3.11}$$

$$\delta = k^a + k_{ab} - k^b - k_{ba} \tag{3.12}$$

$$Q = \left[\delta^2 + 4k_{ab}k_{ba}\right]^{1/2} \tag{3.13}$$

$$k = k^a + k_{ab} + k^b + k_{ba} \tag{3.14}$$

$$l_1 = -\frac{1}{2}(k - Q) \tag{3.15}$$

$$l_2 = -\frac{1}{2}(k + Q) \tag{3.16}$$

We can express the total fluorescence decay as contributions from both the ^1L_b and ^1L_a states.

$$K(t,\lambda) = g^a(\lambda)K^a(t)k_R + g^b(\lambda)K^b(t)k_R \tag{3.17}$$

and we assume as before that $k^a_{NR} = k^b_{NR} = k_R$. Inserting Eqs (3.14) and (3.15) into the above expression, we obtain

$$\begin{aligned} K(t) = {} & \frac{k_R}{2Q}\Big[g^a(\lambda)K^a(0)(Q-\delta) + 2g^a(\lambda)k_{ba}K^b(0) + \\ & g^b(\lambda)K^b(0)(Q+\delta) + 2g^b(\lambda)k_{ab}K^a(0)\Big]\exp(l_1 t) + \\ & \frac{k_R}{2Q}\Big[g^a(\lambda)K^a(0)(Q+\delta) - 2g^a(\lambda)k_{ba}K^b(0) + \\ & g^b(\lambda)K^b(0)(Q-\delta) - 2g^b(\lambda)k_{ab}K^a(0)\Big]\exp(l_2 t) \\ \equiv {} & \alpha_1\exp(-t/\tau_1) + \alpha_2\exp(-t/\tau_2) \end{aligned} \tag{3.18}$$

The total fluorescence decay is described by a double exponential with prefactors α_1 and α_2. The prefactors contain the values of the population of the ^1L_a and ^1L_b states at time zero, $K^a(0)$ and $K^b(0)$. Fleming and coworkers [42] have measured these prefactors for tryptophan under various conditions of excitation and detection with subpicosecond resolution. If we assume [87], as they do, that the relative intensities of the ^1L_a and ^1L_b

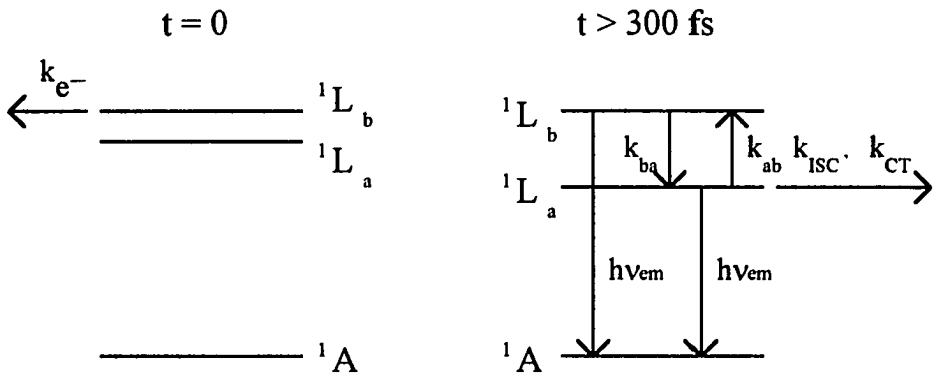

Figure 3.8. Energy level diagram. The scheme is modified from that of Cross et al. [71] in order to take into account ionization from the ^1L_b state. ^1L_b is believed to lie slightly (~ 500 cm^{-1}) above ^1L_a in indole. The ^1L_b - ^1L_a energy gap is expected to be small in 7-azaindole based on its lower steady-state anisotropy values. In 5-methoxy- and 5-hydroxyindole, ^1L_b is believed to lie below ^1L_a, with a significant energy gap, based on steady-state anisotropy data [40]. We have demonstrated that there is excited-state dynamic solvation in 7-azaindole. This occurs in ~ 300 fs in methanol. We attribute this solvation to the ^1L_a state and schematically indicate its position at t = 0 and at a later time when excited-state solvation is accomplished. The ^1L_b level is shown to photoionize only on the left-hand side of the Figure (i.e., at t = 0) because our results indicate that most of the photoionization occurs at this time. After the initially prepared population has moved out of the Franck-Condon region and into the right-hand side of the Figure, other nonradiative processes become significant. (The most cogent evidence for the basic validity of the level kinetics model [71,72] is the observation of the rise time in the time-resolved fluorescence anisotropy [42]. This rise time is controlled by the rate of population of the upper state by the lower state, k_{ab}.)

emission are $g^a(\lambda) = 0.35$ and $g^b(\lambda) = 0.65$ and that $k_{ba} = 0.625\ ps^{-1}$ and $k_{ab} = 0.044\ ps^{-1}$, we can work backwards from their experimentally determined preexponential factors for the population decay and solve for $K^a(0)$ and $K^b(0)$:

$$\frac{\alpha_1}{\alpha_2} = \frac{g^a(\lambda)K^a(0)(Q-\delta)+2g^a(\lambda)K^b(0)k_{ba}+g^b(\lambda)K^b(0)(Q+\delta)+2g^b(\lambda)K^a(0)k_{ab}}{g^a(\lambda)K^a(0)(Q+\delta)-2g^a(\lambda)K^b(0)k_{ba}+g^b(\lambda)K^b(0)(Q-\delta)-2g^b(\lambda)K^a(0)k_{ab}} \quad (3.19)$$

The initial populations obtained from subpicosecond anisotropy and fluorescence decay measurements are summarized in Table 3.5. In every case, the result of the lifetime measurement indicates a much larger ^1L_b population than would have been obtained from a consideration of only the anisotropy measurement. It is this discrepancy that we address in the next section.

3. Modelling Anisotropy Data

We have collected a large body of data on the monophotonic, instantaneous ionization of 7-azaindole, indole, and their derivatives and demonstrated that this ionization is excitation-wavelength dependent. We have also observed that the ^1L_a state is preferentially and dynamically solvated with respect to higher excited states in 7-azaindole [38]. This assignment is based on the observation of preferential solvation of the ^1L_a state in polar media [75]. In the following, we incorporate these factors into the description of the anisotropy decay of indole and demonstrate that the observations presented in this article are consistent with the early-time anisotropy decay measurements [42,73] (Figure 3.8).

We tentatively attribute the photoionization to ^1L_b for the following reasons.

(a) The quantum yields for fluorescence and photoionization are excitation-wavelength dependent (Figure 3.5 and Tables 3.2 and 3.4). If both states were

Table 3.5 Comparison of Initial $^1L_a/^1L_b$ Populations for Tryptophan Obtained from Measurements of Fluorescence and Anisotropy Decay[a]

λ_{ex} (nm)[b]	α_1	α_2	α_1/α_2	$K^b(0)$	$K^b(0)^{r(t)}$
305	0.77	0.23	3.35	0.43	0.01
303	0.66	0.34	1.94	0.70	0.03
300	0.69	0.31	2.23	0.62	0.05
297	0.65	0.35	1.86	0.72	0.11
294	0.59	0.41	1.44	0.92	0.16
292	0.59	0.41	1.44	0.92	0.18
290	0.77	0.23	3.35	0.43	0.40

[a] α_1 and α_2 are the experimentally determined preexponential factors for the excited-state population (fluorescence) decay obtained by Fleming and coworkers [12] with subpicosecond resolution. $K^b(0)$ is the initial relative population of the ^1L_b state predicted from their reported values of α_1 and α_2 by Eqns (3.18) and (3.19). The last column labelled $K^b(0)^{r(t)}$ is the initial relative population of the ^1L_b state required by Fleming and coworkers to fit their experimental anisotropy decay. [b] In each case $\lambda_{em} = 335$ nm.

photoionizable, the excitation-wavelength dependence would be expected to be much weaker or absent.

(b) In 5-methoxyindole, ^1L_b is the lowest excited singlet [40]. 5-Methoxyindole also possesses one of the largest ^1L_b-^1L_a energy gaps among the indoles. Because the solvated electron appears within 1 ps for excitation wavelengths as red as 305 nm for 5-methoxyindole, it is clear that ^1L_b is photoionizable.

We propose that the most of the photoionization occurs only at the moment of excitation, that is, immediately upon excitation, or at t = 0 [38]. At subsequent times, the initially prepared wavepacket will be displaced and photoionization will no longer be possible. Furthermore, at subsequent times, for indole, 7-azaindole, and their derivatives, the ^1L_a state will be stabilized or solvated with respect to the ^1L_b state. This preferential solvation event occurs in ~ 300 fs for 7-azaindole in methanol [38].

If for λ_{ex} = 305 nm at t = 0 the initial populations in the ^1L_b and ^1L_a levels are $K^b(0) = K^a(0) = 0.5$ and $\phi_{e^-} = 0.3$ (Table 3.5), the populations at a later time, t ~ 0, must be correspondingly diminished by the depletion produced by photoionization. Thus at a later time, the normalized populations are $K^b(t \sim 0) = 0.2/0.7 = 0.28$ and $K^a(t \sim 0) = 0.5/0.7 = 0.72$. At λ_{ex} = 300 nm where $\phi_{e^-} = 0.4$, the corresponding populations are $K^b(t \sim 0) = 0.17$ and $K^a(t \sim 0) = 0.83$. Given the resolution of any currently realizable time-resolved experiment, these residual populations not depleted by photoionization are in fact taken as the "zero time" populations measured in steady-state experiments or by time-correlated single-photon counting.

Figure 3.9 presents the anisotropy decay data of Fleming and coworkers for tryptophan at λ_{ex} = 305 and λ_{ex} = 300 nm. Superimposed on their results are our simulations using the "zero time" populations of the ^1L_b and ^1L_a states corrected for photoionization. Our

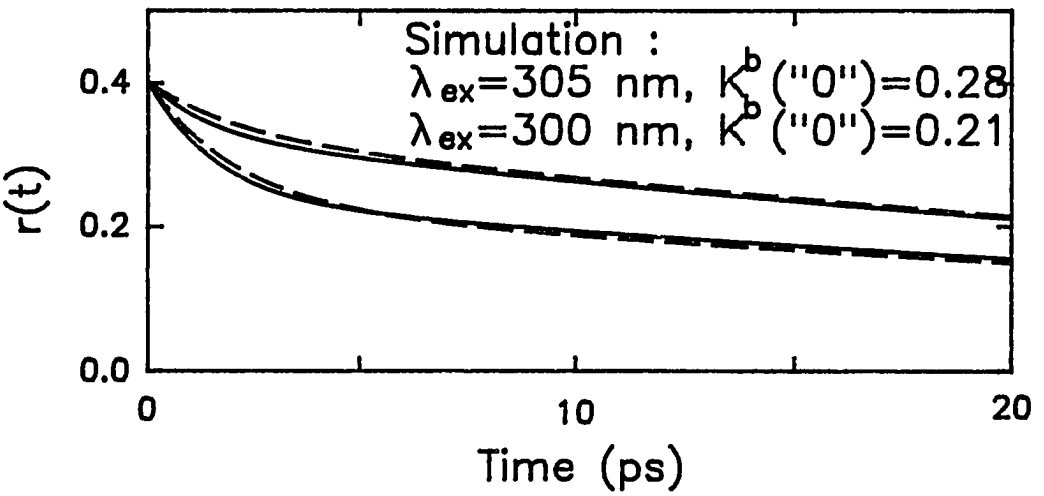

Figure 3.9. Comparison of the global fit (----) of the subpicosecond fluorescence anisotropy data for tryptophan of Fleming and coworkers [42] with a simulation (—) taking into account "zero time populations" of the ^1L_a and ^1L_b states that are corrected for photoionization. As we discuss in the text, "zero time" refers to the population of the excited states that remains after the instantaneous photoionization event. The Figure indicates that we are able to simulate very well the results of Fleming and coworkers by using ^1L_b populations at "zero time" of 0.28 and 0.20 at excitation wavelengths of 305 and 300 nm, respectively. At 300 nm, we use $K^b(0)$ = 0.20 instead of 0.17 because it gives better agreement with the experimental data and because 0.20 is within the bounds of experimental error in our electron yield measurements (Table 3.2). The ^1L_b populations that we estimate from our electron yield measurements are significantly larger than the populations required to fit globally the experimental anisotropy decay data and are closer to the populations obtained from the global analysis of the experimental population decay data (Table 3.5).

simulation is identical with the global fit to the experimental data when noise is taken into account.

The important conclusion to be drawn from this exercise is that the amount of the ^1L_b excited-state population in indole, 7-azaindole, and their derivatives that possess small ^1L_b-^1L_a energy gaps is more than that estimated from subpicosecond anisotropy decay measurements or from steady-state anisotropy measurements. We have discussed this point elsewhere [33]. The agreement of the "zero time" populations of our simulation with those obtained from the subpicosecond lifetime measurements [42] (Table 3.5) illustrates this point.

Crucial to our analysis are the observations that the solvated electron is produced instantaneously (< 1 ps) and that the fluorescence quantum yield is also excitation- wavelength dependent for molecules whose lowest-lying excited state is believed to be ^1L_b and in which there is a relatively large ^1L_b-^1L_a energy gap: 5-methoxy- and 5-hydroxyindole.

Based on these observations, we have assigned the ^1L_b state as the origin of the solvated electron at t = 0. In indole and 7-azaindole, where ^1L_a is lower-lying but where the energy gap is much smaller (based on fluorescence anisotropy measurements), we suggest that ^1L_a is capable of photoionization as long as it is coupled to ^1L_b. As the ^1L_a state is preferentially solvated this coupling will decrease and this state, giving rise to fluorescence in steady-state and conventional time-correlated single-photon counting measurements, will no longer be a source of solvated electrons (Figure 3.8).

E. Conclusion

The description of the excited-states of indole, 7-azaindole, and their derivatives proposed above is useful insofar as it can be used to explain or at least to rationalize the photophysics of more complex molecules — among which is the naturally occurring amino

acid, tryptophan. Essentially all tryptophan derivatives and peptides bearing nonrigid sidechains display nonexponential fluorescence decay [36,78,79]. A notable exception is N-acetyltryptophanamide (NATA), which affords a single exponential fluorescence decay of about 3 ns at 20 °C [36]. 5-hydroxytryptophan has also been observed to have a single-exponential fluorescence decay [80]; we have measured its lifetime at 20 °C and neutral pH to be 3.8 ns.

We have suggested that this nonexponential fluorescence decay arises from two (or more) side chain orientations with respect to the indole moiety. Each orientation is characterized by a different rate of charge transfer from the indole donor to the side chain acceptor [36]. The existence of stable conformational isomers (conformers) of tryptophan is supported by NMR data [79,81]. Molecular dynamics simulations of Engh et al. [82] have suggested different stable conformations between the indole ring and the side chain in tryptophan. Levy and coworkers [60-63] have observed different conformers of tryptophan and tryptophan-containing compounds in supersonic jets.

The fluorescence decay of zwitterionic tryptophan is fit well to two exponentially decaying components, namely to the function [36] $K(t) = 0.22 \exp(-t/620 \text{ ps}) + 0.78 \exp(-t/3200 \text{ ps})$. Measurement of the lifetime as a function of emission wavelength reveals that the short-lived component is blue-shifted with respect to the long-lived component [36,83]. The two components obtained in the fluorescence decay of zwitterionic tryptophan and essentially all tryptophan analogs and tryptophan-containing peptides have temperature dependencies that yield identical Arrhenius activation energies, E_a, but different Arrhenius prefactors [36].

Figure 3.10 provides a means of summarizing the data presented in this article on the photoionization of the excited states of indoles and also provides a qualitative explanation of the nonexponential fluorescence decay kinetics of zwitterionic tryptophan. Figure 3.10 considers the indolyl photophysics in the context of a three-dimensional energy surface. The

Figure 3.10. Potential energy diagrams of indole derivatives as a function of two coordinates. (a): The ^1L_b surface is proposed to be dissociative in one coordinate and bound in the other(s). The bound character of the ^1L_b surface is indicated by the sequence of parabolas tangent to it. Upon light absorption, the initially prepared wavepacket has either "slid down" the dissociative surface, producing the radical cation and the solvated electron, or "spilled out" into an orthogonal coordinate. (b) and (c): The ^1L_a surface of tryptophan is proposed to be coupled to a charge transfer coordinate that involves the amino acid side chain. It is suggested that in certain conformers, this coordinate has a higher frequency than in others (b as opposed to c, for example) and thus manifests a larger rate of charge transfer to the side chain. The barrier to charge transfer is set equal in each case since it is known that in zwitterionic tryptophan the activation barrier is the same for each of the two exponentially decaying components [36]. Finally, it is known that the short-lived (620 ps) component is blue-shifted with respect to the long-lived (3200 ps) component in zwitterionic tryptophan. These spectral shifts are depicted schematically in the Figure. By side chain coordinate we refer to all contributions to the reaction coordinate involved in the charge transfer reaction. The most significant component is obviously the amino acid side chain itself, but the contribution from the solvent cannot be neglected.

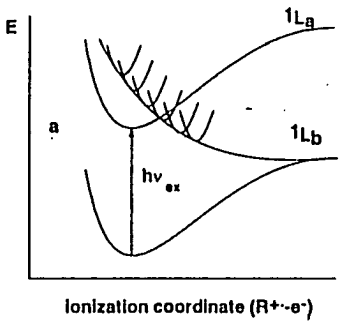
E
^1L_a
^1L_b
a
$h\nu_{ex}$
Ionization coordinate ($R^{+\cdot}$-e^-)

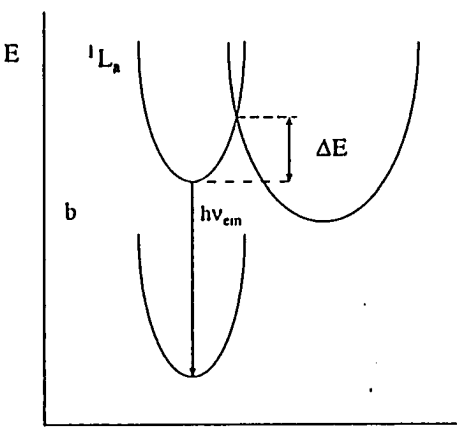
E
^1L_a
ΔE
b
$h\nu_{em}$
charge transfer coordinate

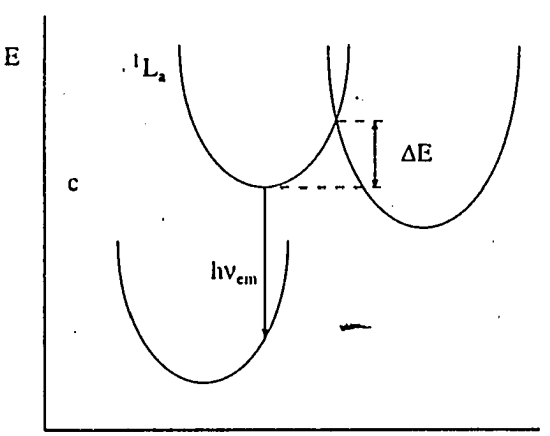
E
^1L_a
ΔE
c
$h\nu_{em}$
charge transfer coordinate

energy is a function of an ionization coordinate determined by an $R^{+\cdot}$ - e^- distance and a charge-transfer-to-side-chain coordinate. The body of data on indole and its derivatives can be rationalized by taking the ^1L_b surface to be highly asymmetric in two coordinates and by using propagating wavepackets [84] to describe excited-state dynamics. Comparison of Figures 3.10a and b show the ^1L_b surface to be dissociative in the ionization coordinate and bound in the side chain or charge transfer coordinate.

In indole and 7-azaindole derivatives, because ^1L_a and ^1L_b lie so close to one another, upon light absorption significant populations of each are excited (Table 3.5, Figures 3.8 and 3.10). The wavepacket projected onto the ^1L_b surface can either slide down the dissociative chute along the ionization coordinate (Figure 3.10a) or spill over into the ^1L_a surface if the ^1L_a surface crosses the ^1L_b surface near its minimum (Figure 3.10b). Thus, about a femtosecond after excitation, the initially prepared population is either photoionized or localized in bound states. This time corresponds to the inverse bandwidth [84] of the indole absorption spectrum.

Fluorescence measurements performed with steady-state or time-correlated, single-photon counting apparatus will only probe areas of the potential energy surfaces illustrated in Figures 10b and c owing to their limited time resolution. The regions of the potential surface displayed in Figures 10b and c are no longer susceptible to instantaneous ionization. It is known, however, that the presence of electrophilic side chain groups in tryptophan induces nonexponential fluorescence decay from, presumably, the ^1L_a state. The activation barrier for this process is determined by the intersection of the surface for the charge-separated state with that of the ^1L_a state. If there is a distribution of ^1L_a states with different frequencies for the side chain mode, it is possible to obtain crossings between the ^1L_a and the charge-separated states that all possess the same activation barrier (Figures 3.10b and c). The rate of passage from ^1L_a to the charge-separated state will now be determined by the curvature [85] of the ^1L_a

surface. The larger the curvature or the higher the frequency of the side chain mode, the larger the rate for the charge transfer process.

The absence of nonexponential fluorescence decay in NATA may now be explained if all its conformers have similar side-chain frequencies and intersect the charge-separated surface at the same position. The absence of nonexponential fluorescence decay in 5-hydroxytryptophan, where ^1L_b is the fluorescent state, can be attributed to a much higher barrier crossing between the ^1L_b and the charge-separated states.

For tryptophan at high pH, the carboxylic acid is depronated and the amino group is uncharged; hence, neither group is a good charge acceptor [36], the fluorescence lifetime becomes insensitive to the side chain distribution, and single exponential fluorescence decay arises [36]. We observe a finite rise time of ~ 3 ns for the appearance of the 10% of the solvated electron produced at pH 12.3 in tryptophan (Figure 3.3b). This rise time corresponds to the 3.2-ns fluorescence decay at pH 12.3. Similarly, Bent and Hayon [37] observe about 10% of the solvated electron produced at pH 10.3 in tryptophan to appear with an ~ 8-ns time constant. Again, this rise time agrees with the fluorescence decay time of the anionic tryptophan. An explanation for this behavior is that when the charge transfer states are no longer accessible at high pH, thermal activation can transfer population from the ^1L_a state back to the dissociative ^1L_b surface. Instantaneous rise times for the solvated electron are observed at high pH for 5-hydroxytryptophan and all other compounds investigated here. In 5-methoxy- and 5-hydroxyindole and 5-hydroxytryptophan, the ^1L_b state is the lowest and hence is the fluorescent state.

Zwitterionic 7-azatryptophan is expected to have the same distribution of conformers in aqueous solution as zwitterionic tryptophan; and although zwitterionic 7-azatryptophan has its ^1L_a state lying slightly below its ^1L_b state [33], it is characterized by a single exponential fluorescence decay over most of the pH range when emission is collected over most of its

band [31,32,35]. This distinguishing characteristic of 7-azatryptophan, which contributes greatly to its amenability as a fluorescent probe [31,34], shall be discussed elsewhere.

CHAPTER IV EXCITED-STATE TAUTOMERIZATION IN THE ANTIVIRAL AGENT HYPERICIN AND ITS FLUORESCENT SPECIES

A. Introduction

The naturally occurring polycyclic quinone, hypericin (Figure 4.1), possesses important and diverse types of biological activity [102]. It has been shown that hypericin deactivates the human immunodeficiency virus (HIV) [103-105]. Antiviral activity was demonstrated in a lentivirus closely related to HIV, equine infectious anemia virus (EIAV), to require light by Carpenter and Kraus [106]. In addition, hypericin is closely related, both structurally and spectrally, to the photoreceptor (Figure 4.1) of the protozoan ciliates, *Stentor coerulus* [107] and *Blepharisma japonicum* [108,109]. Although the singlet oxygen produced from hypericin [110,111] is toxic to *S. coerulus* under high light flux (~ 5000 W/m^2) [112] it is an open question whether the limited exposure to room light in the experiments of Carpenter and Kraus [106] was toxic to EIAV because of photosensitized generation of singlet oxygen by hypericin or because of the presence of additional nonradiative decay processes of the excited states of hypericin. It is of fundamental importance to understand the role of light in the activity of hypericin and hypericin-like molecules.

We provide the first detailed investigation that uses both ~ 1-ps time resolution and a white-light continuum to examine and to unravel the excited-state primary photoprocess of hypericin. In preliminary work, we have observed that hypericin possesses an excited-state absorbance that has a rapid decay component of several picoseconds [113]. The new excited-state absorbance (~ 580-650 nm, in methanol) is of particular interest due to the earlier observations and suggestions of Song and coworkers [112,114,115] that the excited states of hypericin-like chromophores produce protons upon photoexcitation. We had thus tentatively

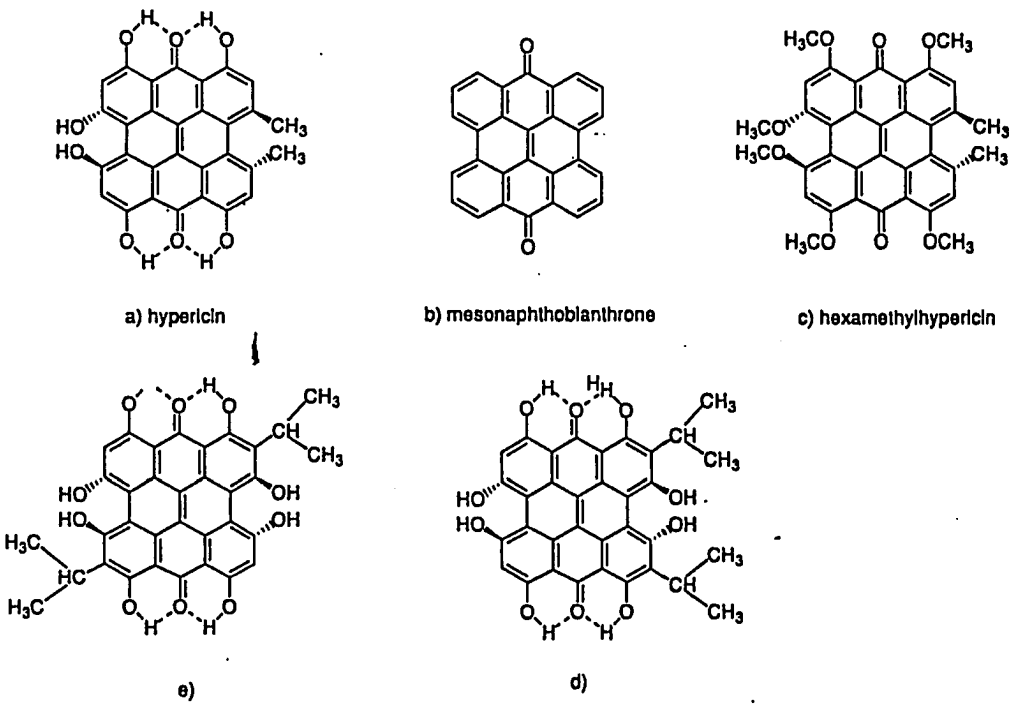

Figure 4.1. Structures of (a) hypericin, (b) the hypericin deshydroxy analog, mesonaphthobianthrone, (c) hexamethylhypericin, and (d) and (e) the two possible structures [107] for the stentorin chromophore.

suggested that a contribution of the excited-state absorption observed in hypericin was due to a species that undergoes excited-state tautomerization [113], and we proposed that deprotonation of the tautomer results in the reported pH decrease.

Because of the attention devoted to the light-dependent properties of hypericin and hypericin-like chromophores by a broad spectrum of investigators, namely those studying antiviral activity [103-106], synthetic pathways [133-137], and the directional responses of microorganisms [107-109], it is imperative that a detailed picture of the primary photoprocesses of hypericin be established. Such is the aim of this article, whose plan is as follows:

(1) Model compounds are investigated that demonstrate that a protonated carbonyl group is required in order to obtain hypericin-like absorption and emission spectra.

(2) Time-resolved absorption (stimulated emission) spectra and kinetics are presented that indicate that the hypericin emission spectrum grows in on a 6-12-ps time scale. Based on the model compounds, the rise time for the appearance of the hypericin emission is taken as evidence for an excited-state proton transfer.

(3) Our results and conclusions are discussed in the context of previous work on hypericin and what is currently known about excited-state proton transfer reactions. We consider possible objections to our assignment of the excited-state reaction to proton transfer.

Finally we note that observation of proton transfer on this time scale is of fundamental importance because its measurement is accessible by "standard" ultrafast spectroscopic techniques. Consequently, theories of proton transfer can be tested using hypericin.

B. Materials and Methods

Hypericin was obtained from Carl Roth GmbH & Co. and used without further

purification. Synthetic hypericin was also generously provided by Professor G. A. Kraus. Solvents were obtained from Aldrich. The hypericin analog, mesonaphthobianthrone (Figure 4.1), was prepared as described by Koch et al. [116].

In order to prepare hexamethylhypericin, hypericin (1 mg) was dissolved in 1 ml of N,N-dimethylformamide (DMF). Two equivalents of NaH were added, and the solution was stirred. Evolution of a gas and a characteristic green color indicated removal of hydroxyl protons from hypericin. Excess CH_3I was then added. This procedure was repeated 3 times No change in color occurred upon addition of NaH the fourth time indicating complete removal of labile protons. The resulting solution was orange and its UV/VIS absorption spectrum agreed with that described in the literature [134].

Deuteration of hypericin was effected by two methods. The first was to equilibrate hypericin in a deuterated solvent such as CH_3OD overnight or longer. The second involved dissolving 0.5 mg of hypericin in 0.5 ml of CH_3OD and adding 2 equivalents of $NaOCH_3$ while stirring. A characteristic green color indicated removal of hydroxyl protons. The solution was diluted up to 1 ml with CH_3OD and consequently changed back to its normal red color indicating deuteration of the hypericin. The solution was then allowed to equilibrate for two days.

Fluorescence spectra were measured with a Spex Fluoromax at room temperature. In certain cases, the spectra were analyzed by fitting to sums of log normal curves (see Figure 4.5 and Table 4.2). The time-resolved absorption and time-correlated single-photon counting experiments are performed with the apparatus described elsewhere [32,33,71]. Transient absorption spectra were obtained with a liquid nitrogen cooled charge-coupled device (CCD) (Princeton Instruments LN/CCD-1152UV) mounted on an HR320 (Instruments SA, Inc.) monochromator with a grating (1200 g/mm) blazed at 5000 Å. The following protocol was employed. The CCD pixels were binned such as to allow simultaneous collection of both the

probe and the reference beams, I and I_0 respectively, of the transient absorption spectrometer. The signal was integrated for 30 seconds. Absorption spectra were constructed from $\log(I/I_0)$. These spectra were corrected by subtraction of background spectra obtained with a probe delay of -20 ps. Five such corrected spectra were then averaged together. Two successive acquisitions at -20 ps and -10 ps yield a flat baseline centered on zero when subtracted from each other. Figure 4.8d compares the absorption spectrum taken at "time zero" of the dye nile blue in ethanol with its steady-state spectrum obtained with a Shimadzu UV-2101PC double-beam spectrometer. The agreement is excellent, especially when it is borne in mind that our laser system operates at 30 Hz and that we generate continuum with ~ 1-ps pulses. For the absorption and stimulated emission experiments, identical kinetics were observed whether the pump beam was rotated parallel, perpendicular, or at the magic angle (54.7°) to the probe beam. Unless otherwise indicated, experiments were performed at room temperature, 22 °C. Sample concentrations for hypericin were ~ 4×10^{-6} M for fluorescence measurements and ~ 5×10^{-5} M for transient absorption measurements.

C. Results

1. Steady-State Absorption and Fluorescence Measurements

a. Hypericin in Protic and Aprotic Solvents

Figure 4.2a presents the absorption and fluorescence spectra of hypericin in DMSO. Table 4.1 presents absorption and emission maxima for various protic and aprotic solvents. The absorption and emission spectra display mirror symmetry. Figure 4.2b presents the fluorescence and absorption spectra of hypericin in H_2SO_4. The shape of both fluorescence and absorption spectra are identical to those obtained in methanol and DMSO although red shifted by 60 and 50 nm, respectively.

Table 4.1. Summary of Hypericin Photophysics

solvent	lifetime (ns)	λ^{max}_{abs} (nm)	λ^{max}_{ems} (nm)
DMSO	6.5	598	598
CH_3CN	5.5	594	594
MeOH	5.5	588	588
MeOH/10mM HCl[a]	3.5	580	580
H_2SO_4	5.5	658	661
H_2O, pH 13[b]	4.5	650	693
40mM β-cyclodextrin[c]	—	~593	593

[a] Song and coworkers [115] reported the fluorescence spectrum of hypericin in a mixture of ethanol and HCl (10 mM). While retaining mirror symmetry, the resultant fluorescence and absorption spectra are blue-shifted 8 and 18 nm from those obtained in methanol and DMSO, respectively. The spectrum in the alcohol/HCl mixture is qualitatively similar to those obtained in protic and aprotic solvents. [b] In water at pH < 3, hypericin is soluble but nonfluorescent. Above pH 11, hypericin is both soluble and fluorescent. [c] The fluorescence intensity was too weak to permit an accurate determination of the excited-state lifetime. The solution was at pH 4.0.

Figure 4.2. Normalized fluorescence spectra (----) and absorption spectra (—) of hypericin in (a) DMSO, (b) H_2SO_4, and (c) a solution of 40 mM β-cyclodextrin at pH 4.0.

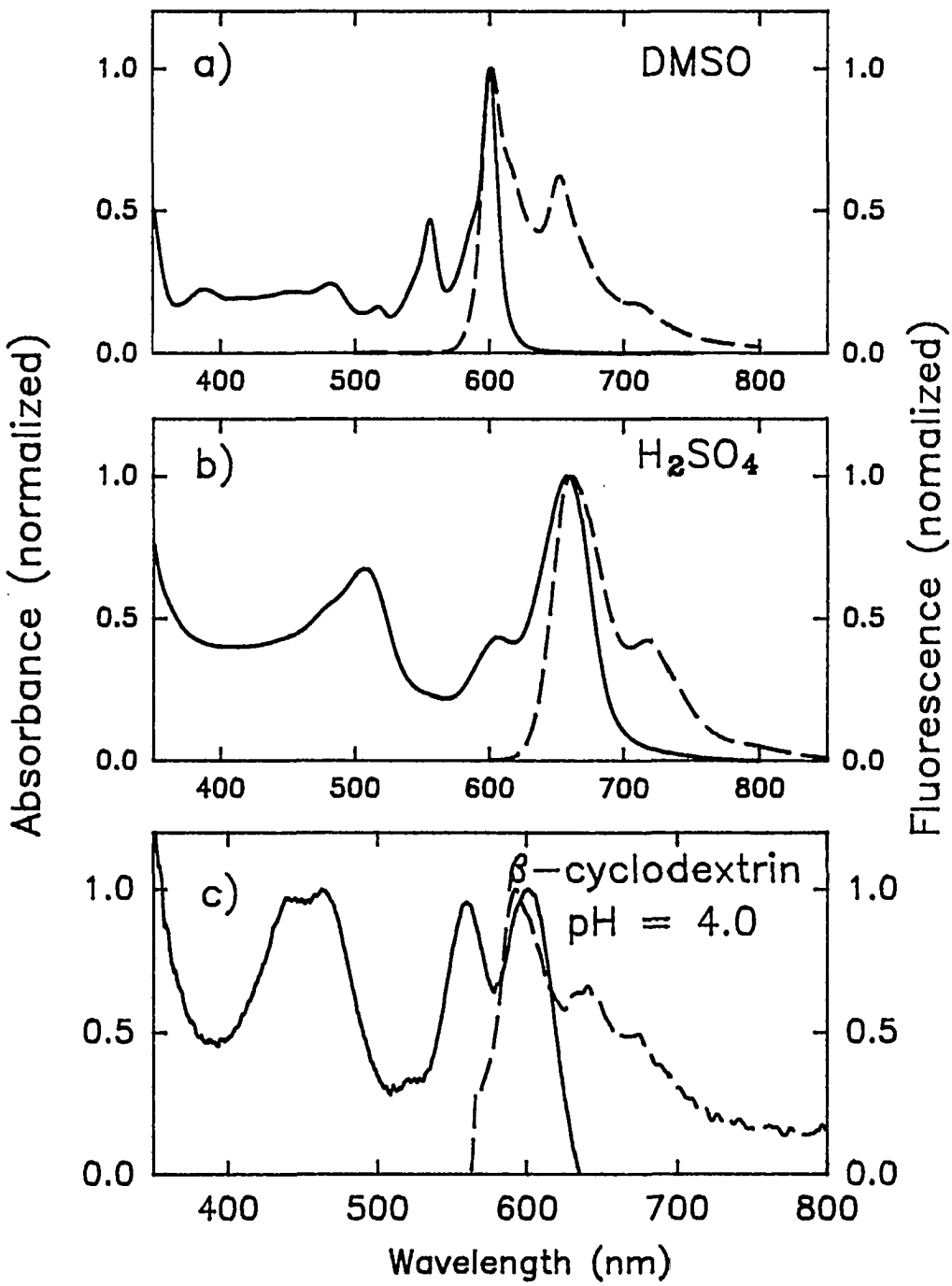
a)
DMSO
b)
H_2SO_4
c)
β—cyclodextrin
pH = 4.0
Absorbance (normalized)
Fluorescence (nomalized)
Wavelength (nm)
1.0
0.5
0.0
400
500
600
700
800

As will be discussed in more detail below, hypericin in water at pH values between 3 and 11 is barely, if at all, soluble and is nonfluorescent. Figure 4.2c and Table 4.1 indicate, however, that hypericin in a 40 mM solution of β-cyclodextrin at pH 4.0 gives rise to fluorescence and absorption spectra very similar to those obtained in less polar solvents in which hypericin is soluble. β-Cyclodextrin is composed of 7 D-(+)-glucopyranose units joined by α-(1,4)-linkages. The result is a cyclic molecule with an inner diameter of ~ 7.0 Å and a depth of ~ 7.0 Å [117]. While such a cavity is too small to accommodate the entire hypericin molecule, which can be crudely approximated as a rectangle of dimensions 12.8 × 9.2 Å, it is spacious enough to hold at least the corner of the molecule bearing the carbonyl group and the β-hydroxyl group adjacent to it. There are examples of β-cyclodextrin forming complexes with both porphyrins [125] and pyrene [126]. It is likely that hypericin forms an inclusion complex with β-cyclodextrin under conditions (water at pH 4.0) where it is otherwise insoluble, and that this complex facilitates proton transfer between the hydroxyl and the carbonyl groups, which is responsible for the distinctive visible absorption and fluorescence spectra. This result is significant because it implies that the photoreceptor complex in the protozoan ciliate *S. coerulus*, for which no x-ray structure exists, most likely efficiently shields the stentorin chromophore from an aqueous environment.

b. Hypericin Analogs in Protic and Aprotic Solvents

In contrast to hypericin, its deshydroxy analog, mesonaphthobianthrone (Figure 4.1) is nonfluorescent in the aprotic solvents DMSO (Figure 4.3a) and CH_3CN. When, however, it is dissolved in a protic solvent such as methanol (in which it is only sparingly soluble), a fluorescence band appears with a maximum at 467 nm (Figure 4.3b). Finally, dissolving it in a strong acid such as sulfuric or triflic acid generates a fluorescence spectrum that has nearly the same shape as that of hypericin in DMSO and that is blue shifted from the hypericin spectrum

by about 14 nm. Its emission maximum is 584 nm. These results demonstrate the importance of a protonated carbonyl group for producing a fluorescent hypericin-like molecule. The visible absorption spectrum of mesonaphthobianthrone in H_2SO_4 is curious in that it resembles a blue shifted duplicate of its fluorescence spectrum and not its mirror image (Figure 4.3c), as is the case for hypericin in DMSO (Figure 4.2a).

In DMF hexamethylhypericin both absorbs and emits in the visible (Figure 4.4b). Its absorption spectrum is distinctly blue-shifted and broader with respect to that of hypericin in DMF (Figure 4.4a). Its emission spectrum is broad and structureless. In H_2SO_4, however, the absorption spectrum shifts to the red and acquires structure similar to that of hypericin. Similarly, the fluorescence spectrum sharpens, and a distinct shoulder appears to the red of the maximum (Figure 4.4c). The change in going from DMF to H_2SO_4 as a solvent for hexamethylhypericin is visually quite striking. In DMF the solution is a faint orange color. In H_2SO_4, it takes on the pink color characteristic of all hypericin solutions.

Regardless of the solvent (DMF, H_2SO_4, or methanol) the fluorescence quantum yield of hexamethylhypericin is always at least 100 times less than that of hypericin in the corresponding solvent. We suggest that this result indicates the importance of intersystem crossing as a nonradiative process in untautomerized hypericin.

c. Mesonaphthobianthrone: Probing Solute Heterogeneity Using Mixed Solvents

In order to assess the extent of inhomogeneity in the ground and the excited states, we measured the fluorescence spectrum of mesonaphthobianthrone in varying H_2SO_4/MeOH mixtures (Figure 4.5). At low H_2SO_4 concentrations (< 45 %), the emission spectra are featureless and broad. At high H_2SO_4 concentrations (> 80 %), the emission spectra are essentially identical to that in pure H_2SO_4 and are characterized by narrower, sharper bands. The width and intensity of these bands, as estimated from a fit to a sum of log-normal

Figure 4.3. Normalized fluorescence spectra (----) and absorption spectra (—) of the hypericin analog lacking hydroxyl groups, mesonaphthobianthrone [116]. The solvents used are DMSO (top), methanol (middle), and sulfuric acid (bottom).

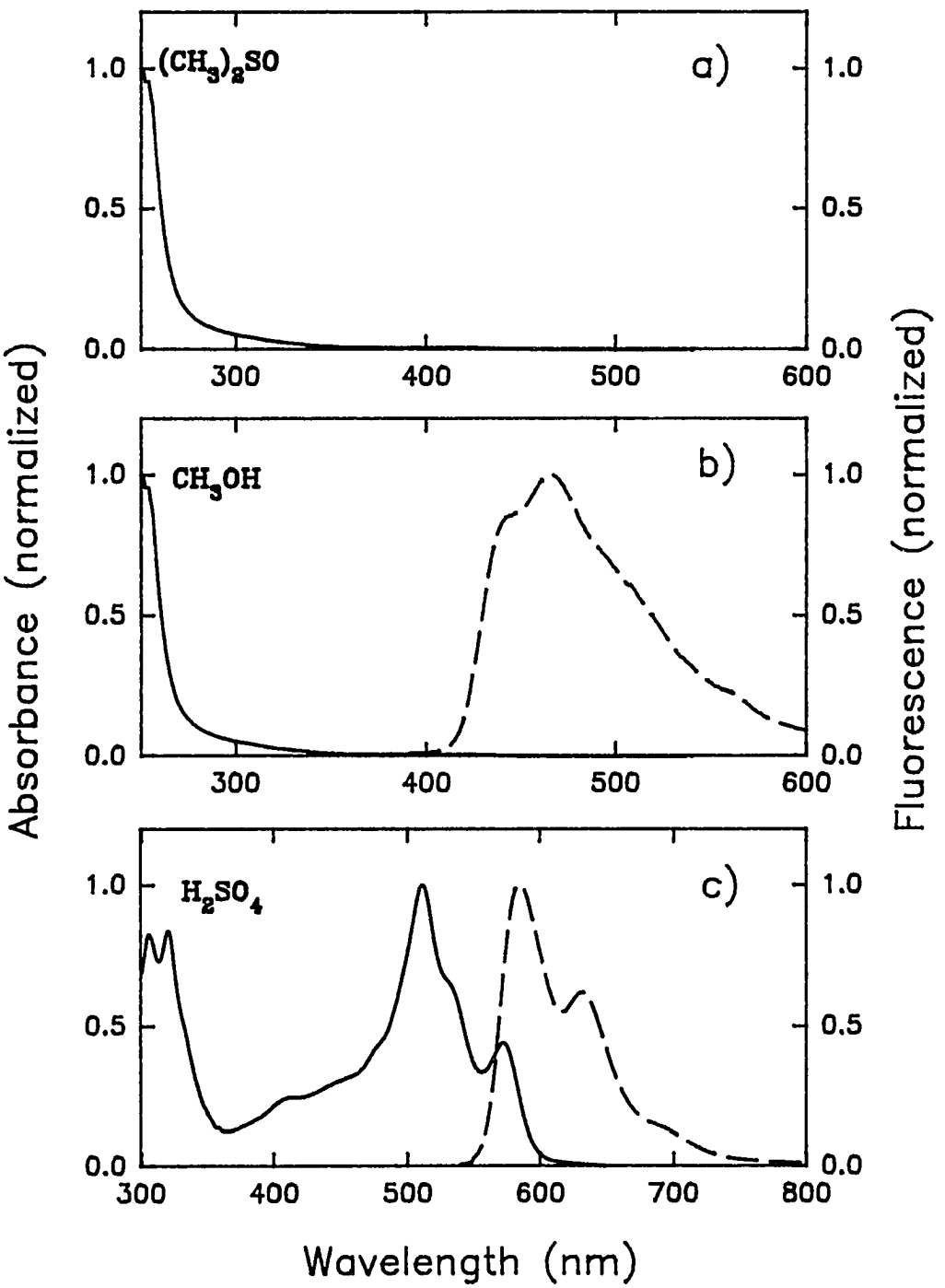
(CH3)2SO
a)
CH3OH
b)
H2SO4
c)
Absorbance (normalized)
Fluorescence (normalized)
Wavelength (nm)
1.0
0.5
0.0
300
400
500
600
700
800

Figure 4.4. Normalized fluorescence spectra (----) and fluorescence excitation spectra (—) of hexamethylhypericin: (a) hypericin in DMF for purposes of comparison; (b) hexamethylhypericin in DMF; (c) hexamethylhypericin in H_2SO_4.

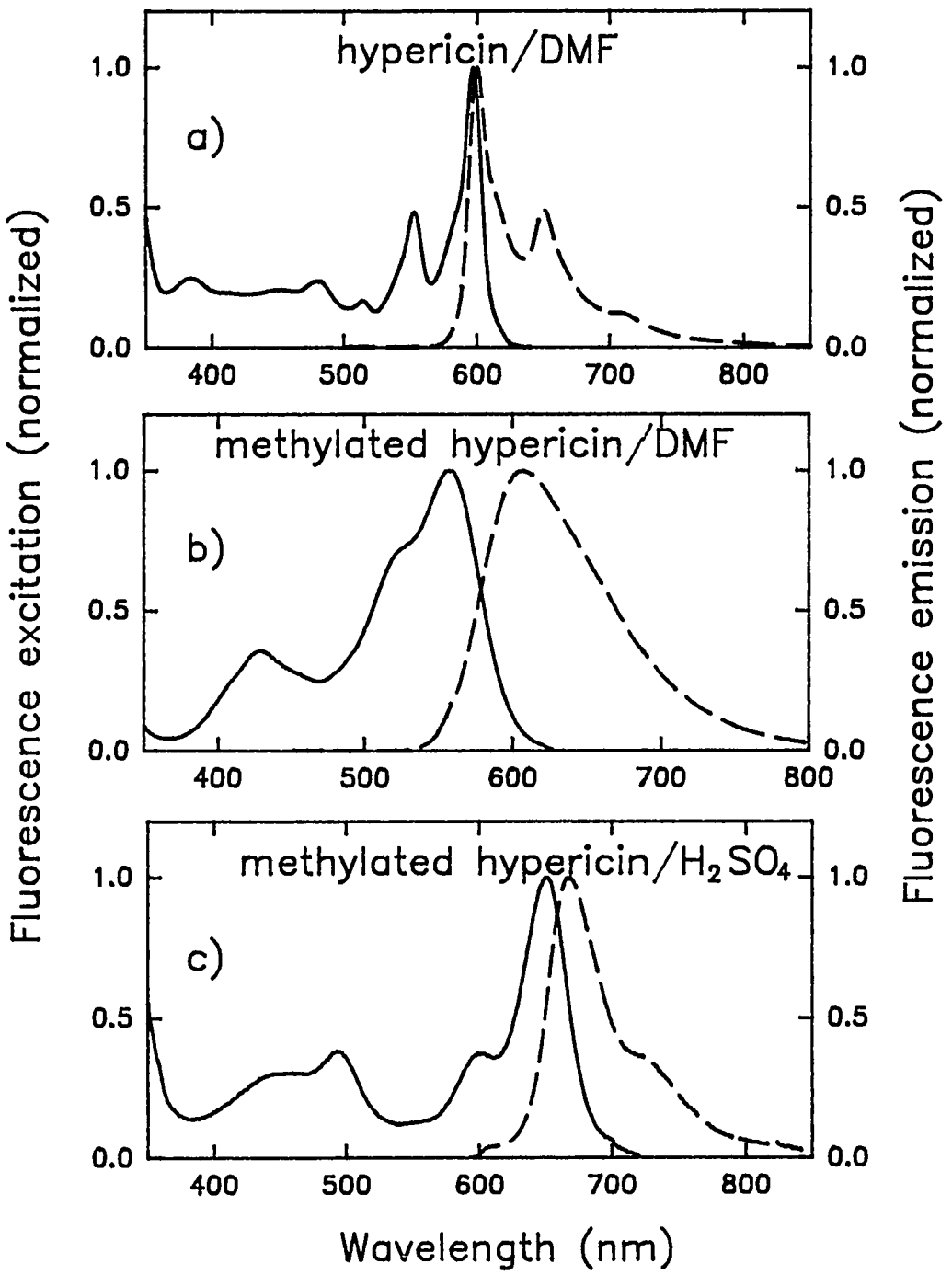
hypericin/DMF
a)
methylated hypericin/DMF
b)
methylated hypericin/H_2SO_4
c)
Fluorescence excitation (normalized)
Fluorescence emission (normalized)
Wavelength (nm)
0.0
0.5
1.0
400
500
600
700
800

Figure 4.5. Fluorescence spectra of the hypericin analog, mesonaphthabianthrone, in mixtures (v/v) of H_2SO_4 and methanol. The percentage of H_2SO_4 in the mixture is indicated in the figure. Spectra are collected at 22°C. The excitation wavelengths used are (a) 256, (b) 511, and (c) 580 nm.

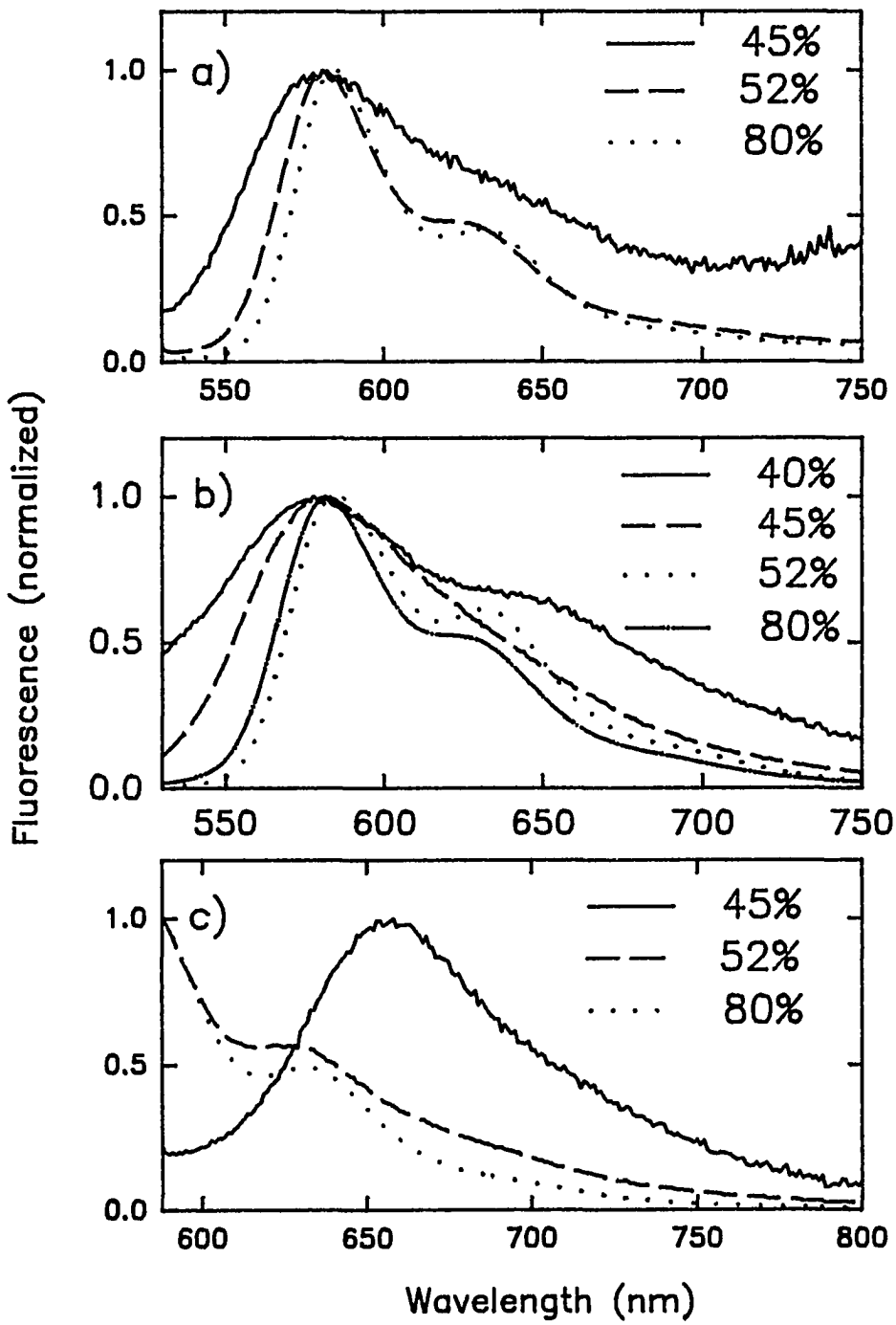
a)
45%
52%
80%
b)
40%
45%
52%
80%
c)
45%
52%
80%
1.0
0.5
0.0
550
600
650
700
750
800
Fluorescence (normalized)
Wavelength (nm)

functions, are summarized in Table 4.2. The ground-state heterogeneity is also illustrated by the variation of the fluorescence spectra with respect to excitation wavelength.

d. Hypericin: Probing Solute Heterogeneity Using Mixed Solvents and pH

As indicated in Figure 4.2b, hypericin in concentrated sulfuric acid is fluorescent. This fluorescence, however, is quenched upon adding water to the solution. A solution that is 33% water exhibits no fluorescence (Figure 4.6b). Figure 4.6c presents the absorbance spectra of hypericin at pH values below 3; Figure 4.6d, at pH values above 11. Although small changes in the absorption spectra are apparent at low pH, the changes are dramatic at high pH.

There are two possible factors for the reduction of hypericin fluorescence upon the addition of water, both of which may contribute. As noted in Table 4.1, hypericin is insoluble in water in the pH range from about 3 to 11. At low pH (< 3), hypericin is soluble but nonfluorescent. It is possible that at pH < 3 hypericin forms nonfluorescent, soluble aggregates. The decrease in fluorescence intensity of H_2SO_4/H_2O mixtures as the amount of H_2O increases (Figure 4.6b) may be attributed to a corresponding increase of such a nonfluorescent aggregate. Alternatively, the second explanation is that water forms very tight complexes with hypericin that prevent protonation of the carbonyl groups either from the internal hydroxyl groups or from external proton sources in solution. There is precedent for such a role for water: the presence of water has been argued to stop excited-state proton transfer in 7-azaindole [32,118]. Hydrogen bonding impurities are known to retard excited-state proton transfer in 3-hydroxyflavone [119,127].

While both of these arguments are plausible, it remains to be explained why hypericin exhibits weak fluorescence in basic solution (pH > 11, Figure 4.6d). Perhaps at high pH hypericin is less likely to form aggregates. Also, at high pH deprotonation of the β hydroxyl group produces an anion whose charge can be delocalized. Such an anion would of course

Table 4.2. Summary of Analog Photophysics in H_2SO_4/Methanol (v/v) Mixtures

$\%H_2SO_4$	τ_1 (ns)	τ_2 (ns)[a,b]	λ^{max}_{ems} (nm)	I_1/I_2[c]	I_1 (fwhm) (nm)	I_2 (fwhm) (nm)
45	1.8	(0.20) 15.5	582, 646	2.98	65.7	84.8
48	2.0	(0.21) 8.2	582, 625	1.93	37.7	55.5
52	2.0	(0.22) 8.2	583, 630	2.12	42.0	54.2
54	1.2	(0.62) 8.8	581, 630	2.08	51.7	61.8
56	1.5	(0.82) 12.0	581, 626	1.92	43.3	56.2
58	1.1	(0.82) 11.2	582, 629	1.98	43.7	55.4
60	0.9	(0.87) 12.5	583, 632	2.04	48.7	56.9
80	1.3	(0.93) 15.1	586, 636	2.05	45.4	53.5
100	—	(1.00) 15.0	586, 635	2.10	44.4	49.2

[a] Owing to the low solubility of mesonaphthobianthrone in these solutions, the fluorescence signal was in all cases very small. Hence only 3000-4000 counts could be collected in the maximum channel of any decay curve. This in combination with the use of a full-scale time base of 20 ns, which limits the dynamic range of the experiments, contributes to the uncertainty in the measured lifetime values. For purposes of discussion, we consider the short- and long-lived components to remain constant over the range of mixtures studied. Mixtures that are less than 45% H_2SO_4 afford very little or no observable fluorescence red of ~ 580 nm. [b] λ_{ex} = 288 nm; $\lambda_{em} \geq$ 550 nm; 20°C. Under these detection conditions, the band at 467 nm, characteristic of pure methanol solutions is not observed. The species giving rise to this band has a fluorescence lifetime of ~ 600 ps. The fluorescence lifetimes are thus fit to only

Table 4.2. Continued

a sum of two exponentially decaying components: $F(t) = A_1\exp(-t/\tau_1) + A_2\exp(-t/\tau_2)$, where $A_1 + A_2 = 1$. The value in parentheses is the amplitude of the longer-lived lifetime component. [c] I_1 and I_2 refer to the intensities of the bands at ~ 580 and ~ 630, respectively. The position of these bands is difficult to determine owing to the large width at lower concentrations of H_2SO_4.

Figure 4.6. Absorbance and fluorescence spectra of hypericin in mixtures (v/v) of H_2SO_4 and water: (a) Changes in hypericin absorbance as a function of H_2SO_4 concentration. (b) Changes in hypericin fluorescence as a function of H_2SO_4 concentration; λ_{ex} = 400 nm. The solution that is 33% H_2SO_4 is completely nonfluorescent and superimposable on the baseline. (c) Absorbance of hypericin at low pH. (d) Absorbance of hypericin at high pH. The titration in this figure most likely represents more than two species. Note that the dotted line whose maximum lies between the other two maxima is not obtained at an intermediate pH. In parts (c) and (d) the pH was adjusted with H_2SO_4 and KOH. In (d) the arrow indicates the fluorescence spectrum at pH 13.8. In each panel, the concentration of hypericin is held constant in order to ensure proper normalization of the data.

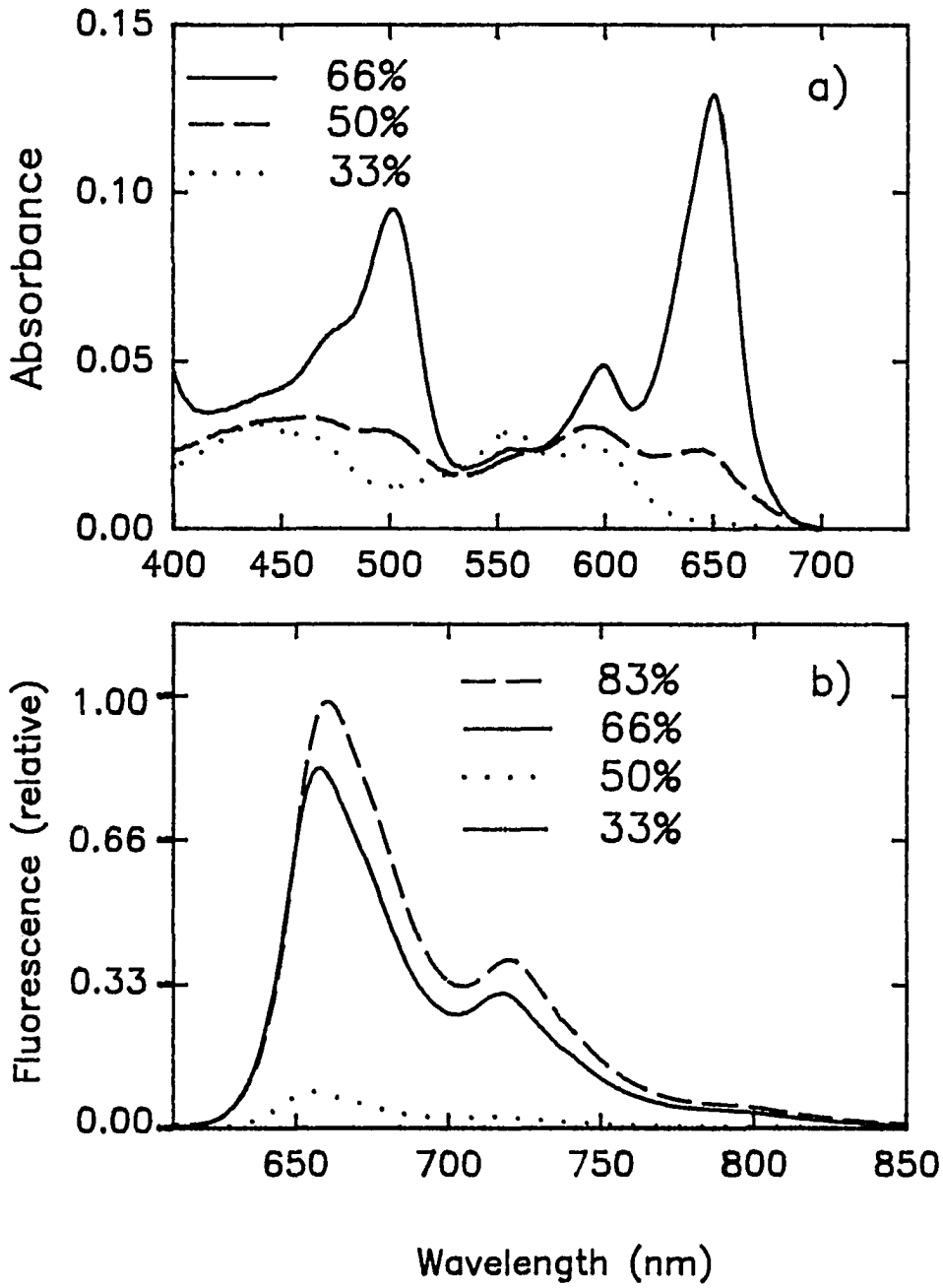
0.15
0.10
0.05
0.00
Absorbance
66%
50%
33%
a)
400
450
500
550
600
650
700
1.00
0.66
0.33
0.00
Fluorescence (relative)
83%
66%
50%
33%
b)
650
700
750
800
850
Wavelength (nm)

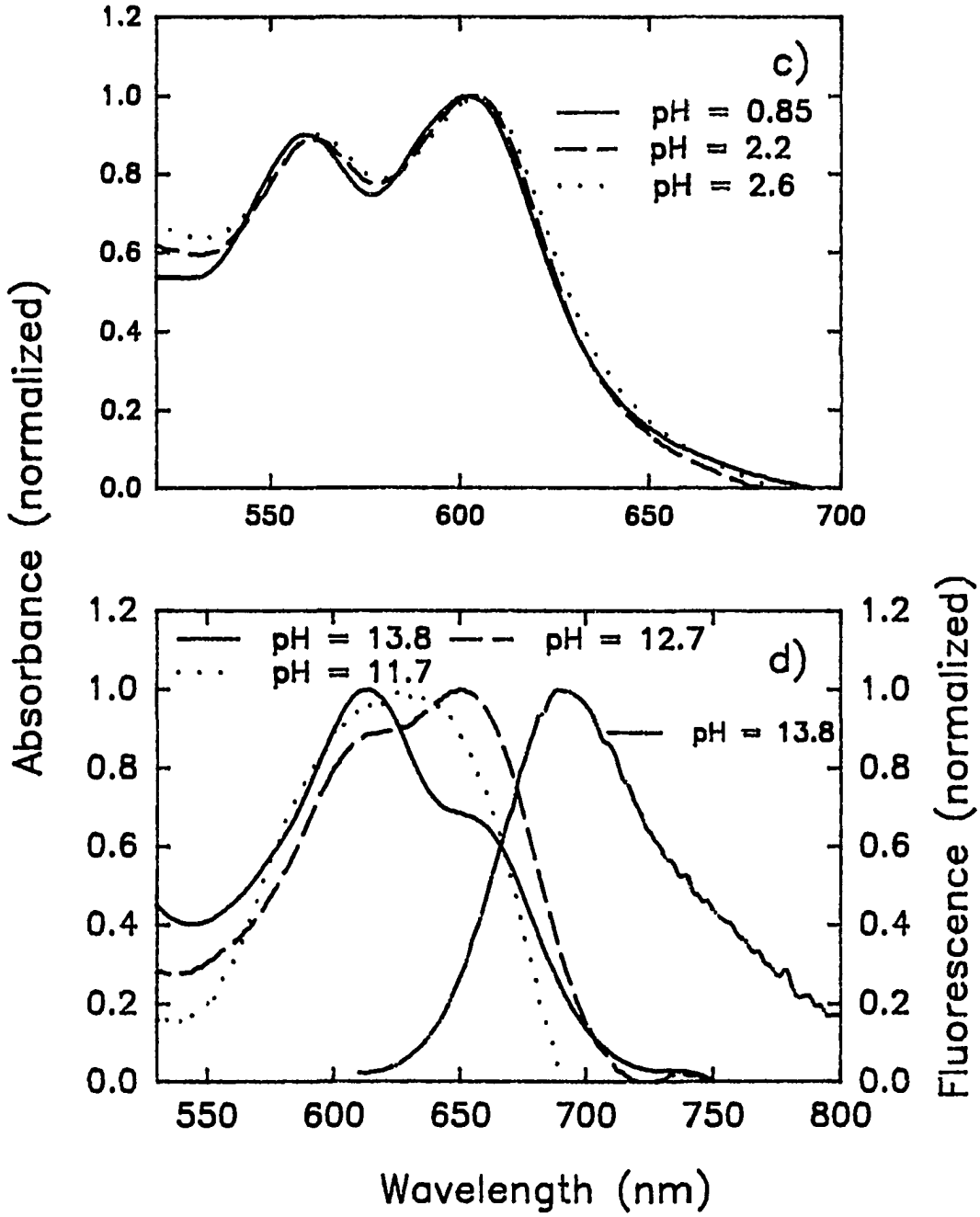

Figure 4.6. Continued

also be produced upon intramolecular proton transfer to the carbonyl.

Further investigation of both ground- and excited-state heterogeneity and the possibility of solute aggregation is afforded by both time-resolved fluorescence and absorption measurements, which are described below.

2. Fluorescence Lifetimes and Anisotropy Decay

Table 4.1 summarizes the fluorescence lifetimes of hypericin obtained in a variety of protic and aprotic solvents. The fluorescence lifetime is always single exponential and usually between 5 and 6 ns in duration. It is relatively insensitive to temperature. Arrhenius plots obtained from the fluorescence lifetime of hypericin in DMSO yield an activation energy of 0.55 kcal/mol. Mesonaphthobianthrone, in either sulfuric or triflic acid yields a single-exponential lifetime of 15 ns (λ_{ex} = 288 nm) either when collecting emission from both bands simultaneously or each band separately.

Lifetime measurements (λ_{ex} = 288 nm, $\lambda_{em} \geq$ 550 nm) were also performed on the mesonaphthobianthrone in mixtures of H_2SO_4 and MeOH. In the solvent mixtures, two lifetime components were obtained whose weights varied as a function of acid concentration (Table 4.2), with the long component (15 ns) dominating at high H_2SO_4 concentrations.

Similar experiments (data not shown) were carried out with mesonaphthobianthrone in H_2SO_4/CH_3CN solutions. The solutions, however, became extremely exothermic at high concentrations of H_2SO_4; and thus solutions with H_2SO_4 higher than 30% were not investigated. The results were identical to those of the H_2SO_4/MeOH experiments with the exception of the lack of a fluorescence band in the blue region of the spectrum (~ 470 nm; see Figure 4.2).

It has been suggested that in water hypericin forms nonfluorescent, high molecular weight (> 8000) aggregates [120]. Since the molecular weight of hypericin is 538, this

corresponds to a complex of > 15 molecules. (Song, Yamazaki, and coworkers [130] have suggested that at moderately high pH hypericin forms dimers that are essentially nonfluorescent.) In order to determine that hypericin in the nonaqueous solutions in which it is fluorescent is not aggregated, we measured its fluorescence anisotropy decay in MeOH and DMSO. Because in all cases, using visible or ultraviolet excitation, within experimental error and using the appropriate time resolution, a limiting anisotropy equal to the theoretical limit (r(0) = 0.40) was observed and because the depolarization was complete within 15 ns (Figure 4.7), we conclude that high molecular weight aggregates are negligible in our experiments and that we are investigating primarily the monomer. The anisotropy decay of hypericin is described well by a sum of two exponentially decaying components. The more rapid of these is approximately 80 ps in methanol (Figure 4.7a). In order to resolve this component and the limiting anisotropy accurately and in order to estimate the duration of the longest depolarizing event, the measurements were performed on two different time scales. The data in Figure 4.7b indicate that the slower event is characterized by a 7.1-ns time constant. Hypericin thus may be considered as an example of an approximately symmetric rotor in which two types of depolarizing motion may be observed. The 80-ps component most likely reflects a spinning motion about an axis perpendicular to the plane of the molecule while the 7.1-ns component can be attributed to overall tumbling of the molecule. A simple calculation indicates that the longer of the two components we observe is consistent with such a motion. The rotational diffusion time [121], τ_r, is given by $1/6D = V\eta/kT$, where V is the molecular volume, η is the solvent viscosity, k is Boltzmann's constant, and T is the absolute temperature. Taking hypericin to be a sphere of radius 6.4 Å, a rotational diffusion time of 1.5 ns is obtained for MeOH at 298 K. This time is certainly a lower limit since the effective molecular volume of hypericin would be expected to be larger owing to hydrogen bonding of the hypericin hydroxyl groups (in the bay region, most likely) to the solvent.

Figure 4.7. Fluorescence anisotropy decay of hypericin in methanol, λ_{ex} = 288 nm, $\lambda_{em} \geq 345$ nm, 20°C. The measurements were performed with the apparatus employing a rotating analyzer polarizer described elsewhere [33] and using a full-scale time base of (a) 3 ns and (b) 15 ns. The results are as follows. (a) $r(t) = 0.23 \exp(-t/79 \text{ ps}) + 0.18$, $\chi^2 = 1.4$. The bump at ~ 0.5 ns in the upper curve (parallel intensity) is due to the instrument function. (b) $r(t) = 0.141 \exp(-t/98 \text{ ps}) + 0.003 \exp(-t/7100 \text{ ps})$, $\chi^2 = 1.7$. Similar results are obtained using visible (576 nm) excitation. Although the 15-ns time base is too coarse to resolve accurately the fast decay component and, more importantly, the limiting anisotropy demonstrates clearly that the curves for the parallel and perpendicular intensities coalesce on this time scale. As discussed in the text, the duration of the slower component of anisotropy decay obtained from the fit, 7.1 ns, is reasonable for a sphere of the dimensions of hypericin undergoing rotational diffusion in methanol.

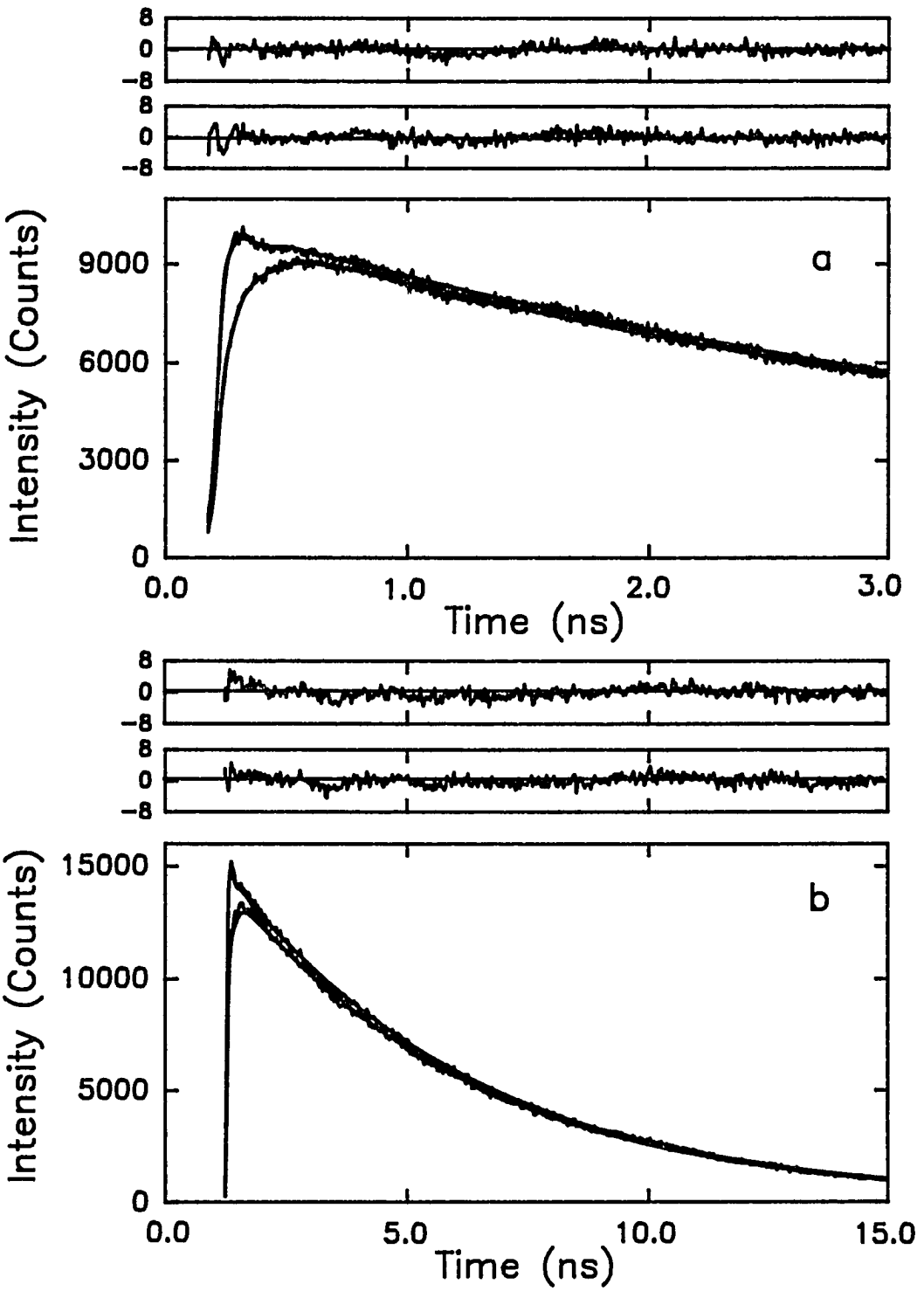
8
0
-8
8
0
-8
Intensity (Counts)
9000
6000
3000
0
a
0.0
1.0
2.0
3.0
Time (ns)
8
0
-8
8
0
-8
Intensity (Counts)
15000
10000
5000
0
b
0.0
5.0
10.0
15.0
Time (ns)

Finally, given the inhomogeneity of the hypericin sample, the observation that in all cases where the appropriate time resolution is employed (Figure 4.7a) the limiting anisotropy of 0.40 is obtained indicates that the distribution of absorbing and emitting transition dipole moments are all parallel, within experimental error.

3. Time-Resolved Absorption Measurements

a. Excited-State Absorption and Stimulated Emission

Figures 4.8a-c present time-resolved spectra of hypericin upon optical excitation. At least three distinct events are apparent in Figure 4.8a: ground-state bleaching; excited-state absorption arising from a newly generated species; and stimulated emission. As we have demonstrated elsewhere [113], the species producing the new absorption decays in 6-12 ps, depending on the solvent. The spectrum of the stimulated emission requires an identical time in order to be fully evolved. In CH_3CN, this time is about 10 ps (Figure 4.8b).

At longer wavelengths (Figure 4.8c) a broad photoinduced absorption is apparent in both hypericin and mesonaphthobianthrone in all the solvents investigated. As we suggested elsewhere [113] and as we conclude below (see Figure 4.11), this broad absorption arises from a solvated electron. The extent to which the spectrum shifts and overlaps that of the stimulated emission can render the determination of whether the electron is produced monophotonically or biphotonically difficult [113].

Figure 4.8d presents a spectrum of nile blue taken with our transient absorption spectrometer superimposed upon a nile blue spectrum obtained with a conventional steady-state double-beam spectrometer. The agreement between the two is excellent and provides a high level of confidence in the results obtained from the time-resolved absorption apparatus.

Tuning the probe wavelength to the absorption feature appearing in the region from 620 to 635 nm for hypericin in MeOH (a similar feature is present from 630 to 645 nm in

Figure 4.8. Time-resolved absorption spectra. (a) Excited-state spectrum of hypericin in DMSO at "time zero". The horizontal line is the control experiment obtained by making the probe precede the pump pulse. At negative delay times no signal is expected, as is observed. This spectrum should be compared to that taken for hypericin in methanol [113] in order to appreciate the spectral shift induced upon changing solvent. At least three events are observed. From shorter to longer wavelength they are bleaching of the ground-state absorption ($\lambda < 630$ nm, compare with the steady-state absorption spectrum, Figure 4.2a); appearance of a new species giving rise to absorption (630 nm $\leq \lambda \leq$ 645 nm); and negative absorption (stimulated emission, $\lambda > 645$ nm), which appears in a region where there is no ground-state absorption and hence cannot be attributed to bleaching. (b) Growth of stimulated emission from hypericin in CH_3CN as a function of time. Spectra are shown for a "zero-time" delay (pump superimposed on probe pulse) and a 10-ps time delay. (c) Excited-state spectrum of hypericin and mesonaphthobianthrone in DMSO at long wavelength (770 nm $\leq \lambda \leq$ 830 nm). As discussed in the text and in the caption to Figure 4.10, this broad absorbance in the red is attributed to a solvated electron that is produced biophotonically. (d) Test of the time-resolved absorption spectrometer by superimposing a spectrum of nile blue in ethanol on one obtained with a conventional double-beam steady-state spectrometer (- - -).

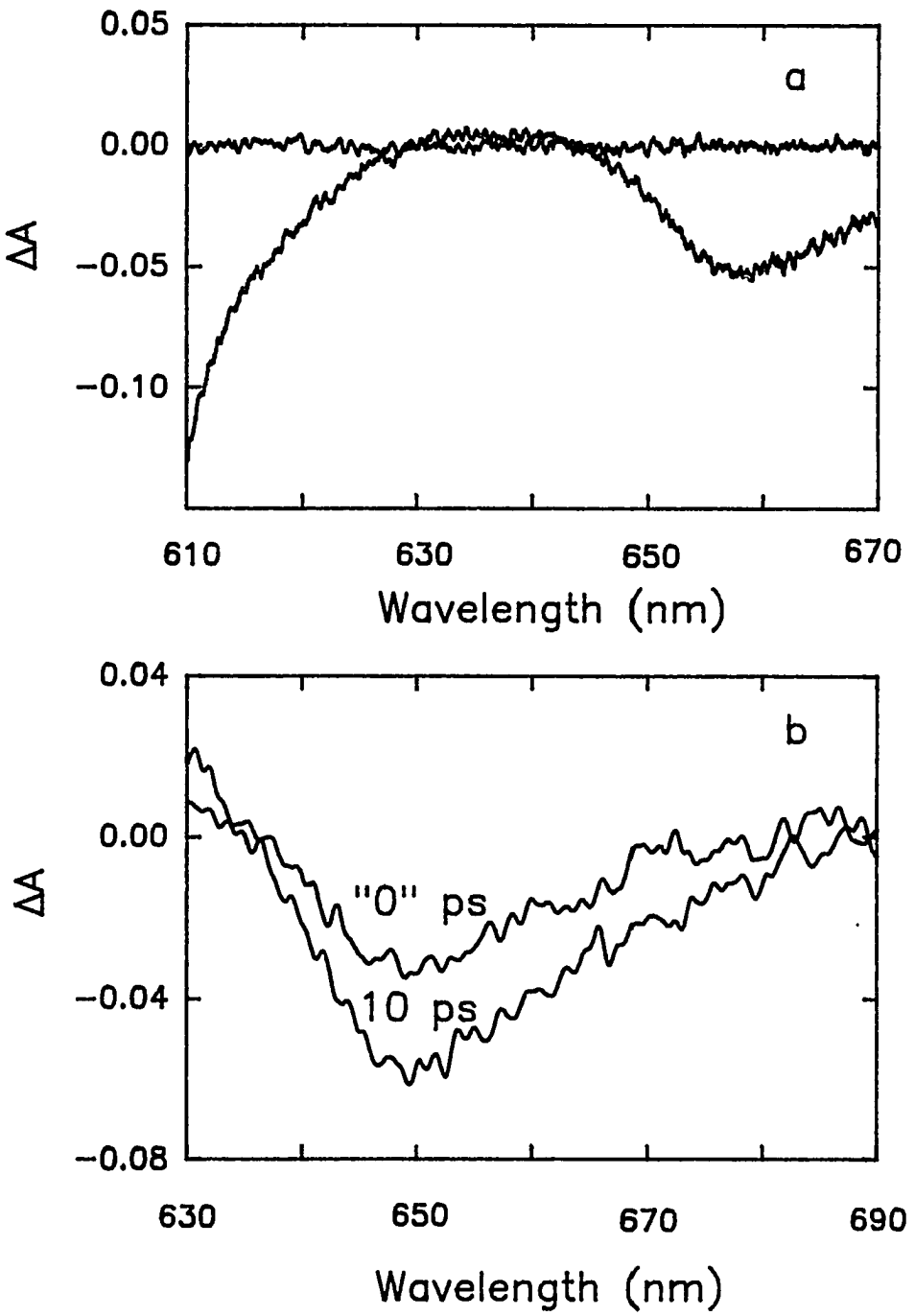
0.05
0.00
−0.05
−0.10
ΔA
a
610
630
650
670
Wavelength (nm)
0.04
0.00
−0.04
−0.08
ΔA
b
"0" ps
10 ps
630
650
670
690
Wavelength (nm)

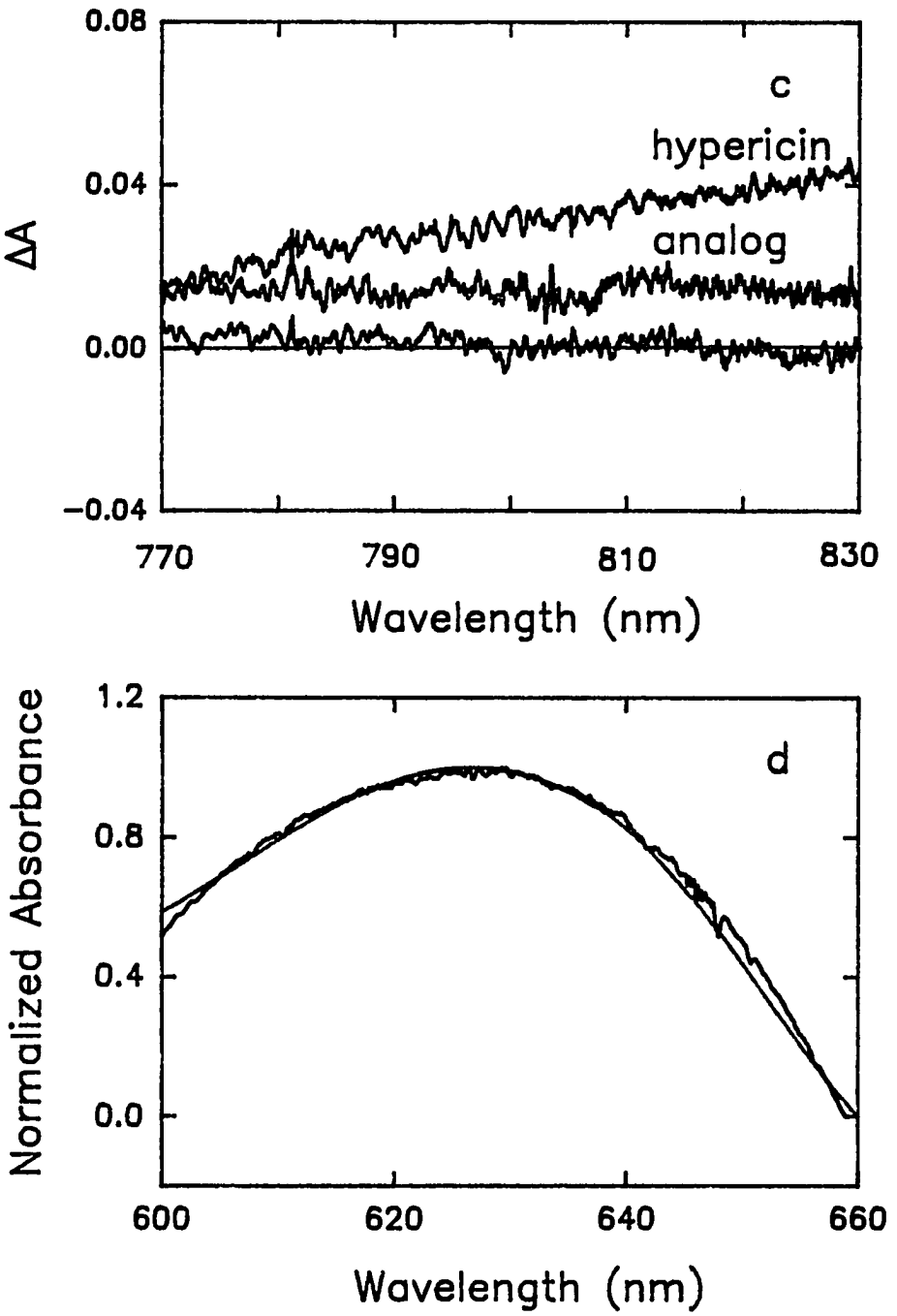

Figure 4.8. Continued

DMSO) permits the observation of a rapid decay component of about 6 ps [113]. Because this excited-state species absorbs in a region where there is ground-state absorbance, bleaching measurements of the ground state of hypericin yield a finite rise time. Thus, measurement of the time required to bleach fully the ground state provides an alternative and, because of the larger signal, more accurate method of determining the lifetime of the short-lived excited state produced upon light absorption. Figure 4.9 presents such ground-state bleaching measurements for hypericin in MeOH, MeOD, and DMSO. Within experimental error, deuteration of the solvent does not affect the decay of the excited state. Also, no isotope effect is observed when deuterated hypericin is used. A similar result has been reported for 3-hydroxyflavone [119] and for benzothiazole [122]. The absence of an isotope effect was used [122] to rule out tunneling as the mechanism of proton transfer and to point out that vibrational degrees of freedom other than O-H or O-D are involved in the proton or deuteron transfer.

The stimulated emission, to which we have referred above, arises from a fluorescent excited-state species. Figure 4.10 demonstrates that the stimulated emission rises with time constants of 6.7 and 9.2 in MeOH and DMSO, respectively. (Figure 4.11f indicates a similar result for CH_3CN.) Within experimental error, the time constants for the rise time of stimulated emission are identical to those obtained, from ground-state bleaching measurements, for the decay of the excited-state produced at time zero. We conclude, therefore, that this excited-state species decays into the fluorescent species, which in turn gives rise to the stimulated emission.

Comparison of the kinetics of the stimulated emission (Figures 4.10 and 4.11f) indicates that in all cases there is a component that appears instantaneously and decays in less than 2 ps. We argue below that this component results from the ground-state heterogeneity of hypericin: that is, from an equilibrium between the untautomerized (or normal) form and a

Figure 4.9. Time delay for the bleaching of hypericin at 22°C.

(a) MeOH, λ_{ex} = 588 nm and λ_{probe} = 600 nm: $\Delta A(t) = 0.10\exp(-t/5.6\text{ ps}) - 0.21$;

(b) MeOD, λ_{ex} = 588 nm and λ_{probe} = 600 nm: $\Delta A(t) = 0.07\exp(t/6.4\text{ ps}) - 0.16$;

(c) DMSO, λ_{ex} = 588 nm and λ_{probe} = 610 nm: $\Delta A(t) = 0.23\exp(-t/9.6\text{ ps}) - 0.41$;

(d) H_2SO_4, λ_{ex} = 588 nm and λ_{probe} = 630 nm. The bleaching is fully developed within the time resolution of the apparatus. This result argues for the protonation of both carbonyl groups of hypericin in the ground state.

Struve and coworkers [123] have also observed a finite rise time for the ground state bleaching of stentorin.

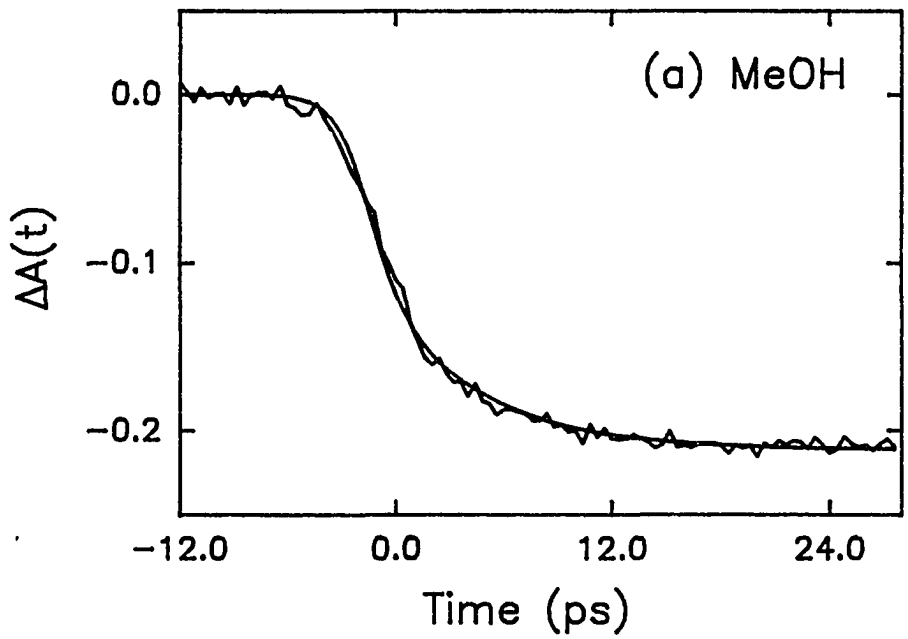
(a) MeOH
0.0
−0.1
−0.2
ΔA(t)
−12.0
0.0
12.0
24.0
Time (ps)

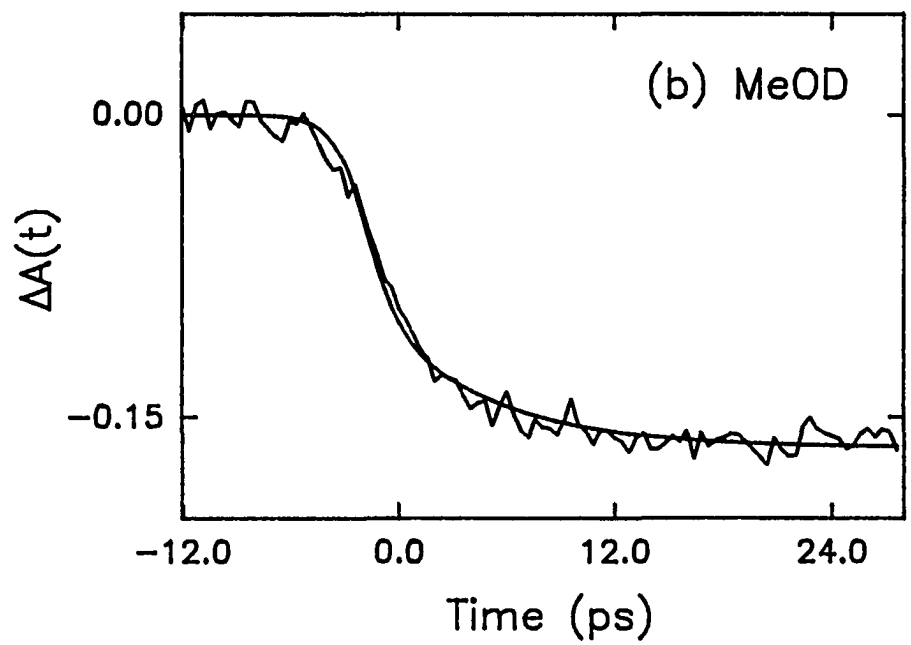
(b) MeOD
0.00
−0.15
ΔA(t)
−12.0
0.0
12.0
24.0
Time (ps)

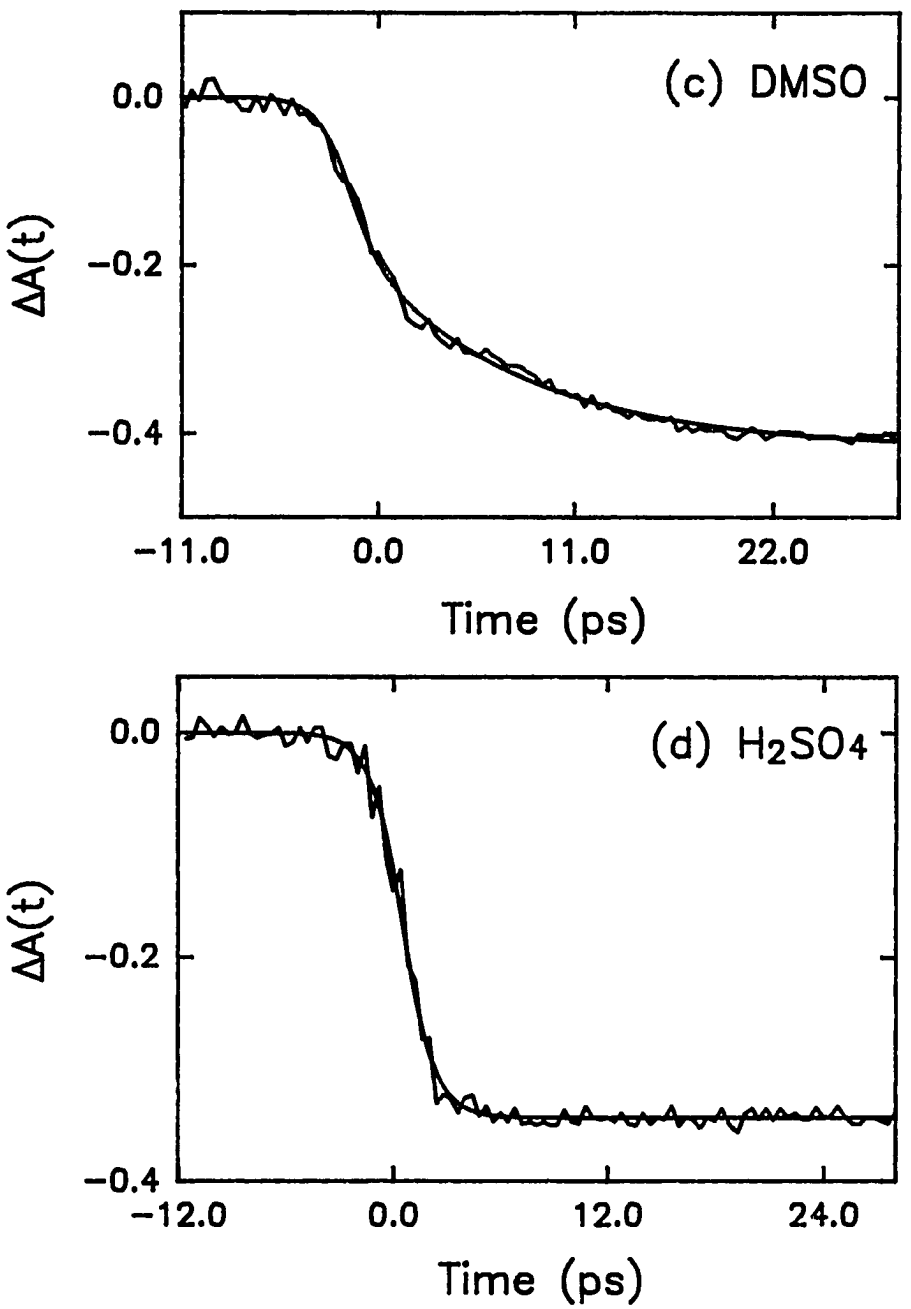

Figure 4.9. Continued

Figure 4.10. Kinetics of stimulated emission in hypericin. Note in each case the component that appears instantaneously. Compare these results also with the data for CH_3CN (Figure 4.11f).

(a) MeOH: λ_{ex} = 588 nm and λ_{probe} = 645 nm: $\Delta A(t) = 0.17[\exp(-t/6.7\text{ ps}) - 1] - 0.14\exp(-t/1.9\text{ ps})$.

(b) DMSO: λ_{ex} = 588 nm and λ_{probe} = 658 nm: $\Delta A(t) = 0.30[\exp(-t/9.2\text{ ps}) - 1] - 0.13\exp(-t/1.9\text{ ps})$.

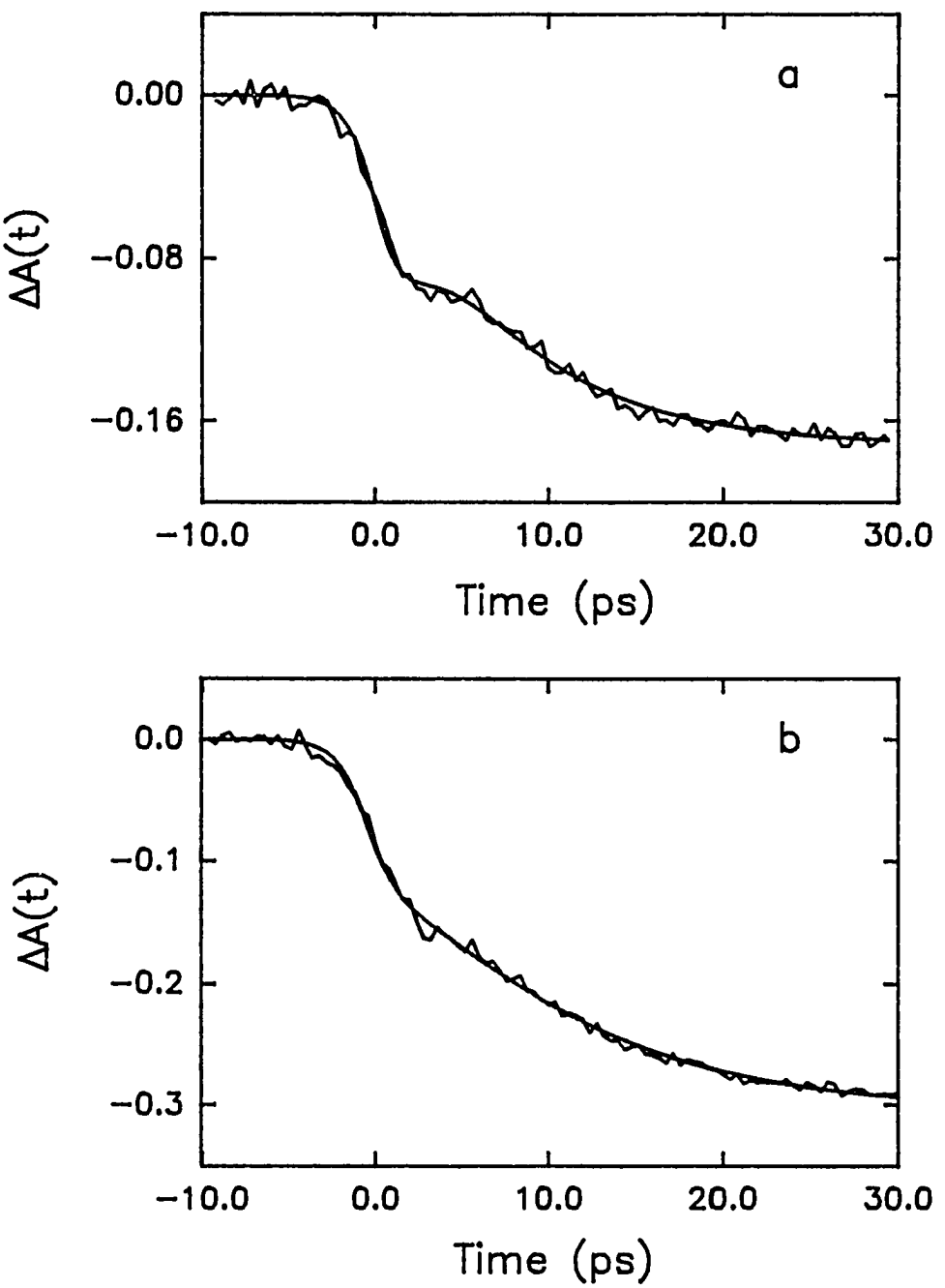
a
0.00
−0.08
−0.16
ΔA(t)
−10.0
0.0
10.0
20.0
30.0
Time (ps)
b
0.0
−0.1
−0.2
−0.3
ΔA(t)
−10.0
0.0
10.0
20.0
30.0
Time (ps)

partially tautomerized form. This component is not observed for hypericin or for the hypericin analog, mesonaphthobianthrone in concentrated H_2SO_4, where in the ground state the two carbonyl sites are expected to be protonated. It is possible that the fast component observed in the stimulated emission signal arises from vibrational relaxation of a "hot" tautomer or other excited state. We tentatively rule out this explanation because the duration of the component is independent of excitation wavelength.

Hypericin in H_2SO_4 (λ_{ex} = 588 nm) exhibits only instantaneous bleaching (Figure 4.9d) at probe wavelengths of 600, 630, 660, and 690 nm. The absence of a finite bleaching time for hypericin in H_2SO_4 is significant. In the light of the discussion below and Figure 4.12, this result can be interpreted in terms of complete protonation of the carbonyl groups in the ground state. For hypericin in H_2SO_4 (λ_{probe} = 755 nm), an absorbance is detected that does not decay on a $\geq$ 20-ps time scale. We have also investigated the transient spectra of mesonaphthobianthrone in both DMSO and H_2SO_4. In DMSO between 500 and 720 nm, no signal was detected. The inability to resolve absorption transients is consistent with the lack of steady-state fluorescence and demonstrates the very short excited-state lifetime (< 1 ps) of the unprotonated species. Between 770 and 830 nm, a positive absorption feature was observed. In all cases, the long-lived transient absorbing at long-wavelengths is assigned to a solvated electron (Figure 4.11 and discussion below).

b. Photoionization Is Biphotonic

Previously we proposed that [113] hypericin (in methanol) produced photoelectrons; but we were unable to determine whether photoionization was monophotonic or biphotonic because of the overlapping spectral contributions of stimulated emission and absorbance from the solvated electron. Figure 4.11 presents a series of results that demonstrates that photoionization occurs in hypericin and that it occurs biphotonically.

Figure 4.11. Demonstration that the species absorbing at long-wavelengths is a solvated electron that is produced biphotonically.

(a) Hypericin in (—) methanol and in (- - -) methanol that is 1.0 M in acetone. Acetone is known to be an electron scavenger [53]. λ_{ex} = 588 nm, λ_{probe} = 750 nm.

(b) Indole, which is known to produce electrons monophotonically [101,37]: Top, indole in methanol; Middle, indole in methanol that is 1.0 M in the electron scavenger, acetone; Bottom, probe pulse at negative delay to provide a baseline or control experiment. λ_{ex} = 294 nm.

(c) Plot of $\log\Delta A(t = 0)_{790\ nm}$ vs $\log(I_{ex})$ for hypericin in methanol. λ_{ex} = 588 nm. Although the blackened circles can be fit to a slope of 0.9 ± 0.3, the presence of stimulated emission in this spectral region renders interpretation of the slope ambiguous [113]. Note that at higher excitation or pump pulse energies, the points deviate from the line of approximately unit slope. The open circles represent a regime where the pump is so intense that the photoelectron signal begins to saturate.

(d) Plot of $\log\Delta A(t = 0)_{790\ nm}$ vs. $\log(I_{ex})$ for hypericin in DMSO. λ_{ex} = 588 nm. In this case, the blackened circles can be fit to a slope of 2.3 ± 0.3. The difference in slope between this example and that of methanol is most likely due to the spectral shifts induced by the solvents. Compare for example Figures 4.2a and 4.8a of this article with the corresponding Figures of reference 113.

(e) Hypericin in CH_3CN, λ_{ex} = 588 nm, λ_{probe} = 645 nm.

(f) Hypericin in CH_3CN, λ_{ex} = 588 nm, λ_{probe} = 645 nm. Here, however, the pump intensity in reduced by a factor of 10 with respect to that for the experiment in panel (e). $\Delta A(t) = 0.19[\exp(-t/11.2\ ps) - \exp(-t/\infty)] - 0.19\exp(-t/1.4\ ps) + 0.025$.

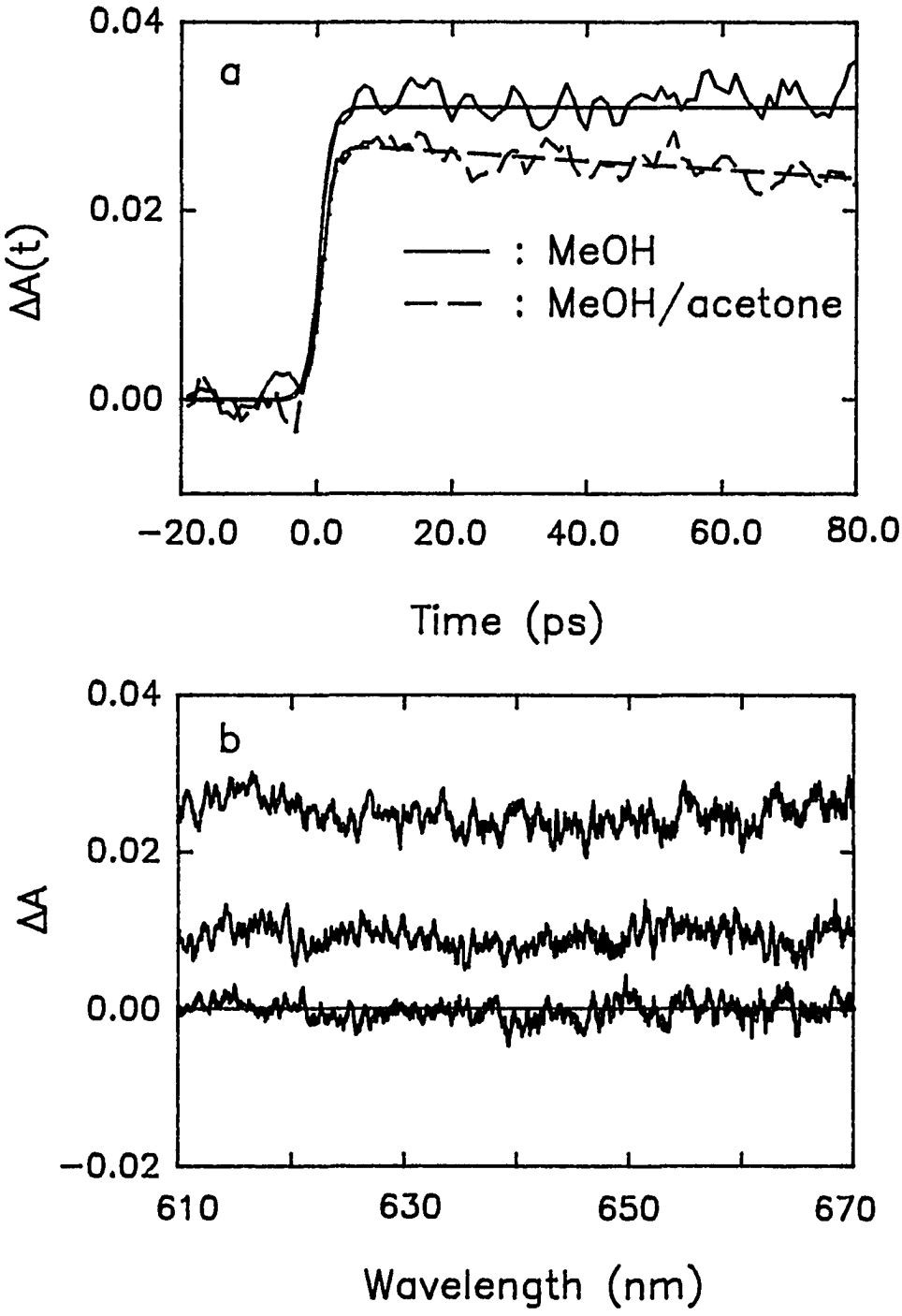
a
0.04
0.02
0.00
ΔA(t)
: MeOH
: MeOH/acetone
−20.0
0.0
20.0
40.0
60.0
80.0
Time (ps)
b
0.04
0.02
0.00
−0.02
ΔA
610
630
650
670
Wavelength (nm)

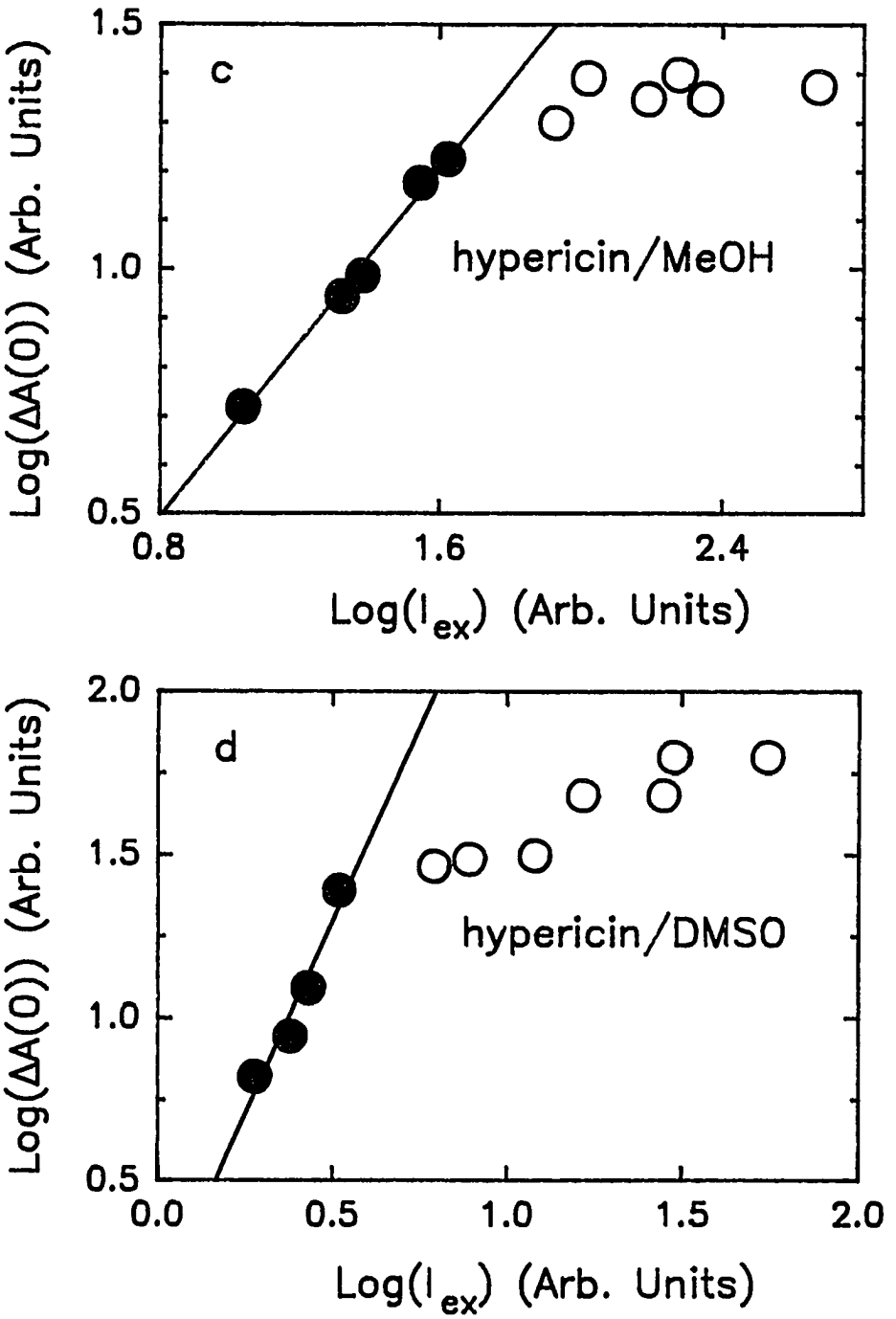

Figure 4.11. Continued

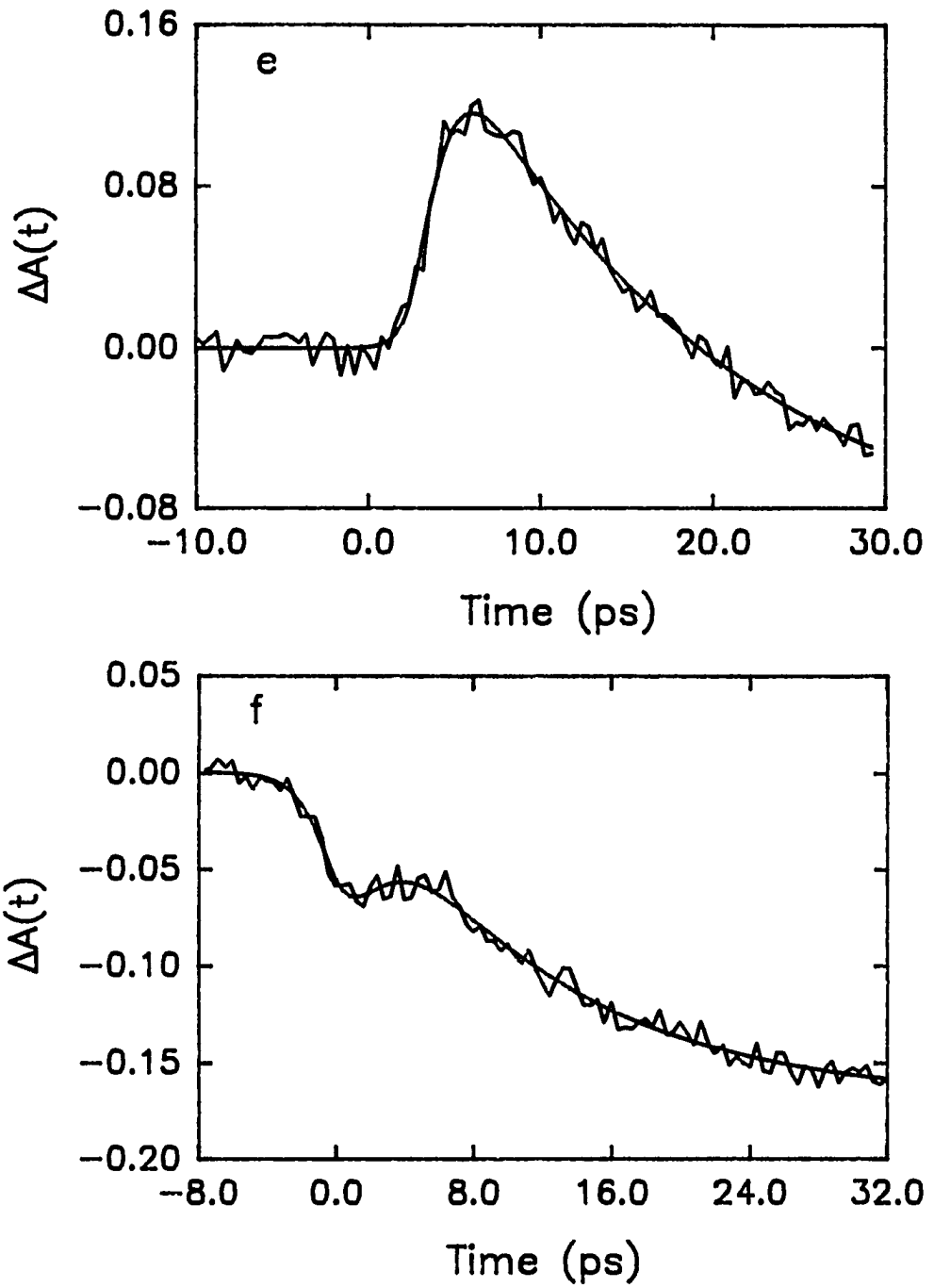

Figue 4.11. Continued

Excited-state absorption at 750 nm is demonstrated in hypericin in methanol upon photoexcitation. This absorption can be quenched by addition of acetone (1.0 M solution), an electron scavenger [53] (Figure 4.11a). The spectrum of this absorbing species in methanol is given in reference 113 and it is consistent with known spectral data for the solvated electron in methanol [58]. Furthermore, as a control experiment we demonstrate the production and quenching of solvated electrons from indole, which is known to photoionize [101,37] (Figure 4.11b). Whether photoionization occurs monophotonically is usually determined [101,37,52] by plotting the logarithm of the electron yield (or something proportional to it, such as its optical density) against the logarithm of the pump intensity. The slope of the resulting line gives the number of photons involved in the ionization process. Although at low pump intensity the slope is 0.9 ± 0.3 for hypericin in methanol, this result is <u>not</u> unambiguous evidence of monophotonic ionization because of the overlapping contribution of stimulated emission, which provides an apparent diminution of the electron absorption (Figure 4.11c). In DMSO, on the other hand, the ground- and excited-state spectra of hypericin are sufficiently different that the log-log plot yields a slope of 2.3 ± 0.3 (Figure 4.11d).

Finally, another convincing piece of evidence for the biphotonic ionization of hypericin is the measurement of the kinetics of transient absorption in a region where both stimulated emission and electron absorption may be present (Figures 4.11 e, f). At high pump intensities an initial strong transient absorbance is observed for hypericin in CH_3CN. When the pump intensity is decreased by a factor of ten, all that is observed is the stimulated emission described above.

D. Discussion

1. Assignment of Excited-State Processes

Figure 4.12 presents ground- and excited-state kinetic schemes for mesonaphthobianthrone that are consistent with the data. Time-resolved fluorescence measurements in H_2SO_4/MeOH mixtures indicate the presence of two lifetime components, ~ 2 and ~ 15 ns, whose amplitudes change with acid concentration. The amplitude of the 15-ns component increases with acid concentration. Furthermore, no rise time for fluorescence is observed for the mesonaphthobianthrone. Similarly, contrary to the case of hypericin, no measurable rise time is observed in the bleaching of the ground-state absorption and no rapid (6-12-ps) decay component is observed in the excited-state absorption of mesonaphthobianthrone.

Bearing in mind these above results and noting that protonation of the carbonyls of mesonaphthobianthrone cannot arise from any intramolecular source and that the fluorescence lifetime of mesonaphthobianthrone is very short-lived, which is demonstrated by the absence of steady-state fluorescence in DMSO and the inability to observe any excited-state absorption even with ~ 1-ps resolution, the ground-state equilibrium is considered in terms of two parallel protonation equilibria. We propose that in the ground state, the unprotonated, the singly protonated, and the doubly protonated species exist together in equilibrium. Upon optical excitation, at time zero, this same ground-state population is projected into the excited state in proportion to the relative extinction coefficients. We note that identical kinetic data are obtained using either excitation wavelengths of 294 or 588 nm. The short fluorescence lifetime of the unprotonated species prevents an excited-state equilibrium from being established with the singly- or doubly-protonated species. The argument against sequential ground-state protonation equilibria is that if, as we propose, the singly- and doubly-protonated

Figure 4.12 Kinetic schemes for (a) mesonaphthobianthrone and (b) hypericin taking into account both ground- and excited-state species. The structures of mesonaphthobianthrone and hypericin are abbreviated; and only two of the six hydroxyl groups of hypericin are indicated in the figure. The schemes presented are the simplest that are consistent with the experimental data. Because of the irresolvably short excited-state lifetime of unprotonated mesonaphthobianthrone (a), an excited-state equilibrium is not expected to be established with either of its protonated forms. For the sake of completeness, we note that for the case of hypericin (b) it may be possible that N^* undergoes a two-proton transfer reaction that converts it directly to DT^*. In part (b) of this figure as well as in Figure 4.1, the proton is shown to interact strongly with the carbonyl oxygen by means of a hydrogen bond. This interaction is reasonable given the rapidity of the excited-state process as well as the observation that hydrogen-bonding solvents do not interfere with the rate of the process [131] (methanol and DMSO give qualitatively similar results), as is observed for example in 3-hydroxyflavone [119]. It must be borne in mind, however, that the proton-transfer reaction is a charge-transfer process and that the tautomer is likely to possess some ionic or charge separated character which is oversimplified by the figures presented here. In support of this ionic character is the observation that the time constant for the excited-state process decreases with increasing solvent polarity [131].

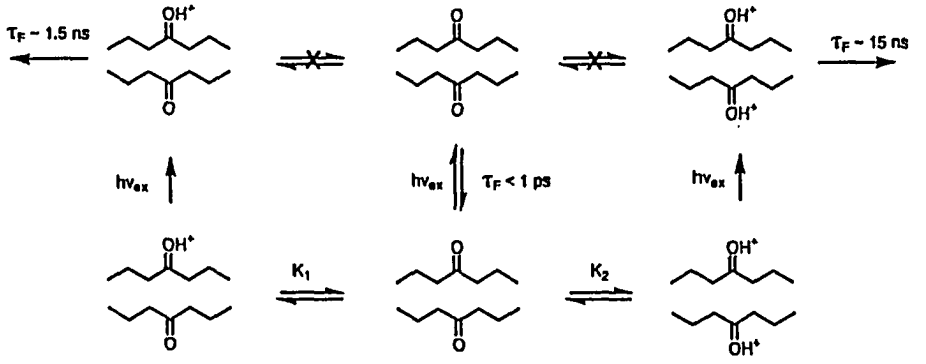

(a) mesonaphthobianthrone

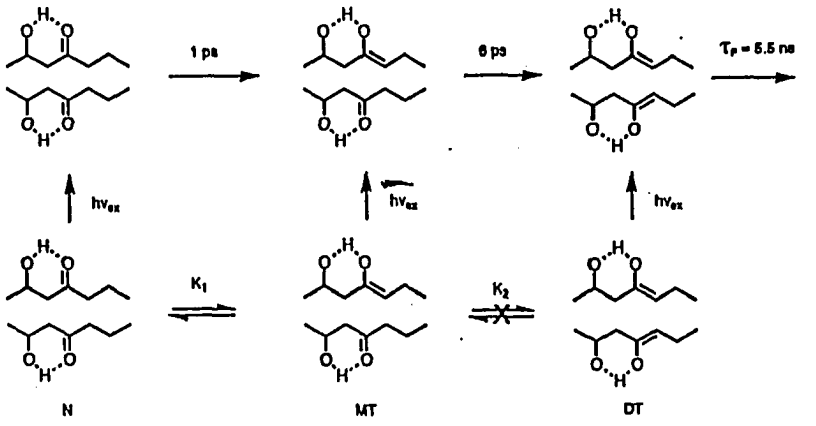

b) hypericin

species have lifetimes of 2 and 15 ns, respectively, then the 15-ns component would be expected to appear with an ~ 2-ns rise time, which is not observed.

The case for hypericin is similar, but not identical to, that of mesonaphthobianthrone. The fundamental difference is that the hydroxyl groups β to the carbonyls provide an intramolecular source of protons that is lacking in the deshydroxy analog. Also, the observation of a finite ground-state bleaching time that corresponds with the decay time of an excited-state absorption and stimulated emission suggest that the protonation equilibria of hypericin are sequential. A possible explanation for the hypericin photophysics is the following. In the ground state, three species (at least) may coexist in equilibrium: the untautomerized or "normal" form, N; the monotautomerized form, MT; and the ditautomerized form, DT. By analogy with mesonaphthobianthrone, DT corresponds to the species with the long (~ 6 ns) fluorescence lifetime. Because stimulated emission corresponding to a long-lived component does not appear instantaneously (within our resolution), we suggest that the population of DT in the ground state is negligible. On the other hand, the heterogeneity of the stimulated emission signal from hypericin in DMSO and CH_3CN may be attributed to significant ground-state population of both N and MT. By analogy with mesonaphthobianthrone in DMSO, the normal form of hypericin is expected to have a very short fluorescence lifetime, whose duration can be estimated from the stimulated emission signals as 1-2 ps. An interesting observation by Weiner and Mazur [30] that is consistent with this description (especially those aspects dealing with ground-state heterogeneity and photoinduced deprotonation of the hydroxyl group) is that hypericin in the absence of light yields an EPR signal that is enhanced upon illumination. They suggest that the EPR signal resembles that of a semiquinone radical.

It is likely that N^* undergoes a rapid one-proton transfer to produce MT^* (Figure 4.12). In order to produce a significant amount of MT^*, the one-proton reaction would need

to occur in 1-2 ps. (It is also possible that N^* executes a double-proton transfer to form DT^* directly.) In several systems excited-state proton transfer has been shown to occur on a time scale of hundreds of femtoseconds [119,122,128]. Of particular relevance to the problem of hypericin are the 1-(acylamino)anthraquinones [128] and disubstituted anthraquinones [129]. For example, Barbara and coworkers have shown that excited-state proton transfer occurs in $\leq$ 100 fs in 1-(dichloroacetylamino)anthraquinone.

We tentatively assign the 6-12 ps rise time in the stimulated emission signals to a one-proton transfer reaction converting MT^* to DT^*. We thus attribute the excited-state species of corresponding decay time in the transient absorption measurements (reference 113 and Figure 4.9) to MT. There are three possible reasons why a 6-12-ps decay component is not observed in the stimulated emission data. The first is that in the ground state [N] > [MT]. The second is that at the probe wavelengths we employ, the emission intensity of MT^* is negligible compared to that of N^* and DT^*. The third is that if indeed the reaction $N^* \rightarrow MT^*$ occurs, the stimulated emission from MT^* at the probe wavelength will be compensated for, at least partially, by the excited-state absorption of MT^*.

Song, Yamazaki, and coworkers [130] have recently presented steady-state spectra and fluorescence lifetimes of hypericin under various conditions. They argue that the excited-state pK_a of hypericin is larger than that of the ground state: 12.2 as opposed to 11.7 (Falk and coworkers [133] have made similar arguments). They also propose, based on comparison of the fluorescence spectra of related compounds, that hypericin has no substantial intramolecular hydrogen bonding. Consequently, they suggest that if excited-state proton transfer is an important nonradiative process in hypericin, such a process is intermolecular and not intramolecular. These conclusions clearly differ from ours. First, it is unlikely that the pK_a of the fluorescent species of hypericin can be measured since it is formed from a species that decays in 6-12 ps. Determination of pK assumes that equilibrium can be established

between the conjugate acid and base. Second, while comparisons with the spectra of analogs such as anthraquinones are instructive, they must take into account the nonaggregated species of hypericin existing in both the ground and the excited states. Third, insofar as we are justified in using the fluorescence spectra of mesonaphthobianthrone and hexamethylhypericin in H_2SO_4 to attribute the long-lived fluorescence in hypericin to a species with protonated carbonyl groups, the presence of the 6-12-ps rise time for long-lived fluorescence in both aprotic and protic solvents demonstrates that in hypericin proton transfer occurs in the excited state and intramolecularly. Fourth, and most importantly, our observation of stimulated emission that rises in 6-12 ps into a long-lived species indicates that steady-state fluorescence and conventional photon counting measurements do not measure the primary photophysical events in hypericin.

2. Potential Difficulties and Unresolved Questions

There are several questions that arise from the results presented upon and from the conclusions drawn from them. We summarize them here and try to respond to them.

(1) A possible objection to the assignment of the excited-state process in hypericin to a tautomerization reaction is the observation of a "mirror symmetry" relationship between the fluorescence spectrum and the visible absorption spectrum (Figure 4.2). We suggest that the observation of a mirror symmetry between the emission and the absorption spectra is consistent with the excited-state proton transfer process if it is kept in mind that tautomerized hypericin, in the form of MT, already exists in the ground state. We argue that MT is similar enough to DT structurally that absorption by MT and fluorescence from DT^* is what produces the mirror symmetry.

(2) The assignment of the excited-state process to intramolecular proton transfer may be criticized because we do not observe an isotope effect. There is precedent for proton

transfer processes that do not exhibit an isotope effect [119,122]. Whether an isotope effect is observed will also depend on such factors as the degree to which the reaction is nonadiabatic and characterized by tunneling through a potential barrier [132] or if the reaction occurs by means of a barrierless (or small barrier) process in which the role of vibrational motions other than the O-H stretch are important. The solvent dependence of the time constant for the excited-state process is also consistent with its assignment to proton transfer. The time constant for the reaction decreases with increasing solvent polarity, as measured by $E_T(30)$, which is consistent for a process that involves the transfer of a charged particle, molecular rearrangement, and charge reorganization [13,139].

(3) Construction of molecular models of hypericin and a recent x-ray structure [136] indicate that the aromatic polycycle is twisted. One might argue that the excited-state transients observed reflect transitions from one form of conformational isomer to another. Because such a process involves a large amplitude motion, it would be expected to be viscosity dependent. In solvents in which the viscosity changes by a factor of 60 we see, however, no more than a change of a factor of two in the time constant of the longer-lived excited-state transient (~ 6-12 ps). Furthermore, the rate of the excited-state process is completely uncorrelated to viscosity: the small variation in rate cited can be effected just a easily when the viscosity is increased by less than a factor of two, i.e. from methanol to acetonitrile [131]. This excludes the assignment to a conformational transition.

(4) The kinetic scheme indicated is not the only one consistent with the data, but it is, we believe, the simplest. There are quite likely more species involved than the few we have depicted. This is certainly suggested by the complexity of the steady-state spectra presented. In particular, we must note that tautomeric forms of DT can exist with the proton being donated from the "upper right" and the "lower left" hydroxyl groups as well as by the "upper left" and "lower left" hydroxyl groups, as indicated in Figure 4.12.

(5) A problem for which at present we do not have a completely satisfactory response is why we observe no emission from MT^*. It may be that there is not a large enough population of the species to be detected in the midst of all the other transients observed. This question requires further investigation.

(6) We have tentatively assigned the rapid decay of N^* to formation of MT^*. Other nonradiative pathways such as internal conversion are also a possibility as is demonstrated by the anthraquinones [128,129]. We note, however, that both the triplet yield and the fluorescence quantum yield of hypericin have been reported to be very high and that $\phi_F + \phi_{ISC} \sim 1$ [110,111]. It thus seems unlikely that other nonradiative processes, besides proton transfer, play a significant role in the deactivation of N^*.

(7) Spectroscopic studies of well-defined synthetically prepared hypericin tautomers will help to clarify the ground- and excited-state chemistry of hypericin. Falk and coworkers [137] have reported the synthesis of a compound, which they identify, based solely upon NMR measurements, as the salt of the hypericin tautomer (DT). This molecule was selected as a target for organic synthesis on the basis of semiempirical calculations (MNDO) [135-138].

The molecule synthesized by Falk and coworkers has an absorption spectrum that is structured and very similar to that of the normal form of hypericin, except that it is slightly blue shifted. Consequently, it bears a mirror image relationship to the fluorescence spectrum of hypericin. This observation is consistent with our argument in point 1 above that partially tautomerized hypericin exists in the ground state. It is also an indication that in the case of hypericin it is not reasonable to require the absence of mirror symmetry between the absorption spectrum of the normal species and the emission spectrum of its fluorescent tautomer.

Falk and coworkers also indicate that upon prolonged heating their compound reforms

the normal species but that irradiation (of an unspecified duration or intensity at an unspecified temperature) is insufficient to convert the normal form to the DT tautomer or vice versa [141]. They argue that the absence of interconvertability in the presence of light precludes an excited-state proton transfer mechanism. Although this conclusion is possible, it is certainly not unique because it assumes that the excited-state potential surface is the same as, or at least very similar to, that of the ground state and because it ignores the multidimensionality of these potential surfaces--that is, the energy must strictly speaking be considered in terms of at least 157 normal coordinates (assuming the solvent coordinates may be neglected).

Figure 4.13 is presented in order to respond to the conclusions of Falk and coworkers. It presents crude approximations of the ground- and excited-state surfaces for hypericin based upon our current knowledge of the system that is summarized largely in Figure 4.12. In the ground state MT lies only slightly in energy above N and is separated from N by a modest barrier. On the other hand, because no long lived fluorescence from hypericin appears instantaneously, DT lies much higher in energy than either MT or N and (based on the work of Falk and coworkers) is also separated from MT by a substantial barrier. The ~ 1-2-ps lifetime of N^* leads us to consider a barrierless transition converting N^* into MT^*. Preliminary temperature-dependent measurements in ethylene glycol [131] indicate that there is a small barrier (~ 1.5 kcal/mol) between MT^* and DT^*. Depending on the location of the minimum of the DT^* potential well with respect to the barrier separating MT and DT, initially prepared N^* will mostly return to MT and ultimately to N.

Figure 4.13 is also capable of explaining the mirror symmetry in the hypericin absorption and emission spectra. The position of the potential well of DT^* affords "cross-well" transitions (both in absorption and emission) between DT^* and MT. A similar cross-well transition has been invoked by Barbara and coworkers to interpret the fluorescence spectra of 1-(acylamino)anthraquinones [128].

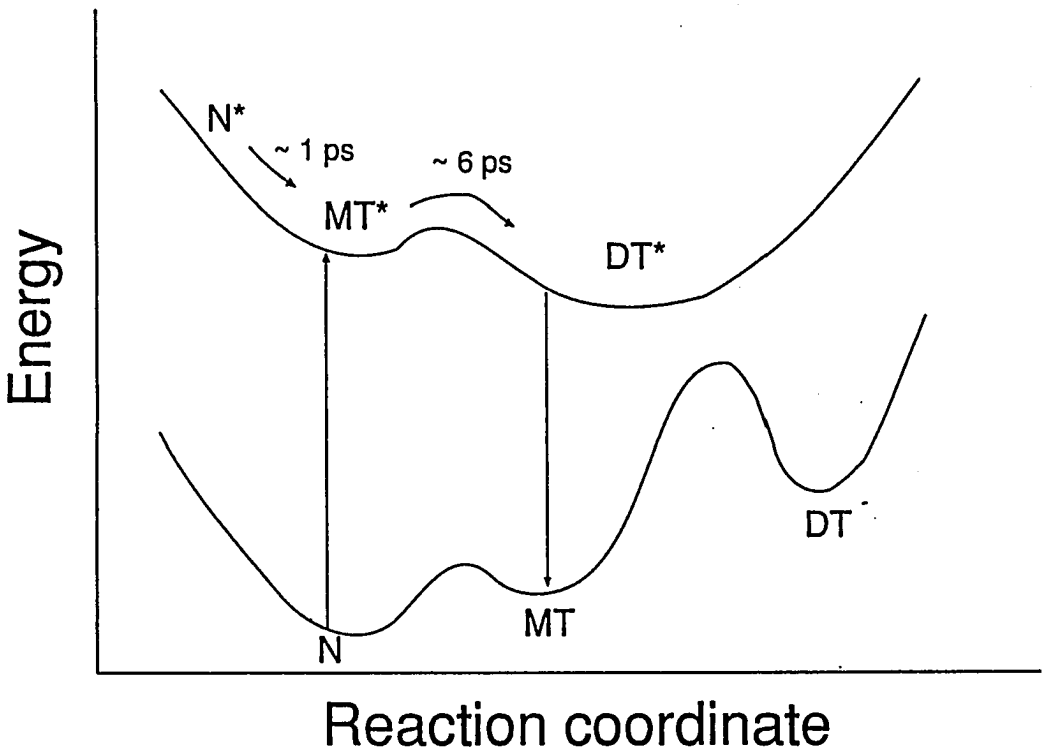

Figure 4.13. Ground- and excited-state energy surfaces of hypericin. See the Discussion. The values given are for methanol. The likelihood of a "cross-well" transition connecting DT^* to MT depends on the coupling of the vibrational levels in the MT^* and DT^* wells. This kind of cross-well transition has been invoked by Barbara and coworkers in their work with anthraquinones [128]. Cross-well transitions have been investigated in detail by Somorjai and Hornig [140].

Finally, it is an open question whether light absorption by the hypericin tautomer, DT, would access the same region of the excited-state potential surface that is probed by exciting the normal form of hypericin, N, and thus allowing it to evolve on this surface. In other words, the fate of N^* is determined by the curvature of the potential energy surface on which it finds itself upon optical excitation, and this in turn is determined by Franck-Condon factors. A priori, there is no reason to assume that the normal form of hypericin, N, will execute a trajectory in which it finishes as DT. The same is true for the hypericin tautomer, DT.

(8) All the results obtained in our laboratory--and elsewhere--support the existence of excited-state tautomerism in hypericin or at least are consistent with it. We have exploited every method currently available to us to verify that excited-state tautomerization occurs in hypericin. The strength of our argument rests on the absorption and emission spectra of the methylated and the deshydroxy hypericins in aprotic and protic solvents taken in conjunction with the transient spectroscopy of hypericin itself. It must be noted, however, that the only indisputable and direct proof for an excited-state proton transfer reaction is the demonstration of the bleaching of the carbonyl stretching frequency as a function of time subsequent to laser excitation. Such measurements require a tunable infrared probe pulse coupled to a visible or ultraviolet pump pulse. Only recently has this type of measurement been performed on molecules generally believed to execute excited-state proton transfer [122]. We are currently preparing an experiment with a picosecond, tunable infrared probe pulse.

E. Conclusions

The deshydroxy hypericin analog, mesonaphthobianthrone, and hexamethylhypericin have proved useful in elucidating the ground- and excited-state kinetics of hypericin. In aprotic solvents such as DMSO, mesonaphthobianthrone is nonfluorescent and exhibits no

absorbance in the visible region of the spectrum. In a strong acid such as H_2SO_4, however, the absorbance and fluorescence spectra of mesonaphthobianthrone closely resemble those of hypericin in aprotic solvents. Similarly, only in sulfuric acid do the absorption and emission spectra of hexamethylhypericin resemble those of hypericin. These results are most easily explained by requiring the fluorescent states of both mesonaphthobianthrone and hypericin to bear protonated carbonyl groups. These results do not indicate what the protonation dynamics are in either the ground or the excited states. Nor do they explain why protonation of the carbonyls so drastically alters the optical spectra.

The presence of two carbonyl groups in the analogs and in hypericin naturally leads to speculation concerning the extent of their protonation in the ground and excited states. Steady-state and time-resolved fluorescence measurements of mesonaphthobianthrone in H_2SO_4/MeOH mixtures proved to be especially useful in investigating solute heterogeneity. The fluorescence spectra in mixed solvents are strongly dependent on the excitation wavelength. Also in the solvent mixtures two lifetime components, ~ 2 and ~ 15 ns, are observed. The shorter component is attributed to a singly protonated carbonyl; the longer component, to a doubly protonated carbonyl. In mixed solvents, both states of protonation are proposed to exist in the ground state because no rise times are detected in the time-resolved fluorescence. In pure H_2SO_4 the doubly protonated species is believed to be predominant because the fluorescence lifetime is 15 ns across the emission spectrum.

Evidence for both ground- and excited-state heterogeneity and for excited-state tautomerization in hypericin comes from transient absorption measurements--and, in particular, the kinetics of stimulated emission from the excited states of hypericin. The finite rise time observed for the appearance of the stimulated emission indicates that a fluorescent species is being created in the excited state. From the titrations of mesonaphthobianthrone, we have inferred that the fluorescent species is protonated at the carbonyl groups. The origin

of the slowly rising stimulated emission component (6-12 ps in the solvents considered here) is attributed to the species that produces a new transient absorption immediately upon excitation (Figure 4.8a) and which is detected either directly through the decay of its absorption or indirectly through the finite bleaching time of the ground state (Figure 4.9). We have suggested that the species producing this absorbance transient is a monotautomer of hypericin that already exists in the ground state in equilibrium with the untautomerized or normal form of hypericin (Figure 4.12). We propose that the normal form of hypericin is revealed in the component of stimulated emission that appears instantaneously and decays in 1-2 ps (Figures 4.10 and 4.11f). Such a rapid decay time of the hypericin species with unprotonated carbonyls is consistent with the absence of fluorescence in mesonaphthobianthrone in aprotic solvents (Figure 4.3). Given the demonstrated heterogeneity of hypericin even in pure solvents (Figures 4.10 and 4.11f), the observation of single exponential fluorescence decay (Table 4.1) is interpreted in terms of the existence of only one species that is long lived enough to produce measurable excited state emission (as detected either by steady-state or traditional photon-counting methods). This fluorescent species is attributed, as discussed above, to a doubly tautomerized hypericin molecule. These conclusions have important implications for the photoinduced biological activity of hypericin and hypericin-like molecules.

The photophysics of hypericin are complicated, and much study is required before the role of light for its antiviral activity and photoreceptor roles is understood. Our results suggest that the primary photoprocess of hypericin is rapid, excited-state proton transfer. Because of the demonstrated antiviral [103-106] and photophobic and phototactic [107] roles played by hypericin and hypericin-like chromophores, elucidating their nonradiative pathways has enormous practical benefits. In addition, this work indicates that hypericin provides an interesting model system with which to study the fundamental aspects of excited-state proton transfer reactions. The influence of the solvents will be discussed in detail elsewhere.

CHAPTER V THE ROLE OF SOLVENT IN EXCITED-STATE PROTON TRANSFER IN HYPERICIN

A. Introduction

Hypericin (Figure 4.1) is a naturally occurring polycyclic quinone that has received recent notoriety for its antiviral capacity—in particular its ability to deactivate the human immunodeficiency virus (HIV) [103,104]. The antiviral activity of hypericin requires light [106]. Hypericin is also very closely related, both structurally and spectrally, to the chromophore of the photoreceptor complexes of the protozoan ciliates, Stentor coerulus [107,123] and Blepharisma japonicum [108,109]. The hypericin-like chromophore is responsible for the photophobic and phototactic responses of the microorganism [107,123]. Optical excitation of hypericin produces both singlet oxygen [102,110,111] and a pH decrease [112,114,115].

Figure 5.1 gives the steady-state absorption and fluorescence spectra of hypericin in octanol. The spectra of hypericin are very similar in all solvents in which it is soluble with the exception of shifts in absorbance and emission maxima. In previous work we have shown that in hypericin the ground state, and consequently the excited state, is inhomogeneous. Figure 5.2 presents a kinetic scheme based upon our current knowledge of the hypericin photophysics, which is discussed in detail elsewhere [113,142]. The salient observations consistent with this scheme are the following:

(1) Immediately upon optical excitation a transient species is produced whose absorption lies between 620 and 650 nm, depending upon the solvent. In methanol measurement of the decay of this absorbance or of the rise time for the bleaching of the

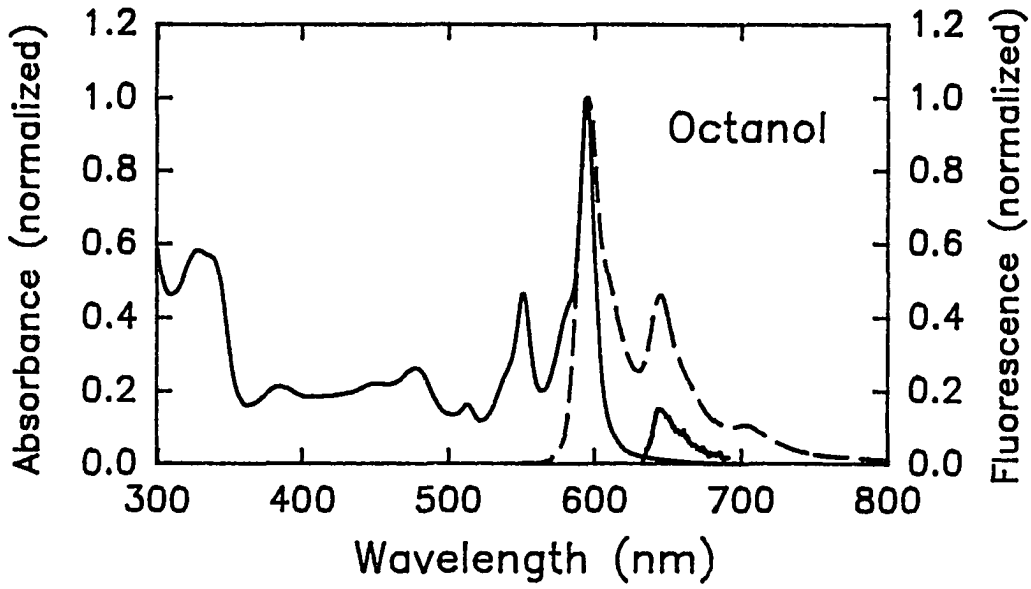

Figure 5.1. Normalized fluorescence spectrum (----) and absorption spectrum (—) of hypericin in octanol. The steady-state emission spectrum bears a "mirror symmetry" relationship to the visible portion of the absorption spectrum. We attribute this part of the absorption spectrum to the presence of ground-state MT (see Figure 5.2). The solid curve centered at ~650 nm is the spectrum of the stimulated emission that appears instantaneously and decays in ~12 ps (Figures 5.4 and 5.6). It is the "zero time" curve from Figure 5.3 scaled according to the relative amplitudes of the components of stimulated emission appearing instantaneously and with a finite rise time in the region from 640-645 nm (Figure 5.6 and Table 5.1). We propose that this emission arises from untautomerized hypericin that exists in equilibrium with a monotautomer in the ground state.

ground-state absorption, which overlaps the spectrum of the newly formed excited state, yields a lifetime of ~ 5-6 ps.

(2) The hypericin analog with no hydroxyl groups and hence no intramolecular proton source, mesonaphthobianthrone, provides no absorption or emission in the visible region of the spectrum in aprotic solvents such as DMSO, unlike hypericin. In concentrated sulfuric acid, however, the absorption and emission spectra of the analog are very similar to those of hypericin. We thus interpreted these data in terms of the necessity of protonated carbonyl groups for the production of fluorescence at wavelengths longer than 580 nm. This result indicates that in the ground state, at least one of the carbonyls of hypericin is protonated. This result also suggests the likelihood of excited-state tautomerization in hypericin.

(3) The occurrence of excited-state tautomerization in hypericin is verified by the rise time of the stimulated emission signal, which measures the excited-state population. In methanol, the rise time of the stimulated emission is within experimental error identical to the decay of the absorption transient produced upon optical excitation. Another confirmation of the excited-state proton transfer process is that in H_2SO_4 there is no transient with time constant > 1 ps [142]. This indicates that in the ground state the entire population of hypericin is already protonated and does not require an excited-state reaction to produce the long-lived fluorescent species (Figure 5.3).

We have suggested that upon light absorption hypericin undergoes excited-state proton transfer in ~ 5 ps in MeOH and ~ 9 ps in DMSO [113,142]. This small variation in rate has led us to inquire in more detail about the role of the solvent on the excited-state proton transfer.

The scheme presented in Figure 5.2 is the simplest that is consistent with the experimental data [113,142]. Two species are believed to be in equilibrium in the ground state, N and MT: normal, or untautomerized, and monotautomerized forms of hypericin.

Figure 5.2. Proposed kinetic scheme for hypericin in the ground and the excited states. The values quoted are for methanol. The time constant of 1 ps given for the conversion of N^* to MT^* is an upper limit determined by the duration of the laser pulse. In other solvents, for example octanol (Figure 4.6), this time constant is larger. Hypericin is represented schematically: only two of its six hydroxyl groups are pictured. We note that the tautomeric forms of DT can exist with the proton being donated from the "upper right" and the "lower left" hydroxyl groups as well as by the "upper left" and "lower left" hydroxyl groups, as indicated in the figure. The delocalization of the double bonds upon tautomerization may contribute significantly to the intramolecular component of the reorganization energy. We have tentatively assigned the rapid decay of N^* to formation of MT^*. Other nonradiative pathways such as internal conversion are also a possibility as is demonstrated by the anthraquinones [128]. We note, however, that both the triplet yield and the fluorescence quantum yield of hypericin have been reported to be very high and that $\phi F + \phi ISC \sim 1$ [102,110,111]. It thus seems unlikely that other nonradiative processes, besides proton transfer, play a significant role in the deactivation of N^*. A problem for which at present we do not have a completely satisfactory response is why we observe no emission from MT^*. It may be that there is not a large enough population of the species to be detected in the midst of all the other transients observed. This question requires further investigation.

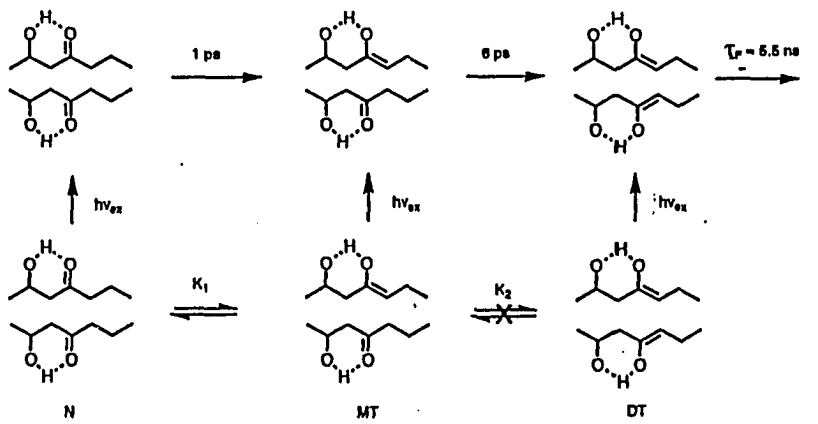
1 ps
6 ps
τ_F = 6.5 ns
$h\nu_{ex}$
$h\nu_{ex}$
$h\nu_{ex}$
K_1
K_2
N
MT
DT

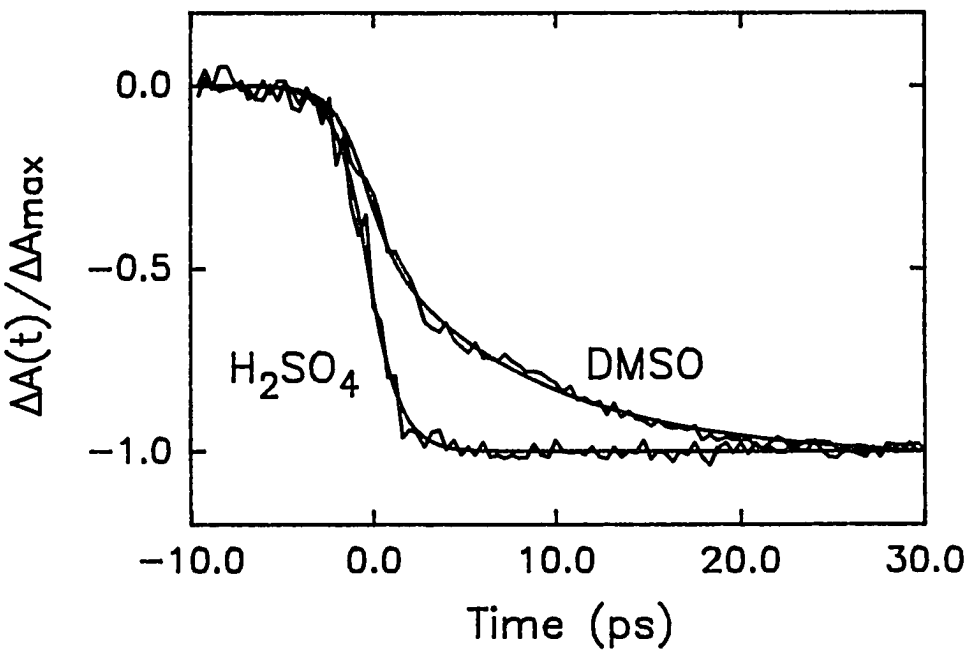

Figure 5.3. Comparison of the rise time for the formation of excited-state transients as measured by the delay time required to bleach maximally the ground-state absorption [113,142] (Table 5.1). This rise time is finite for hypericin in an aprotic solvent where a portion of the ground-state population is not tautomerized (DMSO). But in a solvent where the entire ground-state population is protonated (H_2SO_4), the rise time is instantaneous. The fits to the data are as follows:

DMSO, λ_{probe} = 610 nm: $\Delta A(t) = 0.23\exp(-t/9.6) - 0.41$;

H_2SO_4, λ_{probe} = 630 nm: the bleaching of the ground-state absorption is complete within the time resolution afforded by the system and the excited state formed is long-lived on the time scale of the measurement.

Evidence for this is the appearance in the stimulated emission of an instantaneous component (N^*) decaying with one lifetime and the appearance in transient absorption and bleaching measurements of another component decaying with a different lifetime (MT^*). We propose that negligible amounts of the ditautomerized form exist in the ground state because in the absence of strong acid no long-lived (nanosecond duration) fluorescence appears instantaneously. Measurements of the hypericin analog lacking hydroxyl groups, mesonaphthobianthrone, suggest that protonation of both carbonyl groups of hypericin is a prerequisite for long-lived fluorescence. The decay of MT^* matches the rise of DT^* demonstrating their kinetic relatedness. It is likely that N^* tautomerizes to form MT^* and that this proton transfer step represents the component of stimulated emission appearing instantaneously and decaying rapidly. For completeness, we note that it may be possible that N^* undergoes a two-proton transfer reaction that converts it directly to DT^*. Song, Yamazaki, and coworkers [130] have presented results on hypericin from which they conclude that excited-state intramolecular proton transfer does not occur. All of their conclusions, however, are based on observations of the long-lived fluorescence that is produced from the excited state whose duration is only several picoseconds. While their conclusions are thus not appropriate for the primary photoprocesses of hypericin, they may be relevant to the tautomer, which we refer to as DT^*. The light-induced pH drop produced by hypericin may result from the intermolecular deprotonation of the tautomer by the solvent.

In this article the excited-state tautomerization of hypericin is studied in a range of solvents that vary greatly in their viscosity, their average solvation time, their ability to form hydrogen bonds with the solute, and polarity. The choice of solvents and solvent properties studied was determined by reports in the literature suggesting they play an important role in other proton transfer systems. Of all the solvent properties investigated, only polarity was well correlated with the proton transfer time. We compare results obtained in these model

systems for excited-state proton transfer with those of the more complex system, hypericin, whose fascinating biochemical action and enormous medicinal potential have clearly been demonstrated to depend on light.

B. Materials and Methods

Hypericin was obtained from Carl Roth GmbH & Co. and used without further purification. The hypericin analog, mesonaphthobianthrone (Figure 4.1), was prepared as described by Koch et al. [116]. Solvents were obtained from Aldrich. Fluorescence spectra were measured with a Spex Fluoromax. The time-resolved absorption (stimulated emission) experiments were performed with ≤ 1-ps resolution with the apparatus described elsewhere [32,33,101]. Transient absorption spectra were obtained with a liquid nitrogen cooled charge-coupled device (CCD) (Princeton Instruments LN/CCD-1152UV) mounted on an HR320 (Instruments SA, Inc.) monochromator with a grating (1200 g/mm) blazed at 5000 Å. The CCD pixels were binned such as to allow simultaneous collection of both the probe and the reference beams, I and I_0 respectively, of the transient absorption spectrometer. For the absorption and stimulated emission experiments, identical kinetics were observed whether the pump beam was rotated parallel, perpendicular, or at the magic angle (54.7°) to the probe beam. Unless otherwise indicated, experiments were performed at room temperature, 22 °C. Measuring excited-state kinetics by the increase in probe transmission owing to stimulated emission is a well known technique. See references 23 for an example of its application to a system executing excited-state proton transfer, 3-hydroxyflavone. Temperature dependent measurements were performed with an Air Products system. A helium expander module (DE-202) is connected to a water-cooled compressor (HC-2) for helium exchange. The cryostat is evacuated by a Welch Duo Seal mechanical pump.

In all cases the pump-probe data include a contribution from stimulated emission that grows in with a finite risetime and a contribution from stimulated emission that appears instantaneously. The component with the finite risetime is represented by a rising exponential with a positive prefactor a_1 $[\exp(-t/\tau_1) - 1]$. For large values of t, the amplitude of this term is determined by the stimulated emission corresponding to the long-lived--several nanoseconds--fluorescent state that does not decay on the time scale of the experiment. The instantaneous component of stimulated emission is represented in the data fitting analysis by an exponential with a negative prefactor, $-a_2$. In addition, long-lived absorption owing to the presence of the solvated electron [142] may in some cases need to be taken into account by a constant, c. There are thus four possible factors to be considered in the pump-probe data: (1) stimulated emission with a finite rise time that arises from a long-lived fluorescent state; (2) instantaneous components of stimulated emission; and (3) long-lived transient absorption owing to the presence of the solvated electron. The pump probe data are thus fit to the following form, which takes into account the above contributions in the order in which they have been discussed

$$\Delta A(t) = a_1 [\exp(-t/\tau_1) - 1] - a_2 \exp(-t/\tau_2) + c. \qquad (5.1)$$

The construction of the spectrum (Figure 5.1) of the species, N^*, giving rise to the instantaneous component of stimulated emission that decays rapidly is performed as follows. First, the spectrum of the stimulated emission at "time zero" is obtained (Figure 5.4). Because this spectrum is obtained at zero time, it does not include contributions from the state that grows in with a finite time constant. Second, the amplitude of this spectrum at a given wavelength, with respect to that of the steady-state spectrum, is determined from the ratio of the amplitude of the component of stimulated emission appearing instantaneously, $[N^*]$, to

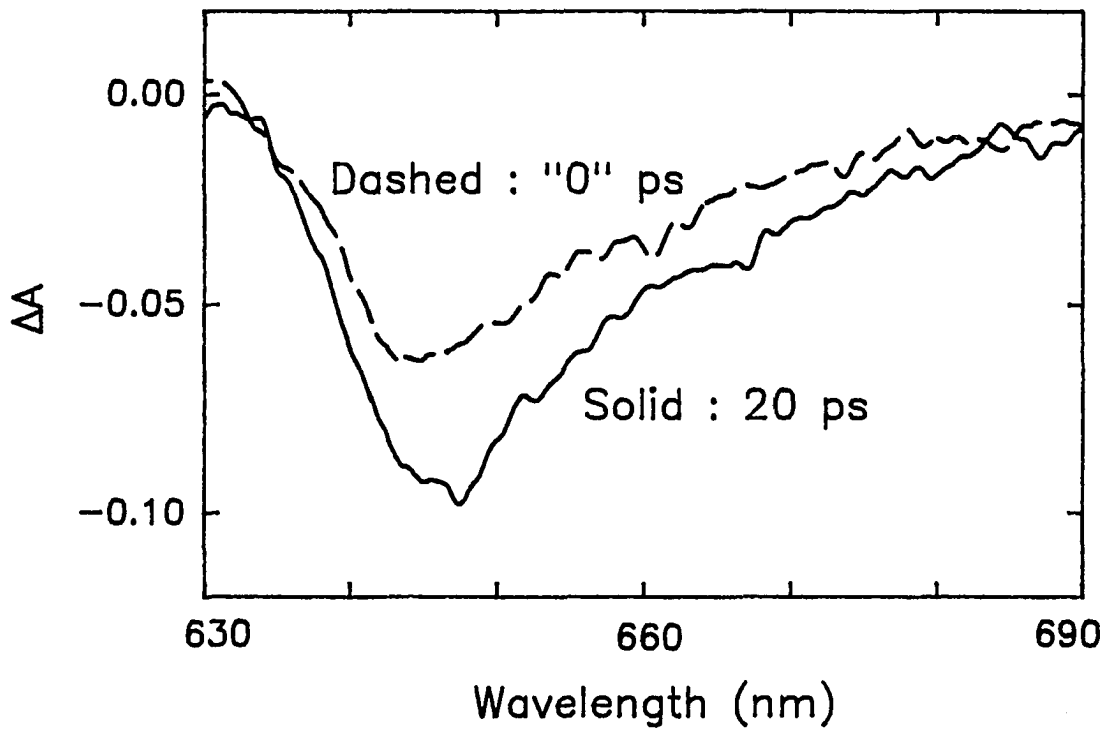

Figure 5.4. Time evolution of stimulated emission of hypericin in octanol.

that of the component appearing with a finite time constant from [MT^*] (Figures 5.2 and 5.6 and Table 5.1). It might be objected that the shape of this spectrum does not accurately represent that of the transient in question because of the presence of other species absorbing at the probe wavelength. The only other transient species with significant oscillator strength in this spectral region is the solvated electron [142]. We note that the absorption spectra of the solvated electrons in methanol, ethanol, and isopropanol are all very broad and that the maximum of the spectrum shifts to longer wavelength with increasing size of the alkyl chain [58]. For isopropanol, for example, the maximum is at ~ 800 nm and the absorbance tails off slowly towards shorter wavelengths. The spectrum of the solvated electron in octanol would be expected to be shifted even farther to the red. We thus conclude that the distortion of the emission spectrum that we attribute to N^* from the solvated electron is negligible and that if any distortion were to be expected, it would appear on the red, not the blue, edge of the spectrum.

C. Results

Figure 5.4 presents the negative-going transient absorbance signal of hypericin in octanol. This signal is attributed to stimulated emission from excited-state hypericin because it is observed in a region where there is no ground-state absorbance. The signal thus cannot be assigned to ground-state bleaching. The salient feature of the Figure is that a finite time is required for the stimulated emission to be fully developed. We have thus used the rise time of stimulated emission as a measure of the time required to produce the long-lived excited-state species. We have argued [142] that measurable fluorescence (by steady-state or conventional photon counting techniques) in hypericin is obtained only from the species with both carbonyl groups protonated.

Table 5.1. Dependence of Proton Transfer Times in Hypericin in Selected Solvents[a]

Solvent	η(cP)[b]	$\langle\tau_S\rangle$[c] (ps)	$E_T(30)$ [33]	decay time[d,f] (ps)	rise time[e,f] (ps)	I_F/I_S[f,g]
MeCN	0.37	0.9	45.6	10.8 (600 nm)	11.6 (645 nm)	1.0 (645 nm)
BuCN	0.57	3.6	43.1	11.7 (600 nm)	10.4 (645 nm)	1.2 (645 nm)
CCl_4/BuCN[h]					12.8 (645 nm)	
MeOH	0.57	3.3, 6.2	55.4	6.4 (600 nm)	6.7 (645 nm)	0.84 (645 nm)
DMSO	1.99[i]	3.1, 1.2	45.1	9.6 (610 nm)	9.2 (658 nm)	0.43 (658 nm)
BuOH	2.75	61	50.2	7.5 (600 nm)	11.0 (645 nm)	0.75 (645 nm)
OcOH	7.36[i]		48.3	10.3 (610 nm)	12.6 (645 nm)	0.49 (640 nm) 0.51 (645 nm)
EgOH	18.25	100	56.3	5.8 (600 nm)	6.4 (645 nm)	1.2 (645 nm) 0.99 (650 nm)

[a] All experiments were performed at room temperature, 22 °C [b] Except where otherwise noted, the solvent viscosity at 22 °C [158]. [c] Average solvation time as determined from measurements of time-resolved Stokes shifts. The cited solvation times are obtained from the tabulation in reference 15. [d] Decay of the excited-state absorption as measured by

Table 5.1. Continued

the rise time for the ground-state bleaching of hypericin. The absence of a value indicates that the measurement was not performed. [e] "Long" component of the rise time of stimulated emission, which is attributed to the intramolecular proton transfer in hypericin. [f] The value in parentheses is the probe wavelength. [g] Ratio of the component of stimulated emission appearing instantaneously, I_F, to that appearing with a finite rise time, I_S. The dependence of this ratio on solvent can be interpreted in terms of a ground-state equilibrium between N and MT (Figure 5.2) insofar as the emission spectra of N^* and MT^* do not change greatly with respect to solvent at the probe wavelength. [h] The ratio of solvents in the mixture is 1/4 and is based on volume. This corresponds to a solution of 0.18 mole fraction in CCl_4. The viscosity of the mixture was not determined. [i] Viscosity at 25 °C [160].

In all the solvents in which we have investigated hypericin, except strong acids such as sulfuric and triflic acid where it is expected to have both carbonyl groups protonated, we observe a finite "rise time" for the ground-state bleaching. Such a phenomenon is most easily rationalized by the presence of an excited-state species, produced within the excitation pulse, that has oscillator strength in the same region as the ground-state molecules. We have directly observed such an excited-state species in transient absorption measurements [113,142]. As indicated by the summary presented in Table 5.1, the agreement between the lifetime of this excited state and the rise time of the "slow" component of the stimulated emission is excellent. We have discovered that measurement of the rise time for ground-state bleaching provides a more accurate determination of the lifetime of the short-lived excited state that is a precursor, MT^*, to the long-lived fluorescent species of hypericin, DT^*. Measurement of the decay of the transient absorbance of MT^* can be obfuscated by the presence of absorption from the biphotonically produced solvated electron [142] as well as from stimulated emission—or transient absorption from the species producing the stimulated emission.

Figures 5.5 and 5.6 also indicate that upon optical excitation a species is created that produces stimulated emission immediately and that subsequently decays. This prompt stimulated emission is consistent with the suggestion made above (and in the caption to Figure 5.2) that at least two ground-state species are optically excited. Figure 5.5 and Table 5.1 suggest that the solvent seems to affect the ground-state equilibrium between N and MT, which is subsequently manifested in the ratio of the components of stimulated emission appearing with an instantaneous or a finite rise time, I_F/I_S. The component of the stimulated emission that appears instantaneously is not attributable to vibrational relaxation because its decay is the same whether the excitation is at 294 or 588 nm. Furthermore, it does not arise from dynamic solvation of the excited state [143] because it decays equally rapidly in acetonitrile and ethylene glycol, whose average solvation times differ by a factor of 100 (Table

Figure 5.5. Time-resolved stimulated emission profiles of hypericin in (from top to bottom) methanol, DMSO, ethylene glycol, and acetonitrile. λ_{ex} = 588 nm. See Table 5.1 for further details.

methanol: $\Delta A(t) = 0.17[\exp(-t/6.7\text{ ps}) - 1] - 0.14\exp(-t/1.9\text{ ps})$;

DMSO: $\Delta A(t) = 0.30[\exp(-t/9.2\text{ ps}) - 1] - 0.13\exp(-t/1.9\text{ ps})$;

ethylene glycol: $\Delta A(t) = 0.45[\exp(-t/6.4\text{ ps}) - 1] - 0.53\exp(-t/2.4\text{ ps}) + 0.26$;

acetonitrile: $\Delta A(t) = 0.19[\exp(-t/11.2\text{ ps}) - 1] - 0.19\exp(-t/1.4\text{ ps}) + 0.025$.

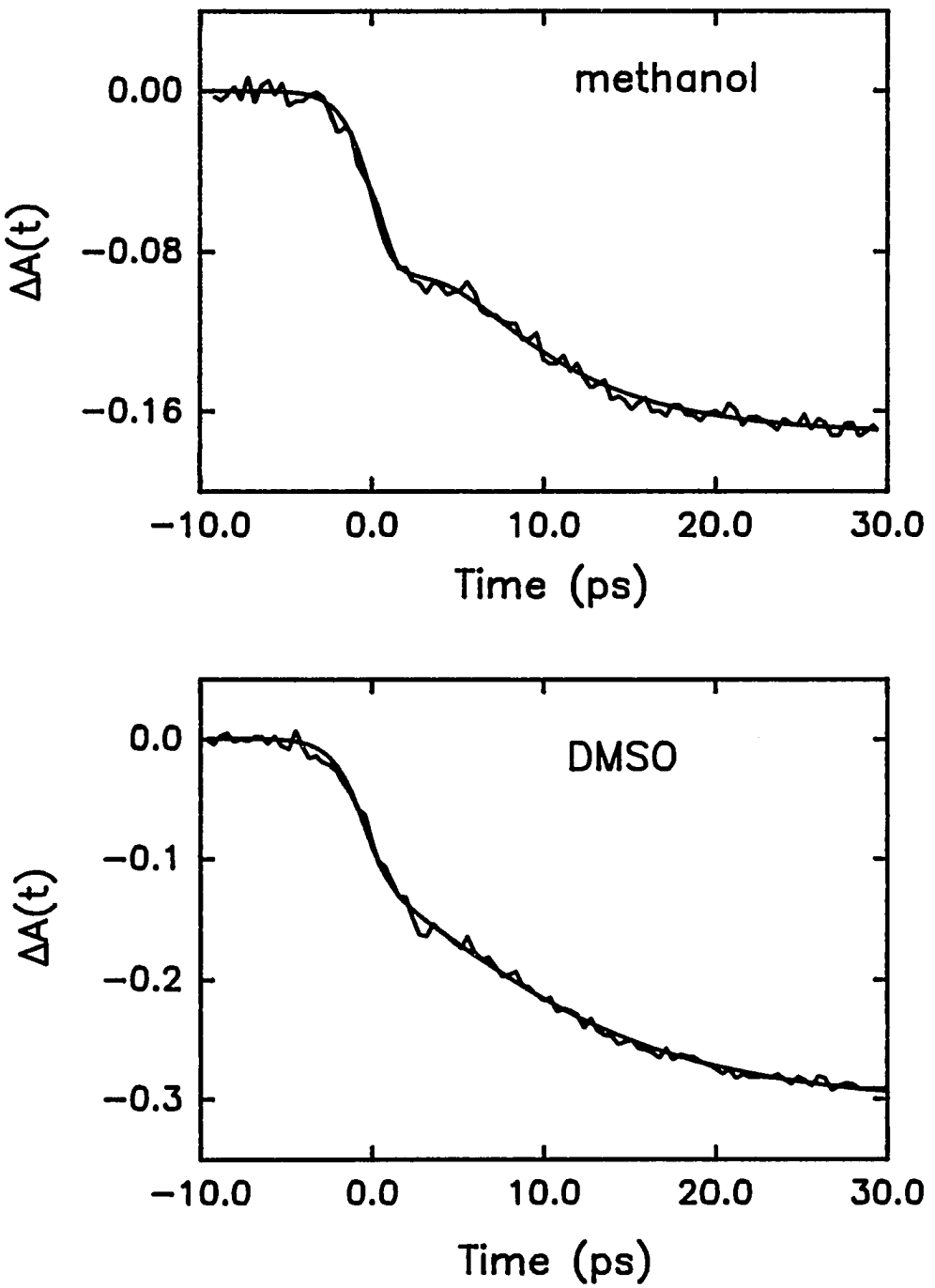
methanol
0.00
−0.08
−0.16
ΔA(t)
−10.0
0.0
10.0
20.0
30.0
Time (ps)
DMSO
0.0
−0.1
−0.2
−0.3
ΔA(t)
−10.0
0.0
10.0
20.0
30.0
Time (ps)

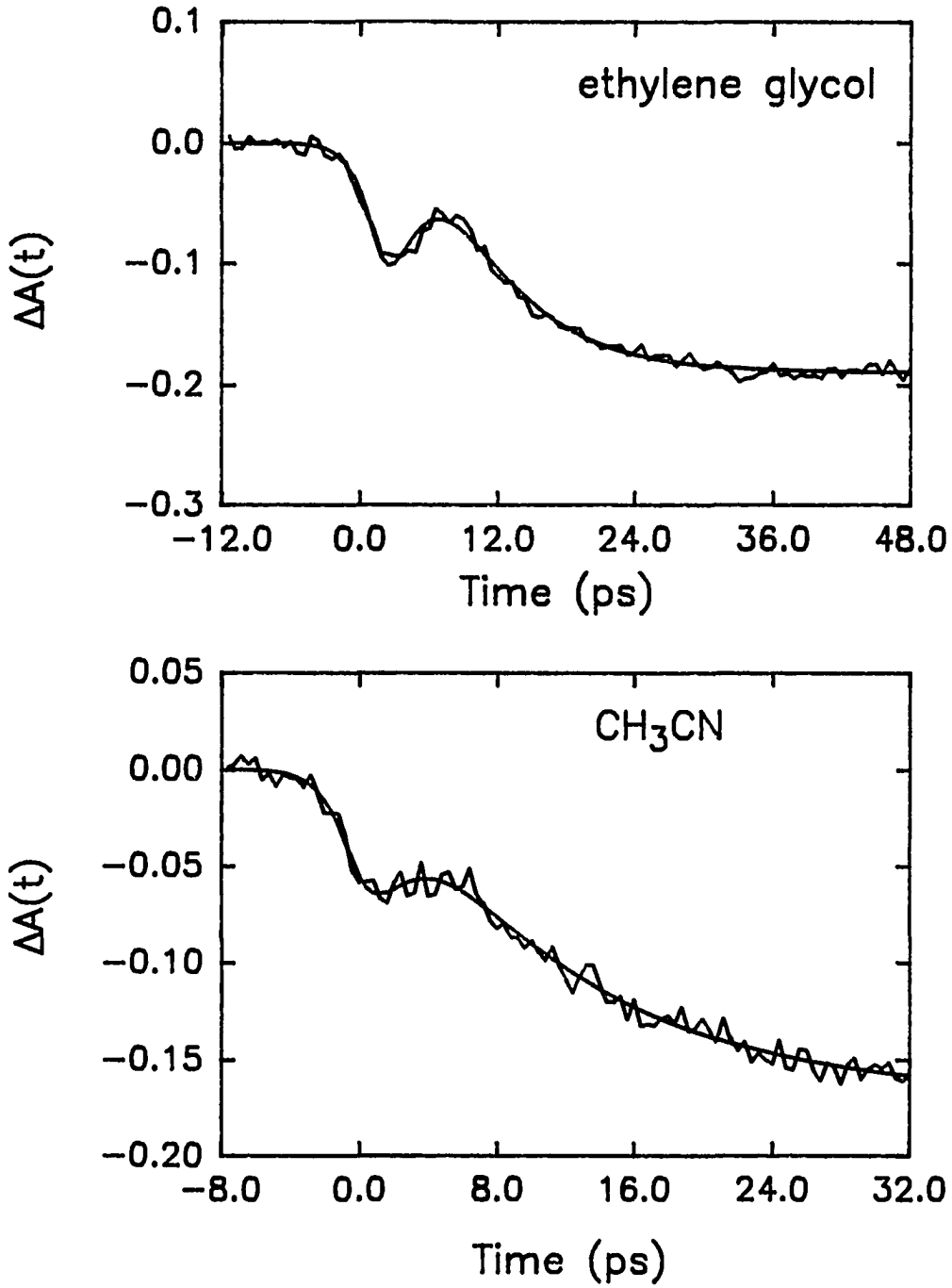

Figure 5.5. Continued

5.1, Figure 5.5). We suggest that the rapid decay of N^* represents a tautomerization step to MT^*. This is discussed in more detail elsewhere [142].

Figure 5.6 demonstrates the variation in the stimulated emission kinetics of hypericin in octanol as a function of probe wavelength. Tuning the probe from 640 to 675 nm reveals smoothly varying contributions of the components of stimulated emission that appear instantaneously and that appear with a finite rise time. The instantaneous component is most easily identified at 640 and 675 nm. The simplest interpretation of these data is that the normal form of hypericin, N^*, which we suggest gives rise to the instantaneous component has a fluorescence spectrum that in some regions is more intense than that of the fully tautomerized form, DT^*. The solid curve centered at ~ 650 nm in Figure 5.1 represents the fluorescence spectrum of N^* obtained from the ratio of the instantaneous to the rising components (Table 5.1).

Measurements of the slower component of the stimulated emission in ethylene glycol over a rather limited temperature range were used to construct an Arrhenius plot (Figure 5.7). The barrier for this proton transfer reaction is thus estimated to be 1.5 kcal/mol in ethylene glycol. Lastly, Figure 5.8 presents a plot of the time constant for the slower component against solvent polarity as measured by $E_T(30)$.

D. Discussion

In a range of solvents, both hydrogen bonding and nonhydrogen bonding and protic and aprotic, over which the viscosity and the average solvation time change by factors of 60 and 100, respectively, the proton transfer time as measured by the rise time of the longer-lived component of the stimulated emission is found to be uncorrelated with these properties and to

Figure 5.6. Stimulated emission profiles of hypericin in octanol at different probe wavelengths, λ_{ex} = 588 nm. Probe wavelengths are indicated in the panels.

λ_{probe} = 640 nm: $\Delta A(t) = 0.086[\exp(-t/11.0\text{ ps}) - 1] - 0.042\exp(-t/13.4\text{ ps})$;

λ_{probe} = 645 nm: $\Delta A(t) = 0.47[\exp(-t/12.6\text{ ps}) - 1] - 0.24\exp(-t/18.8\text{ ps})$;

λ_{probe} = 655 nm: $\Delta A(t) = 0.097[\exp(-t/7.6\text{ ps}) - 1] - 0.054\exp(-t/11.0\text{ ps})$;

λ_{probe} = 665 nm: $\Delta A(t) = -0.12$;

λ_{probe} = 675 nm: $\Delta A(t) = -0.067\exp(-t/16.0\text{ ps}) - 0.022$.

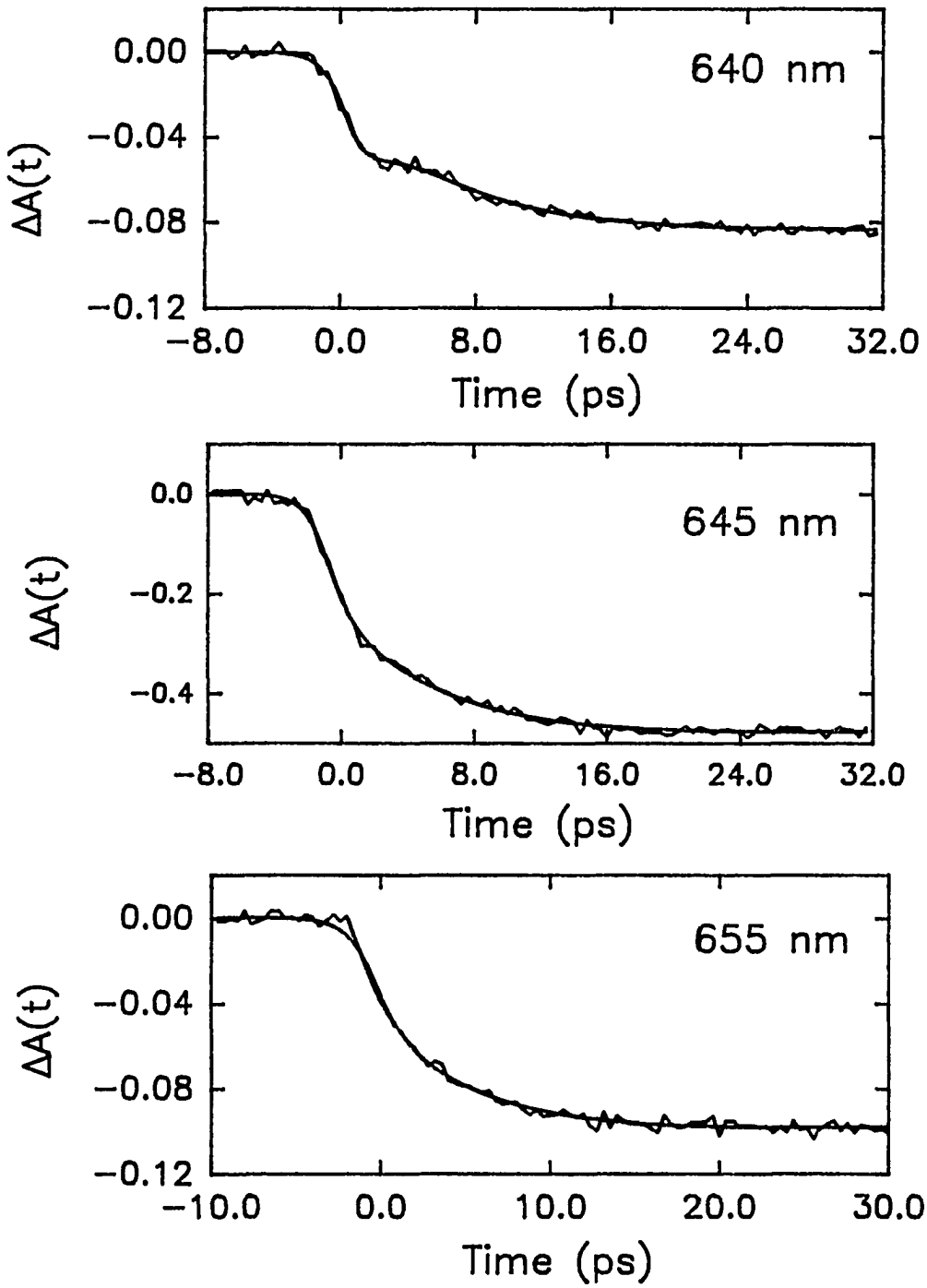
640 nm
0.00
−0.04
−0.08
−0.12
ΔA(t)
−8.0
0.0
8.0
16.0
24.0
32.0
Time (ps)
645 nm
0.0
−0.2
−0.4
ΔA(t)
−8.0
0.0
8.0
16.0
24.0
32.0
Time (ps)
655 nm
0.00
−0.04
−0.08
−0.12
ΔA(t)
−10.0
0.0
10.0
20.0
30.0
Time (ps)

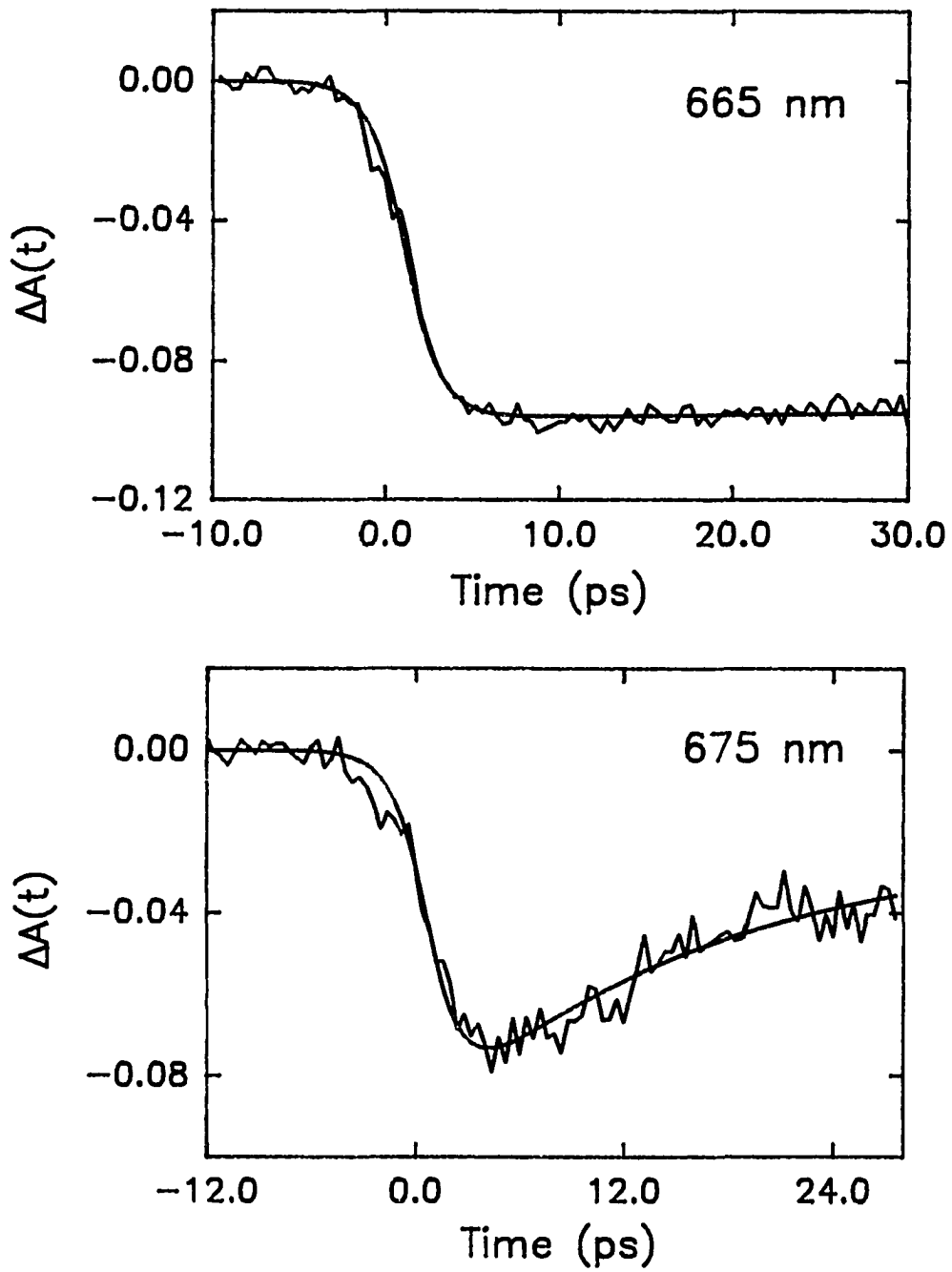

Figure 5.6. Continued

change by at most a factor of two. This result is very surprising when it is considered in the context of other examples of excited-state proton transfer.

Hochstrasser and coworkers [144] have observed proton transfer rates for a 2-phenyl-benzotriazole bearing an octyl group on the 5-position that agree very well with the longitudinal relaxation time of the solvent, τ_L. These data are particularly intriguing because despite this dependence on τ_L no time-dependent Stokes shift is observed in this system.

The time-dependent Stokes shift is related to τ_L and is characterized by an average solvation time $<\tau_S>$ [143,145]. When a solute is promoted to its excited state, its charge distribution is altered. The solvent is no longer in equilibrium and must relax to its new equilibrium structure, thus affording the temporally evolving Stokes shift. Charge transfer reactions similarly alter the charge distribution of the solute, and in many cases the rates of such reactions have been shown to depend on the dynamic response of the solvent, characterized by τ_L or $<\tau_S>$, to the charge-transferred species [144,145].

In hydrogen-bonding solvents such as alcohols, on the other hand, the ability of the solvent to weaken or to break the intramolecular hydrogen bond in 3-hydroxyflavone is the rate determining factor in the excited-state proton transfer reaction [119,127,146-149]. If both the carbonyl and the alcohol groups of 3-hydroxyflavone are strongly coordinated to different solvent molecules, proton transfer occurs relatively slowly, on a time scale of $\geq$ 10 ps [119]. If, however, the intramolecular hydrogen bond of the solute is not perturbed (as occurs in hydrocarbon solvents such as methylcyclohexane) excited-state proton transfer is very rapid. Harris and coworkers have measured this time to be ~ 240 fs [119]. These workers have also proposed that if a single alcoholic solvent molecule can form a cyclic hydrogen-bonding interaction with the carbonyl and the alcohol groups of the solute, an even more rapid transfer time of ~ 80 fs results. Similarly rapid proton transfer times have been observed in benzothiazole derivatives [150,151]. These results have been interpreted in terms of the

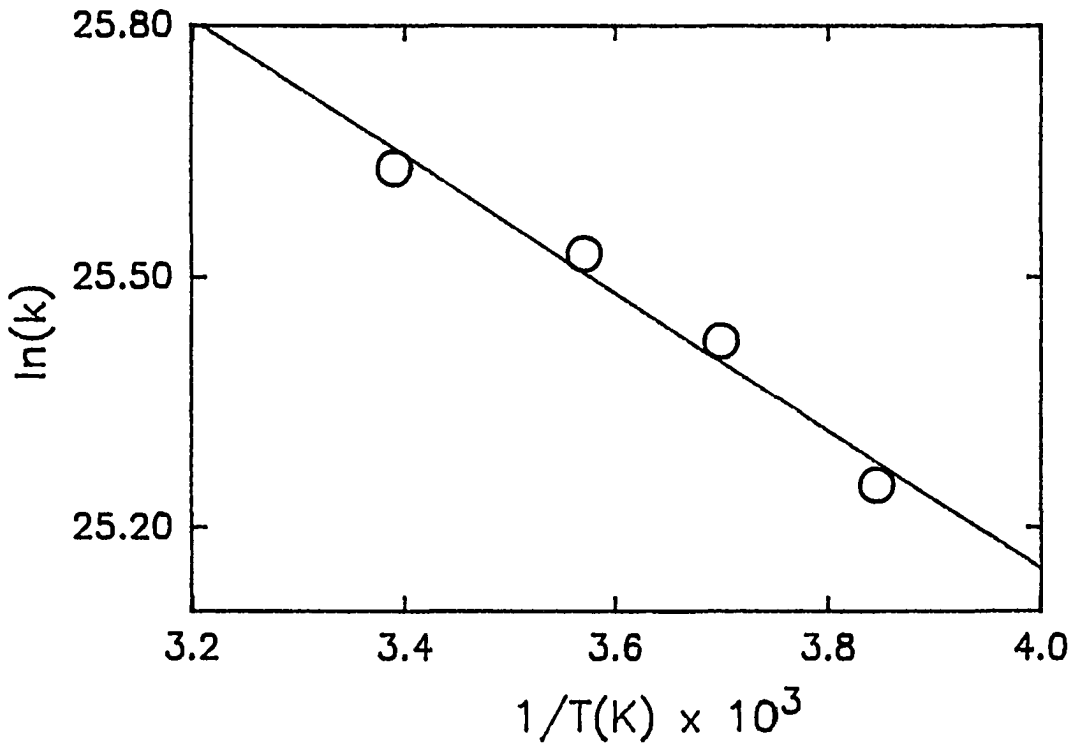

Figure 5.7. Arrhenius plot of the time constant of the longer-lived component of stimulated emission in hypericin in ethylene glycol.

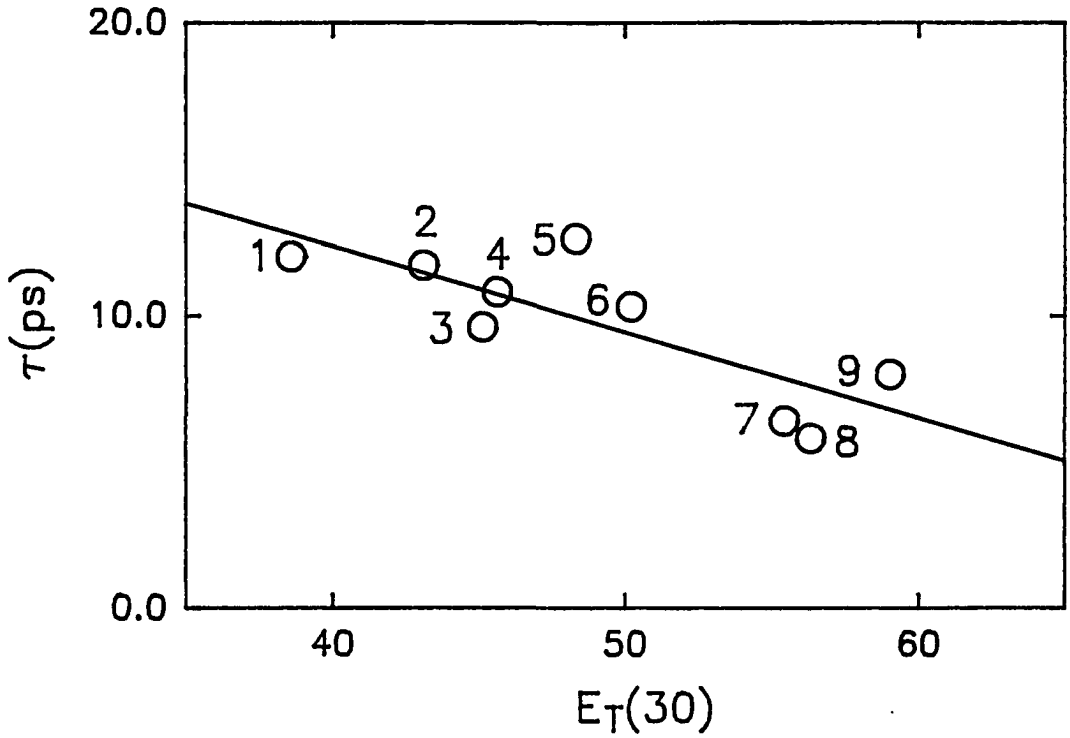

Figure 5.8. The time constant of the longer-lived component of stimulated emission in hypericin plotted as a function of polarity as measured by $E_T(30)$ [159]: 1, diethylene glycol dimethyl ether; 2, butyronitrile; 3, DMSO; 4, acetonitrile; 5, 1-octanol; 6, 1-butanol; 7, methanol; 8, ethylene glycol; 9, 2,2,2-trifluoroethanol.

wavepacket prepared upon optical excitation. The evolution of this wavepacket towards the tautomeric form on the excited-state potential surface will initially depend very strongly on the vibrations displaced upon light absorption [119,150].

The proton transfer time in hypericin ranges from about 6 to 12 ps in the solvents we have investigated and hence is similar to the proton transfer time observed in 3-hydroxyflavone and attributed to solute-solvent structures in which two different alcohol molecules are coordinated to the carbonyl and alcohol groups of the solute [119]. Such a state of solvation cannot, however, explain the proton transfer rates in hypericin because the same results are obtained in both hydrogen-bonding and nonhydrogen-bonding solvents. This suggests that the intramolecular interactions between the O—H•••O group formed by the alcohol oxygen, the proton, and the carbonyl oxygen of hypericin are much stronger than any potential hydrogen bonding interactions with the solvent.

The assignment of the excited-state process to intramolecular proton transfer may be criticized because we do not observe an isotope effect [142]. There is precedent for proton transfer processes that do not exhibit an isotope effect [119,151]. Whether an isotope effect is observed will also depend on such factors as the degree to which the reaction is nonadiabatic and characterized by tunneling through a potential barrier [132,152] or if the reaction occurs by means of a barrierless (or small barrier) process in which the role of vibrational motions other than the O-H stretch are important [153].

Hynes, Borgis, and coworkers [132,152] have presented a theory of proton transfer in both adiabatic and nonadiabatic limits. Three coordinates play an important role: the coordinate for the proton itself; the intramolecular separation of the two atoms (in this case oxygens) between which the proton is transferred; and a collective solvent coordinate. In this treatment, the electrons are always treated adiabatically; but the proton transfer process is considered to be in a nonadiabatic or an adiabatic limit depending on the separation of the

oxygen atoms. For a large (> 2.7 Å) separation, the wavefunction for the proton is localized about one of the oxygens and a sufficiently large barrier exists that proton transfer must be viewed as a nonadiabatic tunneling process. (The rate of this tunneling process is modulated by the oxygen-oxygen separation and the solvent fluctuations.) If, however, the separation is small (< 2.7 Å), the barrier to proton transfer is greatly decreased and the extent to which tunneling contributes to the rate of proton transfer can be greatly reduced. Finally, in reactions that involve the generation of charged or partially charged species, the solvent polarity is expected to accelerate the rate. For example, in a reaction taking covalent reactants to ionic products, the products will be better solvated by a polar substance such as water than a nonpolar substance such a methylcyclohexane. Stabilization of the potential surface for the ionic species with respect to that for the covalent species will lower the point at which they cross and hence decrease the activation energy for the process [154].

In the case of hypericin, the distances [155,156] between the keto and hydroxy oxygens (as measured starting from the 1 and 14 positions and moving clockwise around the polycycle in Figure 4.1) between which the proton is transferred are all consistent with an adiabatic process: 2.45, 2.53, 2.49, and 2.53 Å. The solvent dependence of the time constant for the excited-state process is also consistent with its assignment to proton transfer. The time constant decreases with increasing solvent polarity, as measured by $E_T(30)$, and suggests a process that involves the transfer of a charged particle, molecular rearrangement, and charge reorganization [132,152]. Finally, temperature-dependent measurements in ethylene glycol (Figure 5.7) indicate that there is a small barrier (~ 1.5 kcal/mol) between MT^* and DT^*. This small barrier is in agreement with the short distances between oxygens in hypericin.

Construction of molecular models of hypericin and a recent x-ray structure [155] indicate that the aromatic polycycle is twisted. One might argue that the excited-state transients observed reflect transitions from one form of conformational isomer to another.

Because such a process involves a large amplitude motion, it would be expected to be viscosity dependent. In solvents in which the viscosity changes by a factor of 60 we see, however, no more than a change of a factor of two in the time constant of the longer-lived excited-state transient (~ 6-12 ps). Furthermore, the rate of the excited-state process is completely uncorrelated to viscosity: the small variation in rate cited can be effected just a easily when the viscosity is increased by less than a factor of two, i.e. from methanol to acetonitrile (Table 5.1). This excludes the assignment to a conformational transition.

An obvious question that remains is whether intramolecular vibrational modes other than those modulating the oxygen-oxygen separation play a role in the reaction. Resonance Raman measurements will be indispensable in providing a response. Peteanu and Mathies [153] have shown that in the case of 2-hydroxyacetophenone, which is believed to execute a barrierless excited-state proton transfer, there is no displacement in the O-H stretching coordinate upon optical excitation. This result suggests that vibrations other than proton motion are responsible for the initial displacement of the wavepacket away from the Franck-Condon region of the excited state. Consistent with these Raman measurements are the observations of Harris and coworkers [119] and of Elsaesser and coworkers [150,151] of proton transfer rates that are independent of isotopic substitution. Cotton and coworkers [157] have measured the resonance Raman spectrum of hypericin under various conditions and observed bands in the region from ~ 1620 to 620 cm^{-1}, some of which were tentatively identified.

E. Conclusion

Measurements of the stimulated emission of hypericin with ≤ 1-ps resolution have been used to monitor the creation and decay of excited and hence fluorescent states. The excited-

state characterized by nanosecond lifetimes and observed in steady-state measurements [142,130] appears in roughly 6 to 12 ps. The rise time for the appearance of this emission is attributed to an excited-state proton transfer reaction. The similarity of the rates in both hydrogen-bonding and nonhydrogen-bonding solvents is the most surprising result given what is known about the behaviour of 3-hydroxyflavone in these solvents. Polarity is the only solvent property that is well correlated with the proton transfer time. In addition to the slower, ~ 6-12-ps rise time, a component of the stimulated emission is observed that appears instantaneously. This component is attributed to a ground-state untautomerized (normal, N) form of hypericin that decays rapidly, most probably by forming the excited-state tautomer $M'T^*$. The observation of this component demonstrates the inhomogenous distribution of hypericin structures in the ground state and hence in the excited state. A proton transfer reaction with a time constant of 6-12 ps is relatively slow [127,119,147-151]. Hypericin thus provides an extremely useful system with which to test current theories of proton transfer [152].

In conclusion, the primary photoprocess occurring in hypericin is intramolecular proton transfer, whose rate depends on solvent polarity. Understanding the light induced activity in hypericin is of significance for appreciating its biochemical role in protozoa and exploiting its medicinal activity against viruses.

CHAPTER VI DOUBLE-PROTON TRANSFER REACTIONS: CONCERTED AND STEP-WISE MECHANISMS

A. Introduction

For a multibond reaction, three types of mechanisms may be involved. These mechanisms are (a) step-wise, (b) concerted, and (c) synchronous. A step-wise reaction involves distinct steps. For example, a two-step reaction takes place in two different kinetic processes, and a stable intermediate connects them together. For a concerted reaction, no stable intermediate is involved, the system only passes through one transition state. Dewar [162] defines a synchronous reaction as one where all the bond-making and bond-breaking processes take place in union, and have processed to a comparable extent in the transition state. Usually, synchronous multibond processes are energetically unfavorable and thus prohibited. In the following, we focus only on step-wise and concerted reactions [161].

Double-proton transfer reactions are a topic of current interest. Recent examples appearing in the literature are general base and acid catalysis [169, 170], solvent assisted excited-state double-proton transfer [68], double-proton transfer in dimers [168]. But in practice, it is hard to determine by which mechanism the reaction takes place. Here, we try to answer some basic questions related to the mechanisms of double-proton transfer reactions using isotope effects. Some new results are derived. These results are applied to the double-proton transfer mechanism of 7-azaindole in alcohols.

B. Theory

1. Degenerate Concerted Reactions

For a concerted double-proton transfer reaction, as depicted in Figure 6.1, in the context of transition state theory, only one transition state is involved and the rate constant for the reaction may be written as

$$k^{L_2L_1} = A^{L_2L_1}\exp\left(-E_a^{L_2L_1}/RT\right) \tag{6.1}$$

where $A^{L_2L_1}$ is related to the frequency with which the transferred particle hits the barrier and it is assumed to be the same for all isotopic reactions. $E_a^{L_2L_1}$ is the activation energy of isotopic substitution, L_2L_1. Here L_2 and L_1 means either protium, H, or deuterium, D. In all there are four possibilities, which are HH, HD, DH, and DD (see Figure 6.2). For a degenerate reaction, however, it is expected that the rate constant for HD reaction is the same as that for DH reaction. In the simplest case, the barrier for HD reaction can be taken as the arithmetic mean of the barriers for the HH and DD reactions

$$E_a^{HD} = \tfrac{1}{2}\left(E_a^{HH} + E_a^{DD}\right). \tag{6.2}$$

Substitution of Eq (6.2) into Eq (6.1) gives rise to

$$k^{HD} = \sqrt{k^{HH}k^{DD}}. \tag{6.3}$$

Equation (6.3) can be rearranged as

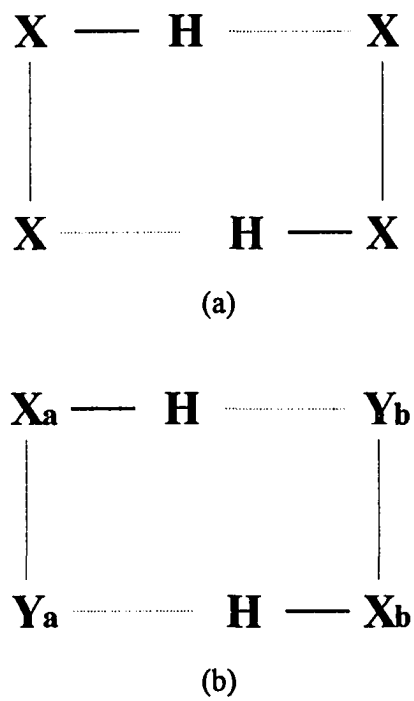

Figure 6.1. (a) Degenerate double-proton transfer reaction between the same molecules and (b) nondegenerate double-proton transfer reaction between different molecules.

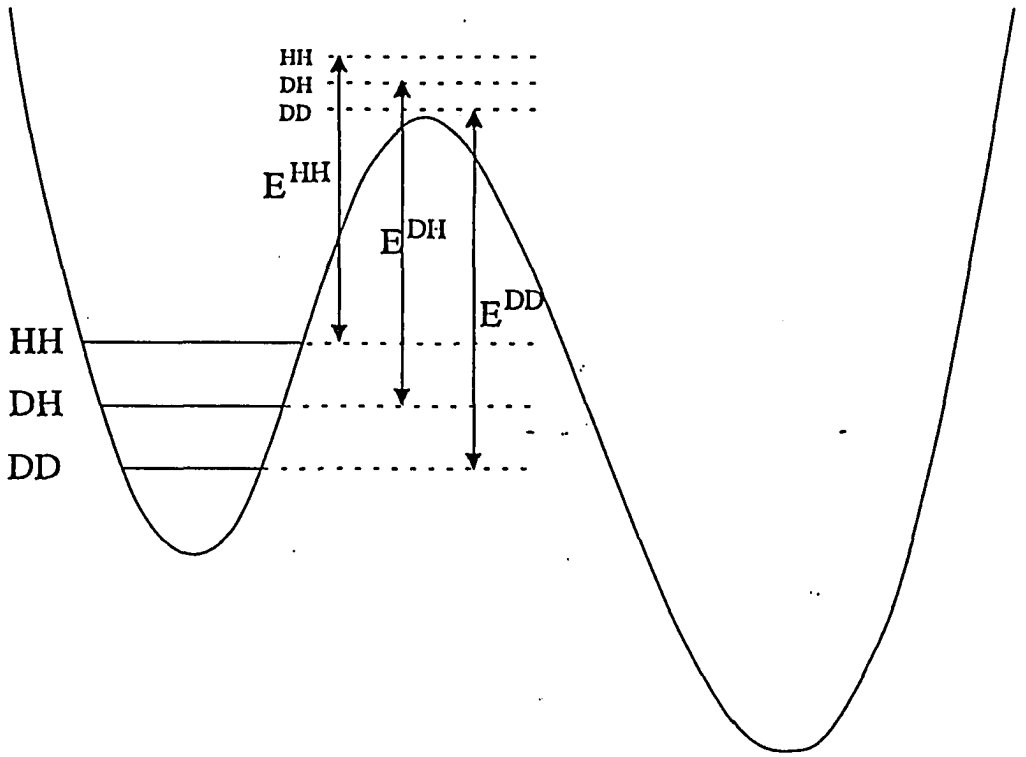

Figure 6.2. Activation energies for HH, DH, and DD in a degenerate reaction.

$$\frac{k^{HH}}{k^{HD}} = \frac{k^{HD}}{k^{DD}}. \tag{6.4}$$

This result is referred to as the rule of geometric mean (RGM). Also, if the difference of the activation energies between HH and DD is given as

$$\Delta\varepsilon = E_a^{DD} - E_a^{HH}, \tag{6.5}$$

by combining Eq (6.5) and Eq (6.2), one obtains

$$E_a^{HD} = E_a^{HH} + \frac{\Delta\varepsilon}{2}. \tag{6.6}$$

Using Eq (6.1) and Eq (6.6),

$$\frac{k^{HH}}{k^{HD}} = \frac{k^{HD}}{k^{DD}} = \exp\left(\Delta\varepsilon/2RT\right). \tag{6.7}$$

Eqs (6.7) and (6.4) are the basic results for concerted reactions. Limbach et al. [2] have obtained similar results. In deriving the above results, the prefactor $A^{L_2L_1}$ has been assumed to be the same for all the isotope substitutions. This assumption may not hold for some cases. However, if A^{HD} can be taken as the geometric mean of A^{HH} and A^{DD}, namely, $A^{HD} = \sqrt{A^{HH}A^{DD}}$, Eqs (6.3) and (6.4) still hold, and Eq (6.7) is modified by the factor $\sqrt{A^{HH}/A^{DD}}$. For all other cases, the above results need to be rederived.

The RGM, however, may not hold for all concerted reactions. In other words, the barrier for HD reaction may not be the arithmetic mean of the barriers for the HH and DD

reactions. So Eqs (6.4) and (6.7) are not the only criteria for judging the mechanisms. Generally, relation (6.2) may be modified to a more general case

$$E_a^{HD} = E_a^{HH} + \alpha\Delta\varepsilon = E_a^{DD} - (1-\alpha)\Delta\varepsilon. \tag{6.8}$$

Where α is a constant for a specific reaction, which has the value of $0 < \alpha < 1$. If $\frac{1}{2} < \alpha < 1$, this indicates that substitution of the first H with D affects the reaction more significantly than the substitution of the second H. From Eq (6.8), two other more general relations can be derived

$$\frac{k^{HH}}{k^{HD}} = \exp\left(\frac{\alpha\Delta\varepsilon}{RT}\right), \tag{6.9}$$

and

$$\frac{k^{HD}}{k^{DD}} = \exp\left(\frac{(1-\alpha)\Delta\varepsilon}{RT}\right). \tag{6.10}$$

Thus, only when $\alpha = 1/2$ do Eqs (6.9) and (6.10) reduce to Eqs (6.4) and (6.7). This explains why the RGM is only a very specific case of a concerted reaction. Usually, $k^{HH}/k^{HD} = k^{HD}/k^{DD}$, but the following relationship holds

$$\frac{k^{HH}}{k^{HD}} = \exp\left(\frac{(2\alpha-1)\Delta\varepsilon}{RT}\right)\frac{k^{HD}}{k^{DD}}. \tag{6.11}$$

If $\alpha \geq \frac{1}{2}$,

$$\frac{k^{HH}}{k^{HD}} \geq \frac{k^{HD}}{k^{DD}}. \tag{6.12}$$

If $\alpha \leq \frac{1}{2}$,

$$\frac{k^{HH}}{k^{HD}} \leq \frac{k^{HD}}{k^{DD}}. \tag{6.13}$$

To the best of our knowledge, we do not know any experimental results that satisfy Eq (6.13). For a degenerate and concerted double-proton transfer reaction, it is likely that Eq (6.12) is the more likely case. One such example is the double-proton transfer in mixed 1:1 dimers of acetic acid and methanol dissolved in THF (tetrahydrofuran), where values of $k^{HH}/k^{HD} \approx 5$, $k^{HD}/k^{DD} \approx 3$, and $k^{HH}/k^{DD} \approx 15$ were found at 298 K [165]. According to Eqs (6.9) and (6.10), if $\alpha \rightarrow 1$, one arrives at the following results

$$\frac{k^{HH}}{k^{HD}} \approx \exp\left(\frac{\Delta\varepsilon}{RT}\right), \tag{6.14}$$

and

$$\frac{k^{HD}}{k^{DD}} \approx 1. \tag{6.15}$$

Also, if one takes the logarithm of Eqs (6.9) and (6.10), one obtains

$$\ln\left(\frac{k^{HH}}{k^{HD}}\right) = \frac{\alpha\Delta\varepsilon}{RT}, \tag{6.16}$$

and

$$\ln\left(\frac{k^{HD}}{k^{DD}}\right)=\frac{(1-\alpha)\Delta\varepsilon}{RT}. \tag{6.17}$$

Eqs (6.16) and (6.17) represent two straight lines, namely, $\ln(k^{HH}/k^{HD})$ vs. 1/T and $\ln(k^{HD}/k^{DD})$ vs. 1/T respectively. The respective slopes are

$$B_1=\frac{\alpha\Delta\varepsilon}{R}, \tag{6.18}$$

and

$$B_2=\frac{(1-\alpha)\Delta\varepsilon}{R}. \tag{6.19}$$

The combination of Eqs (6.18) and (6.19) can be used to solve for α and $\Delta\varepsilon$.

One example of using Eqs (6.9) and (6.10) to solve for α and $\Delta\varepsilon$ is the following. Limbach et al. [165] have measured the proton exchange rates at different temperatures in the mixed solvents of acetic acid, methanol, and tetrahydrofuran. Their measurements yield

$$k^{HH}=10^{7.77}\ s^{-1}\ \exp(-14.0\ \text{kcal mol}^{-1}/RT),$$

$$k^{HD}=10^{8.27}\ s^{-1}\ \exp(-17.5\ \text{kcal mol}^{-1}/RT),$$

$$k^{DD}=10^{8.78}\ s^{-1}\ \exp(-20.4\ \text{kcal mol}^{-1}/RT).$$

Combining these results with Eqs (6.9) and (6.10), one obtains $\alpha = 0.55$ and $\Delta\varepsilon$ = 6.3 kcal mol^{-1} respectively. In order to arrive at these results, we have assumed that all the prefactors in the Arrhenius equations are the same. For an O-H stretching vibration, Bell [171] has determined that the zero point energy of O-H is about 2.57 kcal mol^{-1} higher than that of O-D. For two hydrogens in flight simultaneously, one should expect about 5.14 kcal mol^{-1} difference in the respective activation energies between HH and DD, If this vibration is totally lost at transition state. This value agrees well with the $\Delta\varepsilon$ calculated above.

2. Nondegenerate Concerted Reactions

For a degenerate reaction, it is required that $k^{HD} = k^{DH}$. But for a nondegenerate reaction, as depicted in Figure 6.1b, this need not be the case. If $k^{HD} \neq k^{DH}$, an additional parameter is needed to describe the E_a^{DH}. By analogy to Eq (6.8), it may be defined as

$$E_a^{DH} = E_a^{HH} + \beta\Delta\varepsilon = E_a^{DD} - (1-\beta)\Delta\varepsilon. \tag{6.20}$$

Here, β is a constant like α. So, in order to describe a nondegenerate concerted reaction, two more equations are needed besides Eq (6.9) and (6.10). They are:

$$\frac{k^{HH}}{k^{DH}} = \exp\left(\frac{\beta\Delta\varepsilon}{RT}\right), \tag{6.21}$$

and

$$\frac{k^{DH}}{k^{DD}} = \exp\left(\frac{(1-\beta)\Delta\varepsilon}{RT}\right). \tag{6.22}$$

Dividing Eq (6.21) by Eq (6.9), one obtains

$$\frac{k^{HD}}{k^{DH}} = \exp\left(\frac{(\beta-\alpha)\Delta\varepsilon}{RT}\right). \tag{6.23}$$

Thus, only when $\alpha = \beta$ does $k^{HD} = k^{DH}$. If a plot of k^{LL} vs. T is constructed, one can solve for β, α, and $\Delta\varepsilon$.

3 Step -Wise Reactions

Step-wise reaction is consisted of more than one distinct kinetic step, it involves stable intermediate. Simply, a two step reaction can be expressed as

$$A \underset{k_{-1}}{\overset{k_1}{\rightleftharpoons}} B \xrightarrow{k_2} C \tag{6.24}$$

Where, A stands for the reactants, B the stable intermediate, and C the products. Applying a steady state approximation to the intermediate B in Eq (6.24) leads to an average rate constant [164]

$$k_{av}^{L_2L_1} = \frac{k_1^{L_2L_1} k_2^{L_2L_1}}{k_{-1}^{L_2L_1} + k_2^{L_2L_1}}, \tag{6.25}$$

$k_i^{L_2L_1}$ represents the rate constant for a specific step i (1, -1 or 2), and L_2L_1 is the isotope substitution (see Figure 6.1). Here, subscript 1 and 2 stand for the first and second atom being transferred respectively. For two limiting cases, Eq (6.25) can be simplified. First, if $k_{-1}^{L_2L_1} << k_2^{L_2L_1}$, Eq (6.25) reduces to

$$k_{av}^{L_2L_1} \approx k_1^{L_2L_1}. \tag{6.26}$$

If then we assume that the secondary isotope effects are unimportant, this is usually true, the following conclusions are easily derived

$$\frac{k_{av}^{HH}}{k_{av}^{DD}} = \frac{k_1^{HH}}{k_1^{DD}} \approx P_1, \tag{6.27}$$

$$\frac{k_{av}^{HH}}{k_{av}^{HD}} \approx P_1, \tag{6.28}$$

$$\frac{k_{av}^{HD}}{k_{av}^{DD}} \approx 1, \tag{6.29}$$

$$\frac{k_{av}^{HH}}{k_{av}^{DH}} \approx 1, \tag{6.30}$$

$$\frac{k_{av}^{DH}}{k_{av}^{DD}} \approx P_1. \tag{6.31}$$

Here, P_1 is the primary isotope effect of the first step. Second, if $k_2^{L_2L_2} << k_{-1}^{L_2L_2}$, Eq (6.25) reduces to

$$k_{av}^{L_2L_1} = K_{eq}^{L_2L_1} k_2^{L_2L_1}. \tag{6.32}$$

Here, $K_{eq}^{L_2L_1}$ is the equilibrium constant of the first step. If the isotope effect for this equilibrium is small, then following results are obtained

$$\frac{k_{av}^{HH}}{k_{av}^{DD}} \approx \frac{k_2^{HH}}{k_2^{DD}} \approx P_2, \tag{6.33}$$

$$\frac{k_{av}^{HH}}{k_{av}^{HD}} \approx 1, \tag{6.34}$$

$$\frac{k_{av}^{HH}}{k_{av}^{DH}} \approx P_2, \tag{6.35}$$

$$\frac{k_{av}^{HD}}{k_{av}^{DD}} \approx P_2, \tag{6.36}$$

$$\frac{k_{av}^{DH}}{k_{av}^{DD}} \approx 1. \tag{6.37}$$

Here, P_2 is the primary isotope effect of the second step. In general, for different isotope reactions, the rate constants can be expressed by Eqs (6.38)-(6.41) according to Eq (6.25) and assuming no secondary isotope effect:

$$k_{av}^{HH} = \frac{k_1^H k_2^H}{k_{-1}^H + k_2^H}, \tag{6.38}$$

$$k_{av}^{HD} = \frac{k_1^D k_2^H}{k_{-1}^D + k_2^H}, \tag{6.39}$$

$$k_{av}^{DH} = \frac{k_1^H k_2^D}{k_{-1}^H + k_2^D}, \tag{6.40}$$

$$k_{av}^{DD} = \frac{k_1^D k_2^D}{k_{-1}^D + k_2^D}. \tag{6.41}$$

At the same time, another parameter, ϕ, may be easily defined as

$$\phi = \frac{k_{-1}^{H}}{k_{2}^{H}} = \frac{k_{-1}^{D}}{k_{2}^{D}}. \tag{6.42}$$

Here, ϕ is an index to indicate the ratio between intermediate population which goes to reactant and that which goes to product. If $\phi = 1$, it refers to a symmetric reaction. Using of the last five equations, the following results may be derived without further assumption

$$\frac{k_{av}^{HH}}{k_{av}^{DD}} = \frac{k_{1}^{H}}{k_{1}^{D}} = P_1, \tag{6.43}$$

$$\frac{k_{av}^{HD}}{k_{av}^{DD}} = P_2 \frac{(1+\phi)}{(P_2+\phi)}, \tag{6.44}$$

$$\frac{k_{av}^{DH}}{k_{av}^{DD}} = P_1 \frac{(1+\phi)}{(1+\phi P_2)}. \tag{6.45}$$

When $\phi = 1$, as is expected for a symmetric or degenerate reaction, and if $P_1 = P_2 = P$, both Eqs (6.44) and (6.45) will be reduced to

$$\frac{k_{av}^{HD}}{k_{av}^{DD}} = \frac{k_{av}^{DH}}{k_{av}^{DD}} = \frac{2P}{1+P}. \tag{6.46}$$

This is same as the result of Limbach et al [165] for degenerate reactions. Also, if $\phi \approx 1$ and $P_1, P_2 >> 1$, Eqs (6.44) and (6.45) are simplified as

$$\frac{k_{av}^{HD}}{k_{av}^{DD}} \approx 2, \tag{6.47}$$

$$\frac{k_{av}^{DH}}{k_{av}^{DD}} \approx \frac{2P_1}{P_2}. \tag{6.48}$$

Similarly, Eq (6.49) will be simplified as Eq (6.43), if $P >> 1$

$$\frac{k_{av}^{HD}}{k_{av}^{DD}} = \frac{k_{av}^{DH}}{k_{av}^{DD}} \approx 2. \tag{6.49}$$

Eq (6.49) together with Eq (6.43) are used to be the criteria for step-wise reactions.

C. Experimental Results

In alcohols, the fluorescence spectrum of 7-azaindole is bimodal. The bluer band arises from the so-called "normal" species that decays into the redder band by double-proton transfer. The model of excited-state tautomerization of 7-azaindole in alcohols being mediated by a cyclic solute-solvent complex suggests that only two protons are involved in the transition state for this nonradiative decay process. In this work, we present experimental evidence to support this model. Our experimental procedure consists of measuring the double-proton transfer rates for different isotopic substitution [68]. This is done by measuring the fluorescence lifetimes, using time-correlated single-photon counting techniques, of 7-azaindole in solvent mixtures that vary in the ratio of the amount of protiated to deuterated component.

Formally, the excited-state tautomerization of 7-azaindole (N_1L) with alcohols (ROL) can be considered to be a bimolecular reaction. Here L means either H or D. In mixed

solvents, ROH/ROD, N_1L reacts both with ROH and ROD. Then the reaction rate for N_1H is

$$d[N_1H]/dt = -k^{HH'}[N_1H][ROH] - k^{HD'}[N_1H][ROD]. \quad (6.50)$$

Here $k^{HH'}$ and $k^{HD'}$ are the bimolecular reaction rate constants respectively. The superscripts L_1L_2 means that L_1 is from solute and L_2 is from solvents. If n is the mole fraction of the deuterated solvent, then [ROD] = n[ROL], [ROH] = (1-n)[ROL], and [ROL] = [ROH] + [ROD]. Equation (6.50) is thus

$$\begin{aligned} d[N_1H]/dt &= -\{(1-n)k^{HH'}[ROL] + nk^{HD'}[ROL]\}[N_1H] \\ &= -\{(1-n)k^{HH} + nk^{HD}\}[N_1H]. \end{aligned} \quad (6.51)$$

Where we have introduced the pseudo-first-order rate constants, $k^{HH} = k^{HH'}[ROL]$ and $k^{HD} = k^{HD'}[ROL]$. Equation (6.51) may be written as

$$d[N_1H]/dt = -k_1[N_1H], \text{ where } k_1 = k^{HH} + (k^{HD} - k^{HH})n. \quad (6.52)$$

Similarly for the reaction of N_1D and ROL we have

$$d[N_1D]/dt = -k_2[N_1D], \text{ where } k_2 = k^{DH} + (k^{DD} - k^{DH})n. \quad (6.53)$$

According to the above analysis, the 7-azaindole fluorescence decay curve in mixed solvent can be fit to a sum of two exponentials

$$F(t) = A_1 \exp(-k_1 t) + A_2 \exp(-k_2 t). \tag{6.54}$$

Here the fist term is the contribution of N_1H and the second one is from N_1D. The ratio of the preexponential factors, A_1/A_2, can be derived from the solvent composition. These parameters may thus be fixed during the fit, which yields k_1 and k_2. Since k^{HH} and k^{DD} are known from the experiments in the pure solvents, k^{HD} and k^{DH} may be obtained experimentally as demonstrated in Figure 6.4. The results show that in methanol Eq (6.4) is satisfied, which in turn suggests the concerted double-proton transfer behavior for such a system. Interestingly, the isotope effect of 7-azaindole tautomerization consists of two contributions; one is from the activation energy, the other is from the frequency prefactor. Temperature dependence measurements [11a] of the normal band decays of 7-azaindole in pure methanol and deuterated methanol provide (Figure 6.3)

$$k^{HH} = 24.2 \times 10^{10}\ s^{-1} \exp(-2.07\ \text{kcal mol}^{-1}/RT), \tag{6.55}$$

$$k^{DD} = 1.99 \times 10^{10}\ s^{-1} \exp(-1.15\ \text{kcal mol}^{-1}/RT). \tag{6.56}$$

Equations (6.55) and (6.56) indicate that the isotope effect is mainly from the frequency factors and the activation energies provide a inverse isotope effect. For this case, Eq (6.7) is not valid any more. But Eq (6.7) can be modified to be as

$$\frac{k^{HH}}{k^{HD}} = \sqrt{\frac{A^{HH}}{A^{DD}}} \exp\left(\frac{\Delta\varepsilon}{2RT}\right). \tag{6.57}$$

In order to obtain Eq (57), $A^{HD} = \sqrt{A^{HH}A^{DD}}$ is assumed. By combining Eqs (6.55), (6.56), (6.57) and the ratio of k^{HH}/k^{HD}, which is 1.63 at 20 ^{o}C, $\Delta\varepsilon$ = -0.89 kcal mol^{-1} is obtained.

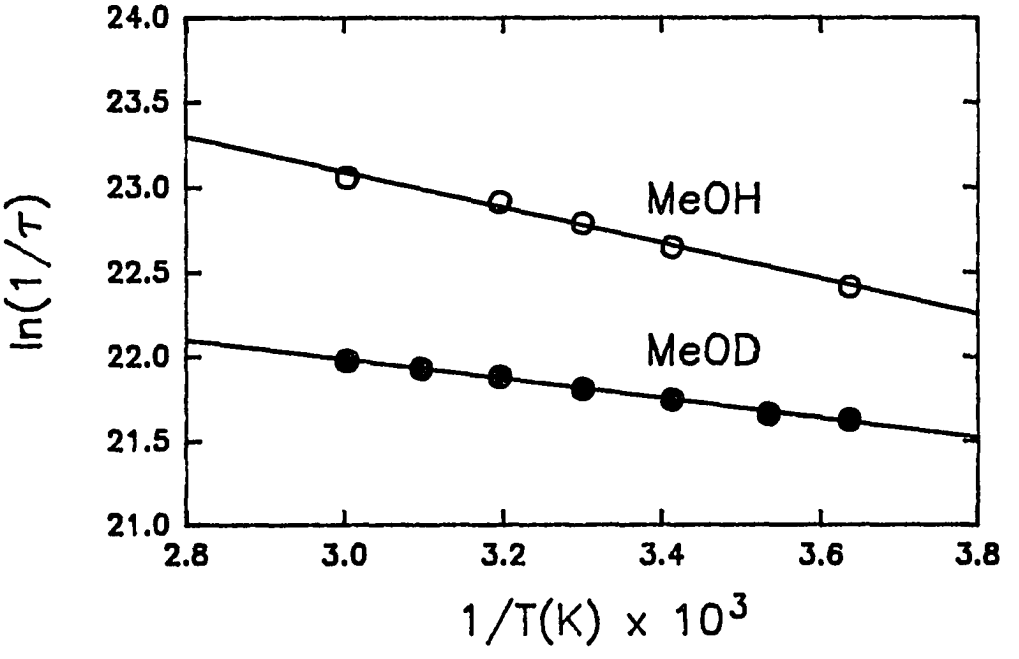

Figure 6.3. Arrhenius plots of 7-azaindole in MeOH and MeOD.

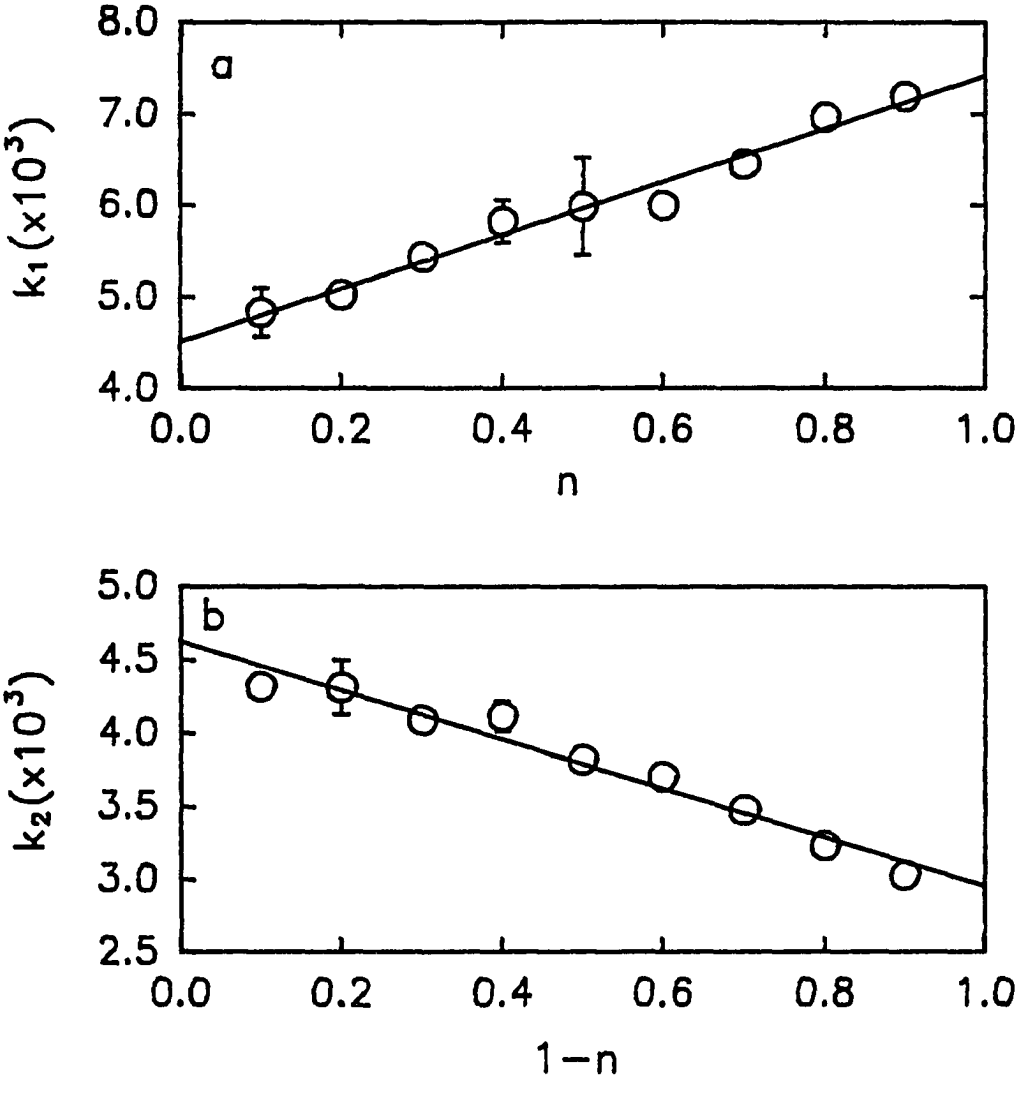

Figure 6.4. (a) k_1 vs. (1-n) for MeOH/MeOD mixtures and (b) k_2 vs. n for MeOH/MeOD mixtures, where n is the mole fraction of the deuterated solvent. The slopes and intercepts of these plots permit the determination of k^{HD} and k^{DH} (see text). The results are $k^{HD} = 4.42 \times 10^9 s^{-1}$ and $k^{DH} = 4.59 \times 10^9 s^{-1}$.

This value matches very well with the experimental difference between E_a^{DD} and E_a^{HH}, which is -0.92 kcal mol^{-1}.

D. Conclusion

Comparison of Eqs (6.14) and (6.15) with (6.34) and (6.36), one can reach the conclusion that it is difficult to distinguish between the concerted and step-wise mechanisms in some cases based on the isotope effects alone since the isotope effects for both mechanisms may be coincidentally the same. So careful attention must be paid when assigning a mechanism. Also, all the above mathematical manipulations are based on the assumption that there is no diffusion process before the reaction. If, however, in the condensed phase the diffusion happens to be important, the isotope effect would be complicated, and all the results derived above cannot be used without further consideration.

The derived results have been employed to judge the mechanism for the excited state double-proton transfer reaction of 7-azaindole in alcohol. The concerted behavior of this reaction is proved experimentally for the first time.

REFERENCES

1. Petrich, J. W. *Ph. D. Thesis* (University of Chicago, **1988**)
2. Weller, A. *Naturwissenschaften* **1955**, 42, 175.
3. Sengupta, P. K.; Kasha. M. *Chem. Phys. Lett.* **1979**, 68,382.
4. Taylor, C. A.; El-Bayoumi, M. A.; Kasha, M. *Proc. Natl. Acad. Sci. U.S.A.* **1969**, 63, 253.
5. (a) Borgis, D; and Hynes, J. T. *Chem Phys. Lett.* **1989**, 162,19; (b) Borgis, D; and Hynes, J. T. *J. Chem. Phys.* **1991**, 94, 3691.
6. (a) Borgis, D.; Tarjus, G.; and Azzouz, H. *J. Phys Chem.* **1992**, 96, 3188; *J. Chem. Phys.* **1992**, 97, 1390; (b) Truong, T. N.; McCammon, J. A.; Kouri, D. J.; and Hoffman, D. K. *J. Chem. Phys.* **1992**, 96, 8136; (c) Haug, K.; Wahnstrom, G.; and Metiu, H. *J. Chem. Phys.* **1990**, 92, 2083.
7. (a) Warshel, A.; and Chu, Z. T. *J. Chem. Phys.* **1990**, 93, 4003; (b) Hwang, J. K.; Chu, Z. T.; Yadav, A.; and Warshel, A. *J. Phys. Chem.* **1991**, 95, 8445; (c) Gillan, M. *Phys Rev. Lett.* **1987**, 58, 563.
8. (a) Makri, N.; and Miller, W. H. J. Chem. Phys. 1987, 87, 5781; (b) Bosch, E.; Moreno, M.; and Lluch, J. M. *Chem Phys.* **1992**, 159, 99.
9. Borgis. D.; and Hynes, J. T. *Chem. Phys.* **1993**, 170, 315.
10. Forster, T. *Naturwiss.* **1949**, 36, 186; Forster, T. *Z. Elektrochem.* **1950**, 54, 43.
11. (a) Négrerie, M.; Gai, F.; Bellefeuille, S. M.; and Petrich, J. W. *J. Phys. Chem.* **1991**, 95, 8663; (c) Chen, Y.; Gai, F.; and Petrich, J. W. *Chem. Phys. Lett.* **1994**, In Press
12. Murnane, M. M.; Kapteyn, H. C.; Huang, C.; Asaki, M. T.; and Garvey, D. *Mode-Locked Ti:Sapphire Laser* **1992** (Private communication).

13. Huang, C.; Asaki, M. T.; Backus, S.; Murnane, M. M.; and Kapteyn, H. C. *Opt. Lett.* **1992**, 17, 1289.

14. Krausz, F.; Fermann, M. E.; Brabec, T.; Curley, P. F.; Hofer, M.; Ober, M. H.; Spielmann, C.; Wintner, E.; and Schmidt, A. J. *IEEE J. Quantum Electron.* **1992**, 28, 2097.

15. Ippen, E. P.; and Shank, C. V. *Picosecond Phenomena* Shank, C. V. and Ippen, E. P. Eds.(Spring-Verlag, New York, **1987**)

16. Murname, M. M.; and Falcone, R. W. *J. Opt. Soc. B* **1988**

17. Koch, T. L.; Chiu, L. C.; and Yariv, A. *Opt. Comm.* **1982**, 40, 364.

18. Sizer II, T.; Kafka, J. D.; Krisiloff, A.; and Mourou, G. *Opt. Comm.* **1981**, 39, 259.

19. Wokaun, A.; Liao, P. F.; Freeman, R. R.; and Storz, R. H. *Opt. Lett.* **1982**, 7, 13.

20. Spence, D. E.; Evans, J. M.; Sleat, W. E.; and Sibbett, W. *Opt. Lett.* **1991**, 16, 1762.

21. Martinez, O. E. and Chilla, J. L. A. *Opt. Lett.* **1992**, 17, 1210.

22. Squier, J.; Salin, F.; and Mourou, G. *Opt. Lett.* **1991**, 16, 324.

23. Jacobson, M. J.; Naganuma, K.; Haus, H. A.; and Fujimoto, J. G. *Opt. Lett.* **1992**, 17, 1608.

24. Maine, P.; Strickland, D.; Bado, P.; Pessot, M.; and Mourou, G. *IEEE J. Quantum. Electron.* **1988**, 24, 398.

25. Fork, R. L.; Brito Cruz, C. H.; Becher, P. C.; and Shank, C. V. *Opt. Lett.* **1987**, 12, 483.

26. Perry, M. D.; Landen, O. L.; Weston, J.; and Ettlebrick, R. *Opt. Lett.* **1988**, 10, 484.

27. Hecht, E. *Optics*, 2nd ed. (Addison-Wesley, Reading, MA, **1987**).

28. (a) Tomov, I. V.; Fedosejevs, R.; and Offenberger, A. A. *IEEE J. Quantum. Electron.* **1982**, 18, 2048. (b) Treacy, E. P. *IEEE J. Quantum. Electron.* QE-19, **1969**, 454. (c)

Fork, R. L.; Martinez, O. E.; and Gordon, J. P. *Opt. Lett.* **1984**, 9, 150. (d) Fork, R. L.; Brito Cruz, C. H.; Becker, P. C.; and Shank, C. V. *Opt. Lett.* **1987**, 12, 483.

29. Kahlow, M. A.; Jarzeba, W.; DuBruil, T. P.; and Barbara P. F. *Rev. Sci. Instrum.* **1988**, 59, 1098.

30. Siegman, A. E. *Lasers.* (University Science Books, **1986**)

31. Négrerie, M.; Bellefeuille, S. M.; Whitham, S.; Petrich, J. W.; Thornburg, R. W. *J. Am. Chem. Soc.* **1990**, 112, 7419.

32. Chen, Y.; Rich, R. L.; Gai, F; Petrich, J. W. *J. Phys. Chem.* **1993**, 97, 1770.

33. Rich, R. L.; Chen, Y.; Neven, D.; Négrerie, M.; Gai, F; Petrich, J. W. *J. Phys. Chem.* **1993**, 97, 1781.

34. Rich, R. L.; Négrerie, M.; Li. J.; Elliott, S.; Thornburg, R. W.; Petrich, J. W. *Photochem. Photobiol.* **1993**, 58, 28.

35. Gai, F.; Chen, Y.; Petrich, J. W. *J. Am. Chem. Soc.* **1992**, 114, 8343.

36. Petrich, J. W.; Chang, M. C.; McDonald, D. B.; Fleming, G. R. *J. Am. Chem. Soc.* **1983**, 105, 3824.

37. Bent, D. V.; Hayon, E. *J. Am. Chem. Soc.* **1975**, 97, 2612.

38. Négrerie, M.; Gai, F; Lambry, J.-C.; Martin, J.-L.; Petrich, J. W. *J. Phys. Chem.* **1993**, 97, 5046; Négrerie, M.; Gai, F.; Lambry, J.-C.; Martin, J.-L.; Petrich, J. W. In *Ultrafast Phenomena VIII*, Eds. Martin J.-L.; Migus, A. **1993**, Springer, New York. p. 621.

39. (a) Valeur, B.; Weber, G. *Photochem. Photobiol.* **1977**, 25, 441; (b) Platt, J. R. *J. Chem. Phys.* **1951**, 19, 263; Yamamoto, Y.; and Tanaka, J. *Bull. Chem. Soc. Jpn.* **1972**, 45, 1363.

40. Eftink, M. R.; Selvidge, L. A.; Callis, P. R.; Rehms, A. A. *J. Phys. Chem.* **1990**, 94, 3469.

41. Still, W. C.; Kahn, M.; Mitra, A. *J. Org. Chem.* **1978**, 43, 2923.

42. Ruggiero, A. J.; Todd, D. C.; Fleming, G. R. *J. Am. Chem. Soc.* **1990**, 112, 1003.

43. Teale, F. W. J.; Weber, G. *Trans. Faraday Soc.* **1957**, 53, 646.

44. Chen, R. F. *Anal. Lett.* **1967**, 1, 35.

45. Børrensen, H. C. *Acta Chem. Scand.* **1967**, 21, 920.

46. Weber, G.; Teale, F. W. J. *Biochem. J.* **1957**, 65, 476.

47. Eisenger, J. *Photochem. Photobiol.* **1969**, 9, 247.

48. Eisenger, J.; Navon, G. *J. Chem. Phys.* **1969**, 50, 2069.

49. Shore, V. G.; Pardee, A. B. *Arch. Biochem. Biophys.* **1956**, 60, 100.

50. Avouris, P.; Yang, L. L.; El-Bayoumi, M. A. *Photochem. Photobiol.* **1976**, 24, 211.

51. Klein, R.; Tatischeff, I. *Chem. Phys. Lett.* **1977**, 51, 333.

52. Lin, S. H.; Fujimura, Y.; Neusser, H. J.; Schlag, E. W. *Multiphoton Spectroscopy of Molecules*; Academic Press; New York, **1984**.

53. Wiesenfeld, J. M.; Ippen, E. P. *Chem. Phys. Lett.* **1980**, 73, 47.

54. Bobrovich, V. P.; Sarzhevskii, A. M.; Senyuk, M. A. *Zh. Prikl. Spektrosk.* **1978**, 30, 1022.

55. Feitelson, J. *Photochem. Photobiol.* **1971**, 13, 87.

56. Robbins, R. J.; Fleming, G. R.; Beddard, G. S.; Robinson, G. W.; Thistelthwaite, P. J.; Woolfe, G. J. *J. Am. Chem. Soc.* **1980**, 102, 6271.

57. Kirby, E. P.; Steiner, R. F. *J. Phys. Chem.* **1970**, 74, 4480.

58. Hart, E. J.; Anbar, M. *The Hydrated Electron*; Wiley-Interscience; New York, **1970**. Data from this text for the extinction coefficient of the solvated electron at 650 nm in units of $M^{-1}cm^{-1}$ can be be plotted against temperature and fit very well to a straight line. We obtain $\varepsilon(T) = 17530 - 66.5\ T(°C)$.

59. Glasser, N.; Lami, H. *J. Chem. Phys.* **1981**, 74, 6526.

60. Rizzo, T. R.; Park, Y. D.; Peteanu, L.; Levy, D. H. *J. Phys. Chem.* **1986**, 84, 2534.

61. Rizzo, T. R.; Park, Y. D.; Levy, D. H. *J. Chem. Phys.* **1986**, 85, 6945.

62. Cable, J. R.; Tubergen, M. J.; Levy, D. H. *J. Am. Chem. Soc.* **1988**, 110, 7349.

63. Tubergen, M. J.; Cable, J. R.; Levy, D. H. *J. Chem. Phys.* **1990**, 92, 51.

64. Hagar, J. W.; Demmer, D. R.; Wallace, S. C. *J. Phys. Chem.* **1987**, 91, 1375.

65. Demmer, D. R.; Leach, G. W.; Outhouse, E. A.; Hagar, J. W.; Wallace, S. C. *J. Phys. Chem.* **1990**, 94, 582.

66. Arnold, S.; Sulkes, M. *J. Phys. Chem.* **1992**, 96, 4768.

67. Lami, H.; Glasser, N. *J. Chem. Phys.* **1986**, 84, 597.

68. Chen, Y.; Gai, F.; Petrich, J. W. *J. Am. Chem. Soc.* **1993**, 115, 10158.

69. Schowen, K. B. J. in *Transition States of Biochemical Processes*, Eds. Gandour, R. D.; Schowen, R. L. (Plenum, New York, **1978**), p. 225.

70. McMahon, L. P.; Colucci, W. J.; McLaughlin, M. L.; Barkley, M. D. *J. Am. Chem. Soc.* **1992**, 114, 8442; Yu, H.-Y.; Colucci, W. J.; McLaughlin, M. L.; Barkley, M. D. *J. Am. Chem. Soc.* **1992**, 114, 8449.

71. Cross, A. J.; Waldeck, D. H.; Fleming, G. R. *J. Chem. Phys.* **1983**, 78, 6455; 79, 3173.

72. Szabo, A. *J. Chem. Phys.* **1984**, 81, 150.

73. Hansen, J. E.; Rosenthal, S. J.; Fleming, G. R. *J. Phys. Chem.* **1992**, 96, 3034.

74. The expressions in references 12 and 41 for l_1 and l_2 must be interchanged.

75. Strickland, E. H.; Horowitz, J.; Billups, C. *Biochemistry* **1970**, 9, 4914; Martinaud, M.; Kadiri, A. *Chem. Phys.* **1978**, 28, 473; Rehms, A. A.; Callis, P. R. *Chem. Phys. Lett.* **1987**, 140, 83; Tatischeff, I.; Klein, R.; Zemb, T.; Duquesne, M. *Chem. Phys. Lett.* **1978**, 54, 394; Meech, S. R.; Phillips, D.; Lee, A. G. *Chem. Phys.* **1983**, 80, 317.

76. Waluk, J.; Pakula, B.; Komorowski, S. J. *J. Photochem.* **1987**, 39, 49.

77. Bulska, H.; Grabowska, A.; Pakula, B.; Sepiol, J.; Waluk, J.; Wild, U. P. *J. Lumin.* **1984**, 29, 65.

78. Petrich, J. W.; Longworth, J. W.; Fleming, G. R. *Biochemistry* **1987**, 26, 2711.

79. Tilstra, L.; Sattler, M. C.; Cherry, W. R.; Barkely, M. D. *J. Am. Chem. Soc.* **1990**, 112, 9176; Colucci, W. J.; Tilstra, L.; Sattler, M. C.; Fronczek, F. R.; Barkley, M. D. *J. Am. Chem. Soc.* **1990**, 112, 9182.

80. Hogue, C. W. V.; Rasquinha, I.; Szabo, A. G.; MacManus, J. P. *FEBS Lett.* **1992**, 310, 269.

81. Skrabal, P.; Rizzo, V.; Baici, A.; Bangerter,; Luisi, P. L. *Biopolymers* **1979**, 18, 995; Kobayashi, J.; Higashijima, T.; Sekido, S.; Miyazawa, T. *Int. J. Pept. Protein Res.* **1981**, 17, 486; Dezube, B.; Dobson, C. M.; Teague, C. E. *J. Chem. Soc. Perkin Trans. 2.* **1981**, 730.

82. Engh, R. A.; Chen, L. X.-Q.; Fleming, G. R. *Chem. Phys. Lett.* **1986**, 126, 365.

83. Szabo, A. G.; Rayner, D. M. *J. Am. Chem. Soc.* **1980**, 102, 554.

84. Heller, E. J. *Acc. Chem. Res.* 1981, *14*, 368; Alvarellos, J.; Metiu, H. *J. Chem. Phys.* **1988**, 88, 4957.

85. Chandrasekhar, S. in *Selected Papers in Noise and Stochastic Processes*, Ed., Wax, N. (Dover, New York, **1954**), p. 3; Frauenfelder, H.; Wolynes, P. G. *Science* **1985**, 229, 337.

86. The presolvated electron is known to appear from 7-azaindole in ≤ 130 fs [38]. This does not, however, place an ~ 100-fs time scale on the event of photoionization but rather indicates a time scale for the localization of the photoelectron.

87. The choice of the values for $g^a(\lambda)$ is motivated by mathematical and physical necessity. The overall population decay, $K(t,\lambda)$ (Eqn 3.17), obtained at a given emission wavelength will only be double exponential, as measured [42], if $g^a(\lambda) \neq g^b(\lambda)$. This

requirement is a consequence of the assumption that $k^a = k^b$ (Eqn 3.9). Given this, the resulting expressions from Eqns 3.12 and 3.13, when substituted in Eqn 3.18, provide $\alpha_2 = 0$, that is K(t) decays as a single exponential if $g^a(\lambda) = g^b(\lambda)$.

88. Internal conversion [76], and N_1H proton abstraction by the solvent [59,65,68,70] are other possible, significant nonradiative pathways. As we discuss elsewhere [32], we do not consider excited-state tautomerization to be an important nonradiative pathway for 7-azaindole in water.

89. Mialocq, J.-C.; Amouyal, E.; Bernas, A.; Grand, D. *J. Phys. Chem.* **1982**, 86, 3173. Santus, R.; Grossweiner, L. I. *Photochem. Photobiol.* **1972**, 15, 101. Pailthorpe, M. T.; Nichols, C. H. *Photochem. Photobiol.* **1971**, 14, 135; Amouyal, E.; Bernas, A.; Grand, D.; Mialocq, J.-C. *Faraday Discuss. Chem. Soc.* **1982**, 74, 147; Kandori, H.; Borkman, R. F.; Yoshihara, K. *J. Phys. Chem.* **1993**, 97, 9664.

90. Pigault, C.; Hasselmann, C.; Laustriat, G. *J. Phys. Chem.* **1982**, 86, 1755.

91. Steen, H. B. *J. Chem. Phys.* **1974**, 61, 3997.

92. Frauenfelder, H.; Sligar, S. G.; Wolynes, P. G. *Science* **1991**, 254, 1598.

93. Lee, J.; Robinson, G. W. *J. Chem. Phys.* **1984**, 81, 1203.

94. Drew, J.; Thistlethwaite, P.; Woolfe, G. *Chem. Phys. Lett.* **1983**, 96, 296; Sadkowski, P. J.; Fleming, G. R. *Chem. Phys.* **1980**, 54, 79; Moore, R. A.; Lee, J.; Robinson, G. W. *J. Phys. Chem.* **1985**, 89, 3648; Lee, J.; Robinson, G. W. *J. Am. Chem. Soc.* **1985**, 107, 6153.

95. Orstan, A.; Ross, J .B. A. *J. Phys. Chem.* **1987**, 91, 2739.

96. Chen, R. F. *Anal. Biochem.* **1967**, 19, 374.

97. Berlman, I. B. *Handbook of Fluorescence Spectra of Aromatic Molecules*; Academic Press; New York and London, **1971**.

98. Parker, C. A. *Photoluminescence of Solutions*; Elsevier Publishing Company; Amsterdam, **1968**.

99. Morris, J. V.; Mahaney, M. A.; Huber, J. R. *J. Phys. Chem.* **1976**, 80, 969.

100. Kaye, G.W.C.; Laby, T.H. *Table of Physical and Chemical Constants*; Longman Group Limited; London, **1973**.

101. Gai, F.; Rich, R. L.; Petrich, J. W. *J. Am. Chem. Soc.* **1994**, 116, 735

102. Durán, N.; Song, P.-S. *Photochem. Photobiol.* **1986**, 43, 677.

103. Meruelo, D.; Lavie, G.; Lavie, D. *Proc. Natl. Acad. Sci. USA* **1988**, 85, 5230.

104. Lavie, G.; Valentine, F.; Levin, B.; Mazur, Y.; Gallo, G.; Lavie, D.; Weiner, D.; Meruelo, D. *Proc. Natl. Acad. Sci. USA* **1989**, 86, 5963; Degar, S.; Prince, A. M.; Pascual, D.; Lavie, G.; Levin, B.; Mazur, Y.; Lavie, D.; Ehrlich, L. S.; Carter, C.; Meruelo, D. *AIDS Res. Hum. Retroviruses* **1992**, 8, 1929.

105. Lenard, J.; Rabson, A.; Vanderoef, R. *Proc. Natl. Acad. Sci. USA* **1993**, 90, 158.

106. Carpenter, S.; Kraus, G. A. *Photochem. Photobiol.* **1991**, 53, 169.

107. Tao, N.; Orlando, M.; Hyon, J.-S.; Gross, M.; Song, P.-S. *J. Am. Chem. Soc.* **1993**, 115, 2526; Song, P.-S.; Kim, I.-K.; Florell, S.; Tamai, N.; Yamazaki, T.; Yamazaki, I. *Biochim. Biophys. Acta* **1990**, 1040, 58; Song, P.-S. *Biochim. Biophys. Acta* **1981**, 639, 1.

108. Cubbedu, R.; Ghetti, F.; Lenci, F.; Ramponi, R.; Taroni, P. *Photochem. Photobiol.* **1990**, 52, 567.

109. Lenci, F.; Ghetti, F.; Gioffré, D.; Passarelli, V.; Heelin, P. F.; Thomas, B.; Phillips, G. O.; Song, P.-S. *J. Photochem. Photobiol. B: Biol.* **1989**, 3, 449.

110. Racinet, H.; Jardon, P.; Gautron, R. *J. Chim. Phys.* **1988**, 85, 971.

111. Bourig, H.; Eloy, D.; Jardon, P. *J. Chim. Phys.* **1992**, 89, 1391.

112. Yang, K.-C.; Prusti, R. K.; Walker, E. B.; Song, P.-S.; Watanabe, M.; Furuya, M. *Photochem. Photobiol.* **1986**, 43, 305.

113. Gai, F.; Fehr, M. J.; Petrich, J. W. *J. Am. Chem. Soc.* **1993**, 115, 3384.

114. Song, P.-S.; Walker, E. B.; Auerbach, R. A.; Robinson, G. W. *Biophys. J.* **1981**, 35, 551.

115. Walker, E. B.; Lee, T. Y.; Song, P.-S. *Biochim. Biophys. Acta* **1979**, 587, 129-144.

116. Koch, W.; Saito, T.; Yoshida, Z. *Tetrahedron* **1972**, 28, 3191.

117. Bender, M. L.; Komiyama, M. *Cyclodextrin Chemistry*; Springer-Verlag; Berlin; **1978**.

118. Chou, P.-T.; Martinez, M. L.; Cooper, W. C.; Collins, S. T.; McMorrow, D. P; Kasha, M. *J. Phys. Chem.* **1992**, 96, 5203.

119. Schwartz, B. J.; Peteanu, L. A.; Harris, C. B. *J. Phys. Chem.* **1992**, 96, 3591.

120. Giese, A. C. in *Photochemical and Photobiological Reviews, Volume 5,* Smith, K. C., Ed. Plenum; New York; **1980**. p. 229.

121. Fleming, G. R. *Chemical Applications of Ultrafast Spectroscopy*; Oxford University Press; New York; **1986**.

122. Frey, W.; Laermer, F.; Elsaesser, T. *J. Phys. Chem.* **1991**, 95, 10391.

123. Tao, N.; Song, P.-S.; Savikhin, S.; Struve, W. S. *J. Phys. Chem.* **1993**, 97, 12379.

124. Weiner, L.; Mazur, Y. *J. Chem. Soc. Perkin Trans. 2.* **1992**, 1439.

125. Dick, D. L.; Rao, T. V. S.; Sukumaran, D.; Lawrence, D. S. *J. Am. Chem. Soc.* **1992**, 114, 2664.

126. Xu, W.; Demas, J. N.; DeGraff, B. A.; Whaley, M. *J. Phys. Chem.* **1993**, 97, 6546.

127. Barbara, P. F.; Walsh, P. K.; Brus, L. E. *J. Phys. Chem.* **1989**, 93, 29.

128. Smith, T. P.; Zaklika, K. A.; Thakur, K.; Walker, G. C.; Tominaga, K.; Barbara, P. F. *J. Phys. Chem.* **1991**, 95, 10465.

129. Flom, S. R.; Barbara, P. F. *J. Phys. Chem.* **1985**, 89, 4489.

129. Flom, S. R.; Barbara, P. F. *J. Phys. Chem.* **1985**, 89, 4489.

130. Yamazaki, T.; Ohta, N.; Yamazaki, I.; Song, P.-S. *J. Phys. Chem.* **1993**, 97, 7870.

131. Gai, F.; Fehr, M. J.; Petrich, J. W. *J. Phys. Chem.* **1994**, In Press.

132. Borgis, D.; Hynes, J. T. *J. Chem. Phys.* **1991**, 94, 3619; Borgis, D.; Hynes, J. T. in *The Enzyme Catalysis Process*, Eds., Cooper, J.; Houben, J. L.; Chien, L. C.; Plenum Press: New York, 1989. p. 293.; Azzouz, H.; Borgis, D. *J. Chem. Phys.* **1993**, 98, 7361. 39.Falk, H.; Meyer, J.; Oberreiter, M. *Monatsh. Chem.* **1992**, 123, 277.

133. Falk, H.; Schoppel, G. *Monatsh. Chem.* **1992**, 123, 931.

134. Etzlstorfer, C.; Falk, H.; Müller, N. *Monatsh. Chem.* **1993**, 124, 431.

135. Etzlstorfer, C.; Falk, H.; Müller, N.; Schmitzberger, W.; Wagner, U. G. *Monatsh. Chem.* **1993**, 124, 731.

136. Etzlstorfer, C.; Falk, H.; Oberreiter, M. *Monatsh. Chem.* **1993**, 124, 923.

137. Semiempirical methods are known not to handle intramolecular hydrogen bonding well. See, for example: Jensen, J. H.; Gordon, M. S. *J. Am. Chem. Soc.* **1991**, 113, 7917 (and references therein). Other doubly tautomerized forms exist, and it is possible that a higher-level calculation with incorporation of solvent will show they are lower in energy than suggested [71-73].

138. Keirstead, W. P.; Wilson, K. R.; Hynes, J. T. *J. Chem. Phys.* **1991**, 95, 5256.

139. Somorjai, R. L.; Hornig, D. F. *J. Chem. Phys.* **1962**, 36, 1980.

140. Falk and coworkers state that the compound they identify as the hypericin

141. Gai, F.; Fehr, M. J.; Petrich, J. W. *J. Phys. Chem.* **1994**. In Press

142. Barbara, P. F.; Jarzeba, W. *Adv. Photochem.* **1990**, 15, 1.

143. Kim, Y. R.; Yardley, J. T.; Hochstrasser, R. M. *Chem. Phys.* **1989**, 136, 311.

144. Kosower, E. M.; Huppert, D. *Ann. Rev. Phys. Chem.* **1986**, 37, 127; Maroncelli, M.; MacInnis, J.; Fleming, G. R. *Science* **1989**, 243, 1671; Barbara, P. F.; Walker, G. C.; Smith, T. P. *Science* **1992**, 256, 975.

145. Brucker, G. A.; Swinney, T. C.; Kelley, D. F. *J. Phys. Chem.* **1991**, 95, 3190; Swinney, T. C.; Kelley, D. F. *J. Phys. Chem.* **1991**, 95, 10369; Swinney, T. C.; Kelley, D. F. *J. Chem. Phys.* **1993**, 99, 211.

146. Strandjord, A. J. G.; Barbara, P. F. *J. Phys. Chem.* **1985**, 89, 2355.

147. McMorrow, D.; Kasha, M. *J. Phys. Chem.* **1984**, 88, 2235.

148. Brucker, G. A.; Kelley, D. F. *J. Phys. Chem.* **1987**, 91, 2856.

149. Laermer, F.; Elsaesser, T.; Kaiser, W. *Chem. Phys. Lett.* **1988**, 148, 119.

150. Frey, W.; Laermer, F.; Elsaesser, T. *J. Phys. Chem.* **1991**, 95, 10391.

151. Borgis, D.; Lee, S.; Hynes, J. T. *Chem. Phys. Lett.* **1989**, 162, 19; Borgis, D.; Hynes, J. T. *J. Chim. Phys.* **1990**, 87, 819; Borgis, D. in *Electron and Proton Transfer in Chemistry and Biology*, eds Müller, A.; Ratajczak, H.; Junge, W.; Diemann, E. Elsevier; Amsterdam, **1992**; p. 345; Azzouz, H.; Borgis, D. *J. Chem. Phys.* **1993**, 98, 7361.

152. Peteanu, L. A.; Mathies, R. A. *J. Phys. Chem.* **1992**, 96, 6910.

153. Keirstead, W. P.; Wilson, K. R.; Hynes, J. T. *J. Chem. Phys.* **1991**, 95, 5256.

154. Etzlstorfer, C.; Falk, H.; Müller, N.; Schmitzberger, W.; Wagner, U. G. *Monatsh. Chem.* **1993**, 124, 731.

155. Falk, H. Personal communication.

156. Raser, L. N.; Kolaczkowski, S. V.; Cotton, T. M. *Photochem. Photobiol.* **1992**, 56, 157.

157. Viswanath, D. S.; Natarajan, G. *Data Book on the Viscosity of Liquids*; Hemisphere publishing: New York, **1989**.

158. Reichardt, C. *Solvents and Solvent Effects in Organic Chemistry*; VCH: Weinheim, **1988**.

159. Riddick, J. A.; Bunger, W. B.; Sakano, T. K. *Organic Solvents: Physical Properties and Methods of Purification*; Wiley: New York, **1986**.

160. Inoue, H.; Hida, M.; Nakashima, N.; Yoshihara, K. *J. Phys. Chem.* **1982**, 86, 3184.

161. Gai, F.; and Petrich, J. W. *Chem. Phys.* **1994**, In Press.

162. Dewar, M. J. S. *J. Am. Chem. Soc.* **1984**, 106, 209.

163. Meschede, L.; Limbach, H. H. *J. Phys. Chem.* **1991**, 95, 10267.

164. Rumpel, H; Limbach, H. H. *J. Am. Chem. Soc.* **1989**, 111, 5429.

165. Limbach, H. H.; Hennig, J.; Gerritzen, G.; Rumpel, H. *Faraday. Discuss. Chem. Soc.* **1982**, 74, 229.

166. Arnaut, L. G.; Formosinho, S. J. *J. Photochem. Photobiol. A: Chem.* **1993**, 75, 1.

167. Amaut, L. G.; Formosinho, S. J. *J. Photochem. Photobiol. A: Chem.* **1993**, 75, 21.

168. Fuke, K.; and Kaya, K. *J. Phys. Chem.* **1989**, 93, 614.

169. Gerritzen, D.; and Limbach, H. H. *J. Am. Chem. Soc.* **1984**, 106, 869.

170. Cox, M. M.; and Jencks, W. P. *J. Am. Chem. Soc.* **1981**, 103, 580.

171. Bell, R. P. *The Tunnel Effect in Chemistry*; Chapmam and Hall; London, **1980**.

ACKNOWLEDGMENTS

I would like to express deep appreciation and gratitude to my research advisor, Dr. Jacob W. Petrich, for his support, guidance, knowledge, and assistance throughout this endeavor. His valuable advice, enthusiasm, and vast repertoire of scientific knowledge served to motivate and inspire.

I would also like to thank the fellow members of Dr. Petrich's group, particularly to Rebecca Rich, Mike Fehr, and Yu Chen for their encouragement, friendship, and help. Without their collaboration, this study would never have been possible. Special appreciation is offered to Dr. Michel Négrerie. He taught me how to use lasers.

I would like to thank my wife, Xiaoyan Shao, and my daughter, Yanjiao Gai. Their love, patience, understanding, and support was always there when I needed. Their many sacrifices have enabled the completion of this doctoral program. I would also like to thank my parents and siblings for their love and support.